Report No. FHWA-KS-98-3
Interim Report

REPAIR OF THERMALLY CRACKED BITUMINOUS PAVEMENTS WITH FIBER REINFORCED PLASTIC COMPOSITES

Jeffrey A. Frantzen

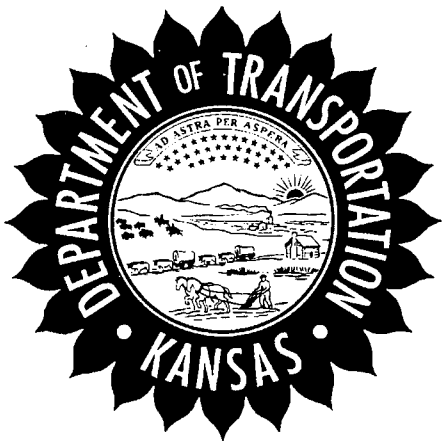

September 1998

KANSAS DEPARTMENT OF TRANSPORTATION

Division of Operations
Bureau of Materials and Research

1. Report No. FHWA-KS-98/3	**2. Government Accession No.**	**3. Recipient Catalog No.**
4 Title and Subtitle Repair of Thermally Cracked Bituminous Pavements with Fiber Reinforced Plastic Composites		**5 Report Date** September 1998 **6 Performing Organization Code**
7. Author(s) Jeffrey A. Frantzen		**8 Performing Organization Report No.** FHWA-KS-98/3
9 Performing Organization Name and Address Kansas Department of Transportation Materials and Research Center, Research Unit 2300 SW Van Buren Street Topeka, Kansas 66611-1195		**10 Work Unit No. (TRAIS)** **11 Contract or Grant No.** RE-0114-01 RE-0114-02
12 Sponsoring Agency Name and Address Kansas Department of Transportation Docking State Office Building Topeka, Kansas 66612		**13 Type of Report and Period Covered** Interim Report December 1995-September 1998 **14 Sponsoring Agency Code**

15 Supplementary Notes
Prepared in cooperation with the U.S. Department of Transportation, Federal Highway Administration.

16 Abstract

The apparatus under development in this project is a structural component or beam fabricated from a fiber reinforced composite (FRPC). The FRPC beam is a structural repair component intended to bridge a deteriorated thermal crack in full depth bituminous pavements or partial depth bituminous pavements over portland cement concrete. The bridging action provided by the FRPC beam is intended to minimize roughness through the repaired area for up to five years, eliminate reappearance of the deteriorated crack, and provide a controlled expansion crack that can be treated with standard sealing techniques. The apparatus is designed for maintenance use as a field expedient, semi-permanent repair using tools that are commonly available at the Area Maintenance level.

Three FRPC beams were constructed for field trial in a thermally cracked, fully bituminous pavement on US-36 east of Hiawatha, Kansas. Each of the beams were instrumented with bonded metal foil strain gages and field installation by KDOT maintenance forces was done in August and September of 1997. The FRPC beams have been evaluated since installation and this evaluation will continue for up to five years from the date of installation. Evaluation of the beams has been accomplished through static load tests using the stain gage instrumentation and Falling Weight Deflectometer measurements. The FRPC beams have performed satisfactorily as of the date of writing.

17 Key Words Composites, fiber reinforced composites, load transfer, transverse cracking, thermal cracking, bituminous pavements, maintenance and repair.		**18 Distribution Statement** No restrictions. This document is available to the public through the National Technical Information Service, Springfield, Virginia 22161	
19 Security Classification (of this report) Unclassified	**20 Security Classification (of this page)** Unclassified	**21 No. of pages** 159	**22 Price**

Repair of Thermally Cracked Bituminous Pavements with Fiber Reinforced Plastic Composites

Interim Report
FHWA-KS-98/3

by

Jeffrey A. Frantzen

Kansas Department of Transportation

September 1998

PREFACE

This report presents the interim results of a development project for using fiber reinforced composites as a structural repair component in full depth bituminous pavements. The purpose of the project was to develop a fiber reinforced composite beam that could act as a bridge over a deteriorated thermal crack in a full depth bituminous pavement or a partial depth bituminous pavement over portland cement concrete. The composite beam is designed for maintenance use as a field expedient, semi-permanent repair using tools that are commonly available at the Area maintenance level. Three composite beams were constructed and installed in a thermally cracked, full depth bituminous pavement on US-36 east of Hiawatha, Kansas in August and September of 1997. Two of the composite beams are still in service after one year and are performing satisfactorily. These beams will continue to be evaluated for as long as they remain in service, or until five years of service life has been completed.

ACKNOWLEDGEMENTS

I wish to express my appreciation to the many individuals who contributed time, effort, and advice to this project. First of all, I want to thank the Federal Highway Administration and the Kansas Department of Transportation for their financial support and their willingness to believe in my concept. Special thanks are due to Richard McReynolds, Steve Woolington, Roy Rissky, and Clay Adams for

their support of this project. I want to acknowledge the enormous technical and moral support of Dr. Ray Moore, Dr. Stan Rolfe, Dr. Steve Cross, Dr. Jim Locke, Dr. John Easley, Dr. Steve McCabe, Dr. Francis Thomas, Dr. Rob Sorem, and Mr. Ron Hurst of the University of Kansas. Their advice and guidance was crucial in the design phase of the project. I also want to thank the university for the loan of strain gage equipment during the field testing phase.

Finally, I want to thank the fine people of the Area 1 maintenance office at Horton for their assistance and patience in installing the composite beams. Without their help, this project would still be a paper study.

NOTICE

The author and the State of Kansas do not endorse products or manufacturers. Trade and manufacturer's names appear herein solely because they are considered essential to the object of this report.

DISCLAIMER

The content of this report presents the view of the author who is responsible for the accuracy of the data and the facts contained within. The content of this report does not necessarily reflect the policies or views of the Federal Highway Administration or the State of Kansas. This report does not constitute a standard, specification, or regulation.

Table of Contents

Table of Contents (cont.)

List of Figures

List of Figures (cont.)

Page

List of Figures (cont.)

Page

List of Tables

Chapter I

INTRODUCTION

The repair of deteriorated transverse cracks in full and partial depth bituminous pavements is an ongoing problem for the maintenance organizations of transportation departments in the colder geographic areas of the North American continent. Most methods of repair require contract maintenance by external forces and specialized equipment to achieve an adequate repair. This report describes an approach to the repair of deteriorated transverse cracks that can be implemented by highway agency maintenance forces. The approach makes use of a fiber reinforced epoxy composite structural component to provide adequate long-term load transfer over the deteriorated pavement.

This report describes the design, production, and use of a composite structural component in the repair of a deep transverse crack on a high truck traffic volume bituminous pavement. These topics are discussed in a two-tier fashion. The body of the report is structured as a general overview of the project with sufficient detail to permit a general understanding of the procedures and results. The detailed analyses, design, and construction features of the project are contained in the appendices, which may be consulted for more detail as desired.

HYPOTHESIS AND OBJECTIVE

When transverse cracks in full depth bituminous pavements are small, they are usually treated by routine maintenance techniques using highway agency forces. When the cracks have deteriorated to the point that they have considerable roughness or surface depression associated with them, they are usually repaired by external contract maintenance forces. A photograph of a deteriorated thermal crack is

presented in Figure 1-1. Contract maintenance forces are used when the equipment required for repair is not normally part of the highway agency maintenance organization's equipment or the repair requires special knowledge or materials.

A maintenance repair technique is needed that does not require complete removal of all deteriorated pavement and that can be done within a few hours with equipment that is commonly issued to maintenance forces. The subsequent chapters describe the development of materials and procedures that will allow highway agency maintenance organizations to make long term repairs on deteriorated transverse cracks without resorting to contract maintenance.

Figure 1-1. - Thermal Crack on US-36, Brown County.

The maintenance technique that has been developed involves the use of a fiber reinforced plastic composite (FRPC) structural member. The FRPC structural member is intended to be placed in a shallow milled area over the deteriorated crack, covered with hot mixed asphalt concrete, and is designed to transmit the wheel loads

from vehicular traffic to sound pavement on either side of the crack with minimal surface deflection.

APPROACH

Development of the FRPC structural member involved the design and production of a structural unit consisting of two fiber reinforced plastic skins that cover a core of expanded plastic foam or structural honeycomb. The FRPC member is designed to have sufficient structural rigidity to transmit wheel loads with minor deflection from the deteriorated area to sound material on either side of the crack. The surface deflection standard for design purposes is 0.020 inches for a 9000 pound wheel load.

A series of test models of the FRPC beam have been produced for laboratory testing of the concept and as a development aid to check materials compatibility. After evaluating the information from the laboratory tests, three full size FRPC units were produced for installation by Kansas Department of Transportation maintenance forces at suitable transverse cracks on US-36 just east of Hiawatha, Kansas. These units are instrumented to record the deformation characteristics, installation, and field aging effects on the FRPC structural members over an anticipated five year period.

Chapter 2

LOAD-DISPLACEMENT BEHAVIOR AND SERVICEABILITY

The desired level of service of a repaired thermal crack is a pavement that behaves like an undeteriorated pavement when subjected to a wheel load. That is, the repaired area should deform at the surface like the undeteriorated pavement on either side of the thermal crack.

Designing a successful crack repair requires a reasonably accurate and simple pavement deformation model. The model selected for use in design is a homogeneous, linearly elastic, isotropic material model for the pavement and subgrade. A simple model was selected because little benefit would be gained by using a complex material model for initial design.

After selecting the model, the next step is the selection of a procedure to identify the pavement and subgrade modulus and Poisson's ratio. A decision was made to measure the pavement material's elastic characteristics using the non-destructive Falling Weight Deflectometer (FWD) test rather than use laboratory test results on pavement cores and subgrade soil samples. The FWD consists of a trailer carrying the test instrumentation and a van containing signal conditioning and data processing equipment. The trailer carries a calibrated falling weight which impacts a loading plate that rests on the pavement surface. The deflection basin caused by the impact load is sensed by six geophones suspended from a bar on the trailer. The impact load signal from a load cell beneath the falling weights and the geophone

signals are converted into load and deformation data and are stored on a floppy disk and printed out inside the van. Each FWD test consists of three test loadings at each location. A line drawing of the FWD is presented in Figure 2-1. The use of the FWD allows for repeated measurements of the pavement modulus through most of the year. This technique permits measurement of the effects of the environment on the pavement and subgrade modulus values and also allows for better estimation of the modulus value through repeated sampling.

Pavement system modulus values derived from laboratory tests on pavement cores and subgrade samples obtained from the field are "one-shot" measurements subject to many sources of variability. These sources include the effects of sampling disturbance, non-uniformity in resilient modulus values due to test machine variability, and difficulty in simulating environmental effects in the laboratory. Repeated measurements on one sample to limit variability are not possible due to the destructive nature of the test methods. Also, the use of multiple samples involves considerable expense. Furthermore, multiple samples taken from a small area have a biasing effect on the field location as the voids left by sampling must be filled and are usually filled with material that is not representative of the site under study.

The determination of pavement and subgrade modulus values from FWD test results involves fitting the observed surface deformation of the pavement with a

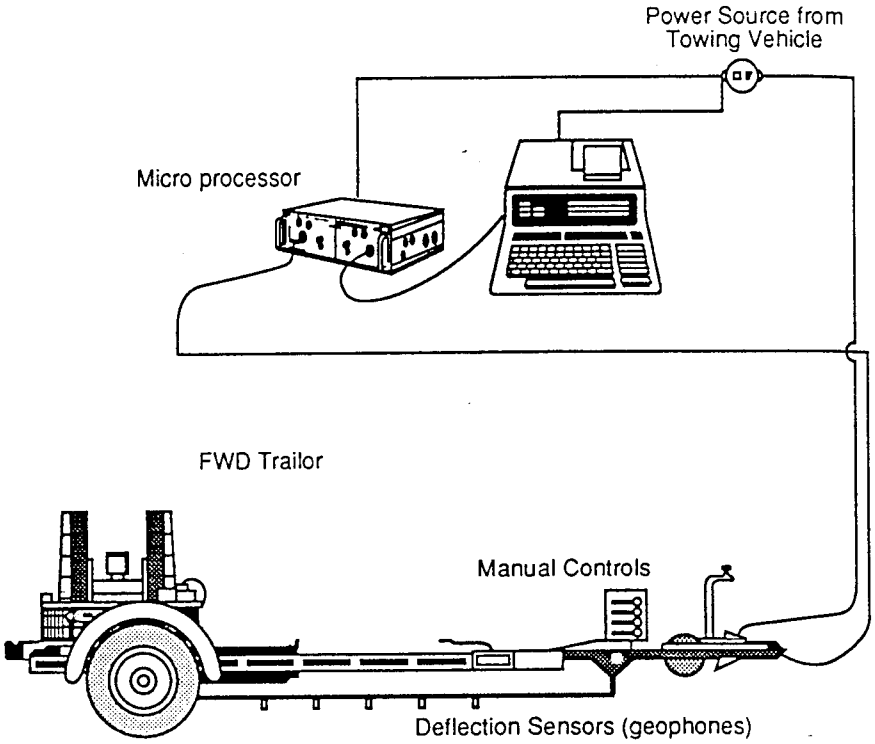

(a) FWD in Operating Position

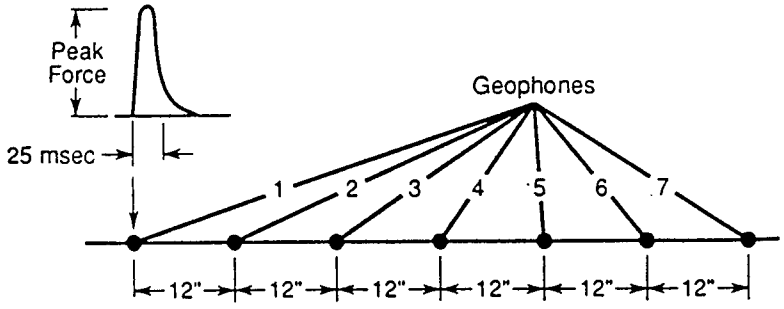

(b) Geophones Configuration

Schematic diagram of Dynatest Model 8000 FWD (Note 1 in. = 25.4 mm)

Figure 2-1. - FWD Configuration (AASHTO, 1986).

theoretical deflection based on elastic layer theory. The theoretical deflection is computed using a FORTRAN program written by ARE, Inc. called MATCH (Austin Research Engineers, 1985). The program relies on an assumption of plane strain and axial symmetry and involves the solution of the biharmonic equation

$$\nabla^4 \varphi = 0$$

for a multilayered elastic solid with a circular surface load. The method of solution implemented in the computer program follows that outlined by Burmeister (1944) and Jones (1962) wherein the stress function which is the solution to the biharmonic equation is integrated and evaluated numerically to obtain the surface deformations. The required input for the program consists of the surface load, thickness of the pavement and subgrade layers, assumed values for Poisson's ratio and the elastic moduli, and the points at which surface deformation values are desired.

Operation of the program with FWD data involves making initial assumptions for the values of the elastic modulus and Poisson's ratio for each of the pavement layers. Typically, a Poisson's ratio value of 0.35 to 0.40 is selected for asphaltic concrete, 0.42 to 0.45 for aggregate bases, and 0.45 to 0.49 for the subgrade soils. Initial assumed modulus values are usually in the range of 2500 to 40000 psi for subgrade soils, 80,000 to 200,000 psi for aggregate base courses, and 100,000 to 2,500,000 psi for asphalt concrete. Once the initial values are selected, pavement deflections are calculated using MATCH and compared to the FWD measurements. New values are selected for the pavement moduli and the process is repeated until

reasonable agreement between the calculated and observed deflections are reached. The resulting moduli can then be used for design purposes. A sample output from MATCH is presented in Figure 2-2.

Once pavement modulus values were calculated for the field test site, the required thickness of the FRPC structural member could be determined. Pavement moduli for initial design were calculated using MATCH for a location on I-70 in Russell County, Kansas. The data set from this location was used because it was the original candidate location for the field trials. Using the moduli from the FWD runs, two finite element models of the pavement structure at the field location were constructed. One finite element model was an axisymmetric model and the other a 2 dimensional plane strain model. Both models used continuous strain triangle (CST) elements. The computer programs used for the finite element analysis are the author's modification of a program originally presented by Zienkiewicz (1972). The mesh used in the analysis is shown in Figure 2-3.

Both finite element models were checked against the FWD field deflections. There is a 10 percent error in the surface deformation as predicted by the 2-D plain strain analysis when compared to the field results. The reason for this difference arises from the initial assumptions underlying a plane strain analysis. A plane strain analysis assumes that the body and the imposed loads extend continuously for a long distance along an axis perpendicular to the section under consideration. This assumption is not correct for the FWD loading condition, which is axisymmetric and

```
Enter Poissons Ratios for Each Layer (from the top-down):0.4,0.45

Enter FWD Load Magnitude (pounds): 9220.

Enter Field Deflections for All Sensors (milli-inches):3.29,2.67,2.19,1.76,1.46

Enter Elastic Moduli for Each Layer (from the top-down, in psi):310000.,25500.

LAYER Program Running ...

DEFLECTION PLOT:

Sensor +---------+---------+---------+---------+---------+  Field  Theor
   1                                              T         F  3.290  2.930
   2                                  T      F                 2.670  2.446
   3                        T    F                            2.190  2.047
   4              TF                                         1.760  1.718
   5    *                                                     1.460  1.451

Try New Modulus Values? (N=No):



Enter Poissons Ratios for Each Layer (from the top-down):0.4,0.45

Enter FWD Load Magnitude (pounds): 9220.

Enter Field Deflections for All Sensors (milli-inches):5.75,3.76,3.29,2.67,2.19

Enter Elastic Moduli for Each Layer (from the top-down, in psi):310000.,25500.

LAYER Program Running ...

DEFLECTION PLOT:

Sensor +---------+---------+---------+---------+---------+  Field  Theor
   1                                                    *    5.750  5.768
   2                          T F                            3.760  3.593
   3                   T     F                              3.290  2.930
   4           T  F                                         2.670  2.446
   5    T F                                                 2.190  2.047
```

Figure 2-2. - Sample Output from MATCH.

limited in extent. However, the error was not deemed sufficiently detrimental to invalidate the use of this method, especially for initial design and selection of the thickness of the FRPC beam.

After calibrating the finite element model, a crack was simulated in the 2 dimensional plane strain model by reducing the modulus of the elements along a vertical line from the subgrade to the surface of the pavement. The softening of these elements produced a depressed zone at the surface much like that observed in the field surrounding a deteriorated thermal crack. The number of elements with reduced modulus values was adjusted until a depressed surface profile was formed extending 12 inches on either side of the crack.

The next step involved simulating the placement of a FRPC structural member 2 inches below the surface of the pavement. This was done by assigning an elastic modulus of 7.5 million psi and a Poisson's ratio of 0.25 to the elements in a layer 36 inches wide and two inches down from the surface. A surface load simulating an FWD test was applied to the model and the surface deformations were noted. FRPC members 1, 2, 3, and 4 inches thick were examined. A three inch thick FRPC member was found to be sufficient to restore the pavement deflection in the finite element analysis to the value of an undeteriorated pavement.

Once pavement modulus information was calculated for the field test site, the required thickness of the FRPC structural member could be determined. Pavement moduli for initial design were calculated using MATCH for a location on I-70 in

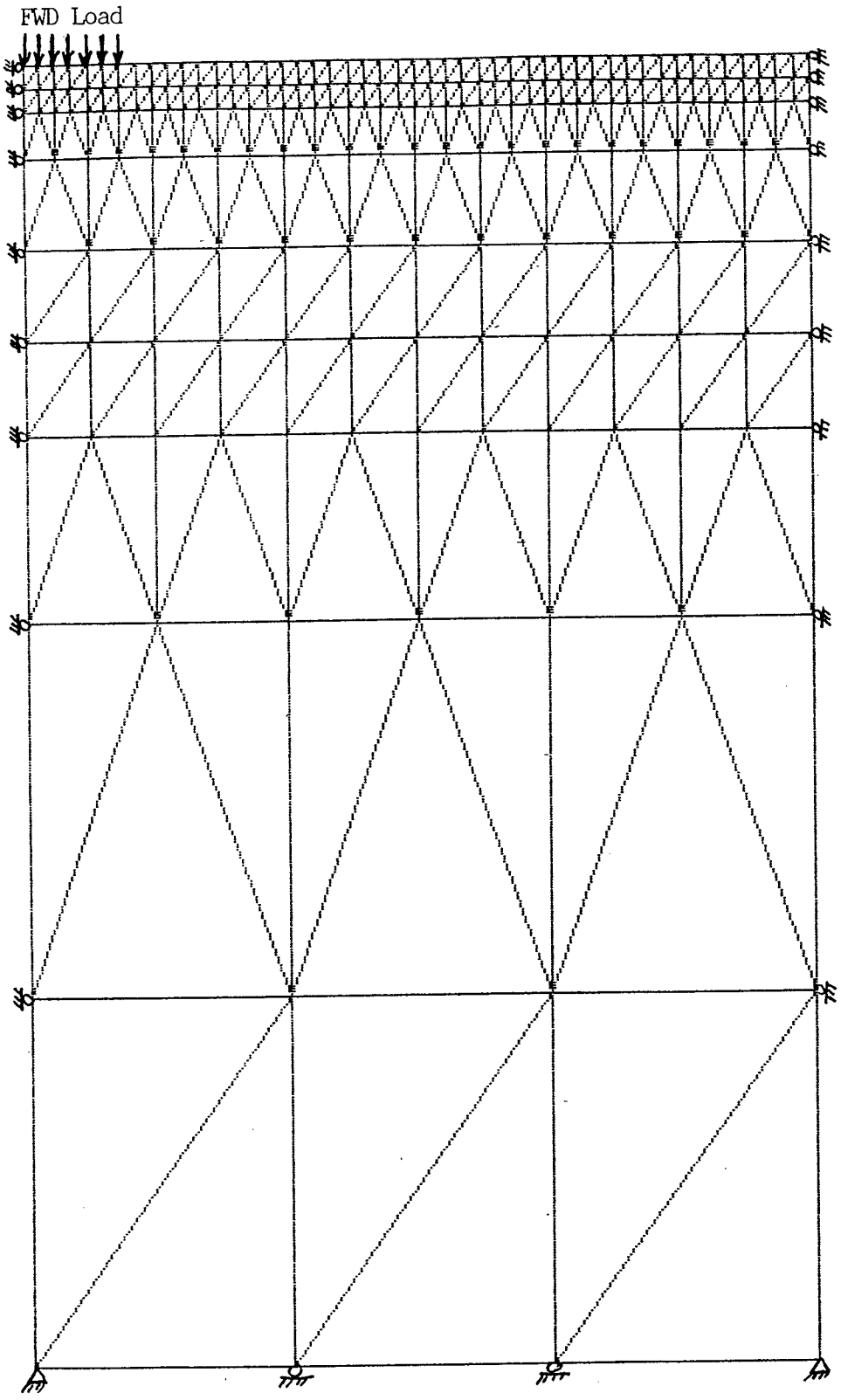

Figure 2-3. - Finite Element Mesh for Pavement.

Russell County, Kansas. The data set from this location was used because it was the original candidate finite element method in that the subgrade soils are modeled using a Winkler spring foundation model rather than an elastic continuum. The asphalt concrete pavement section is modeled as an elastic beam. Determination of the subgrade response involves selecting a modulus of subgrade reaction, k, for the soil springs that gives a pavement surface deformation equivalent to that produced by the FWD. In the beam on an elastic foundation approach, the pavement was modeled as a beam with a modulus equivalent to that determined using the FWD data. A one foot wide section of the pavement was used to determine the moment of inertia for the section. The deformation basin measured by the FWD and the FWD load were used to calculate the k value for the soil springs that would be representative of the elastic characteristics of the subgrade. Given a 16 inch thick pavement with a modulus of 373,000 psi and a subgrade modulus of 20,000 psi, the equivalent k value is 3000 pounds/inch.

Once k was determined, the modulus of the asphalt concrete pavement beam was reduced to 100,000 psi to develop a deflection basin equivalent to a deteriorated pavement. This was done to gauge the benefit a 3 inch FRPC beam would have on a weak pavement section. A composite beam EI value for the repaired pavement made up of the FRPC member and deteriorated pavement sections was substituted into the analysis and a new maximum deflection was calculated. The results of the beam on elastic foundation and finite element analyses with identical material properties are

presented in Table II-1. Also presented are the measured field deformation for an undeteriorated pavement and an estimated deformation using the beam on elastic foundation method for a pavement modulus of 100,000 psi.

Table II-1 Pavement Surface Deflections

Analysis Type	Maximum Deflection (inches)
Surface Deformation (Existing-Measured)	0.00576
Surface Deformation (Existing-Predicted) (Axisymmetric CST Finite Element analysis)	0.00560
Surface Deformation (Existing-Predicted) (Plane strain using CST elements)	0.00610
Surface Deformation (Finite Element Method) (For 100 ksi pavement moduli)	0.00780
Beam on Elastic Foundation (For 100 ksi pavement moduli)	0.00710

The procedures described in the preceding paragraphs indicated that a 3 inch thick FRPC beam approximately 36 inches long would be sufficient to improve a deteriorated pavement and limit deformation. The next step in the design involves selection of a structural configuration that will achieve the required stiffness and be easy to construct.

Chapter 3

DESIGN OF FIBER REINFORCED COMPOSITE BEAMS FOR CRACK REPAIR

Once an initial estimate of the required size of the FRPC member was made, an efficient design for the member needed to be made. A structural plate constructed of a large number of layers of epoxy and glass or carbon fiber cloth would be structurally inefficient and too heavy to be lifted by two men. Accordingly, several conceptual combinations of structural members and configurations were initially examined. These included plates and angles or I sections, foam cores with face sheets, bonded triangular tubes, and box beams. A series of bonded box beams was chosen for detailed analyses. The box section was chosen because it could be designed rapidly and constructed easily by hand with simple tooling. This type of member could also be fabricated and tested singly and in bonded combinations, allowing a natural progression from prototype to finished assembly. A series of bonded box beams also yielded some structural redundancy.

The design method selected for the initial design of the FRPC box sections was the simplified method of Chamis (1986). His method consists of a series of closed form approximate equations which use a weighted average of the individual lamina characteristics to predict the behavior of an orthotropic structural member. The general design philosophy is to size the composite panels of the box beam to resist vertical loading and to add plys for lateral loads and twist moments. Displacement

and buckling criteria are also addressed in the procedure. The design procedure identifies the number of plys required to resist the design loads without failing, their orientation, and the stacking sequence. Chamis's design procedure is shown in full for the succeeding design in Appendix B.

The configuration of the box section as designed is shown in Figure 3.1. The design requirements chosen for the box beam were a load factor of 2.0 and a design load of 4500 pounds. This was representative of a 9000 pound dual wheel load being shared by two box beam sections. An assumption was made that no box would fail under this load and there would be no imposed twist moment or lateral load.

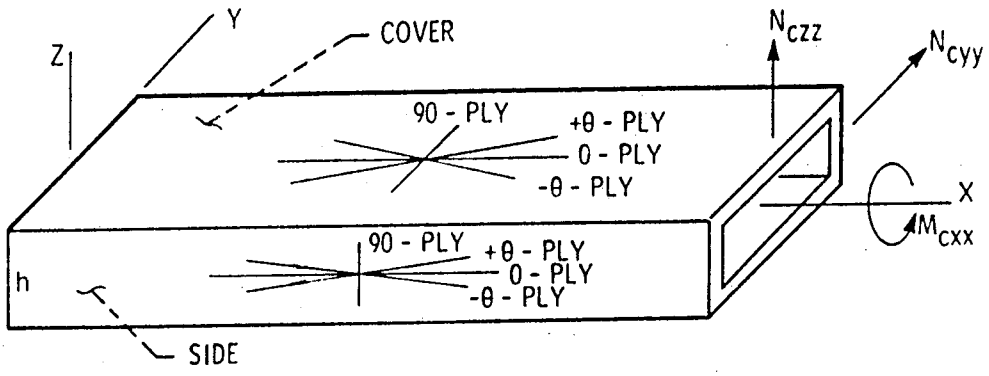

Figure 3-1. - Box Beam (Chamis, 1985).

Two different designs were produced. One used E-glass/epoxy as the material and the other graphite/epoxy. The E-glass/epoxy design had a configuration of 20 plys in the 0 degree orientation (along the axis of the beam), 2 plys in the 90 degree orientation (cross-beam axis), and 8 plys oriented at ±45 degrees (or $[\pm 45_8/0_{20}/90_2]$).

The graphite/epoxy design allowed a reduction in the number of plys required to one half that of e-glass/epoxy or [$\pm 45_4/0_{10}/90_2$]. This also reduced the weight of the member by about one half. However, the cost of graphite/epoxy is about four times that of E-glass, which resulted in a member that would cost twice that of e-glass. Therefore, the E-glass /epoxy alternate was selected for construction.

The FRPC member could not be constructed by simply bonding the individual box beam units together. Additional coupling between the units was required to insure that the box beams would act as a unit. The requirement for coupling meant that a skin needed to be placed on the top and bottom surfaces of the FRPC unit. The best way to accomplish this was to divide the number of plys equally between the skin and the box units. This provides symmetry for the entire unit and inhibits any undesirable twist in the unit that might occur from thermal or mechanical stress. The configuration chosen for the box beams and the skin is shown in Figure 3-2.

Each box section has a cross-sectional size of 6 inches by 3 inches. Two lengths of box section are used in the design, 30 and 34 inches in length. Box sections of each length are alternately bonded together to form a sawtooth pattern along one edge. The purpose of the sawtooth pattern is to provide a dowel-like action at one end of the repair. The flat end of the FRPC unit is cemented in place while the sawtooth end is coated to allow movement between the pavement sections.

After a preliminary design for the beam was obtained from Chamis's method, classical lamination theory for plates (Jones, 1975) was used to check the resulting

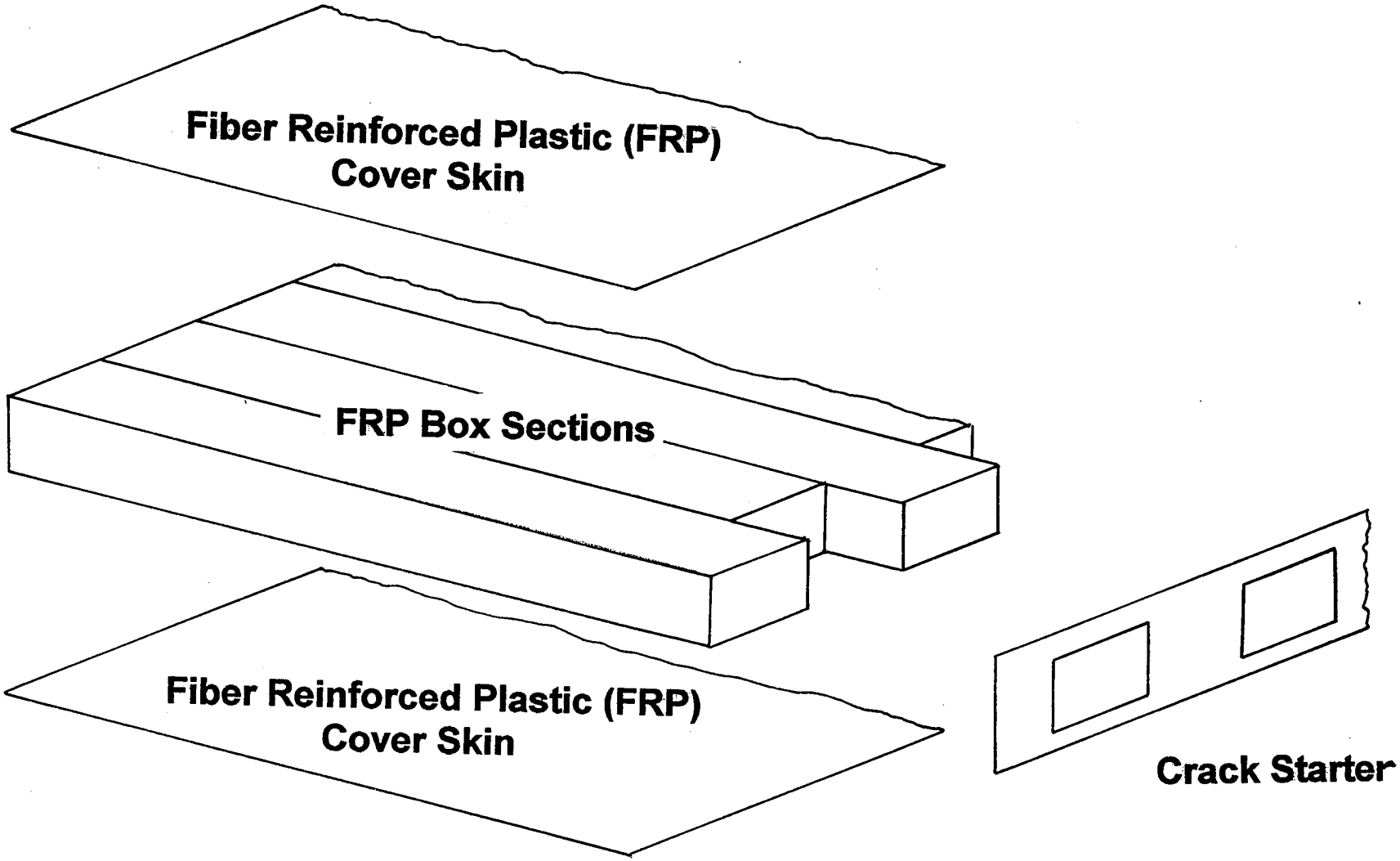

Figure 3-2. Configuration of the FRPC Beam

design. In classical laminated plate theory, the stiffness of each of the individual layers is calculated first. Then each layer stiffness and its the corresponding thickness are combined and used to calculate the extensional stiffnesses A_{ij} , the coupling stiffnesses B_{ij}, and the bending stiffnesses D_{ij} for the complete laminate. These stiffnesses are used to calculate the strains in the laminate from imposed thermal and mechanical loads. The strains can then be used to determine the stress level in each individual ply. This procedure is presented in flow chart form in Figure 3-3.

All isotropic materials have extensional and bending stiffnesses. However, an oriented fiber reinforced composite may exhibit coupling between extension and bending. This may not occur if the laminate is an orthotropic laminate where the fibers in the laminate are oriented at 0 and 90 degrees to the major axis of loading. However, if the laminate is constructed such that all of the fibers are oriented at an angle between 0 and 90 degrees, there is extensional deformation with load, but there is also twisting and bending. This twisting and bending can be overcome by designing the laminate so that it is balanced. The term balance means there is symmetry through the laminate if one looks at the ply arrangement with respect to the center of the laminate.

The method for calculating stiffness and stress in a laminated plate described above was automated by writing a FORTRAN program titled CSTRESS. A listing of the program is located in Appendix C. Input for the program consists of orientation, thickness, strength and elastic properties for the fiber and epoxy matrix for each of the

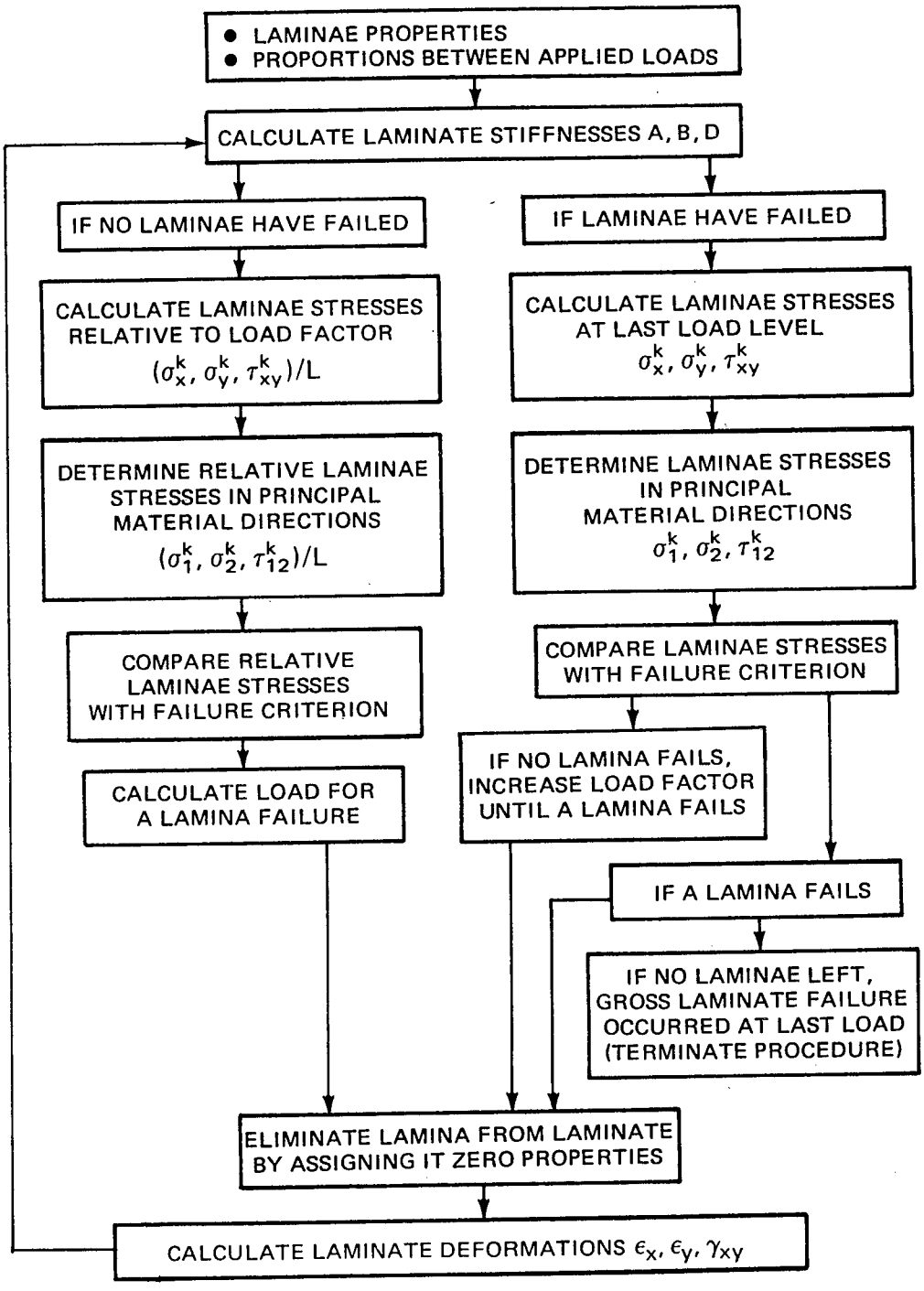

Figure 3-3. - Design Procedure for CLP Theory (Jones, 1975).

fiber reinforced plys. Loads and service temperature data are entered for the entire laminate as well. The program calculates the laminate stiffnesses A_{ij}, B_{ij}, and D_{ij}, the stresses and strains in each of the individual plys, and notifies the user if failure has occurred according to the criteria outlined in the Tsai-Hill failure criterion.

CSTRESS was used to check the initial design by examining the properties of stresses and strains in each of the individual plys, and notifies the user if failure has occurred according to the criteria outlined in the Tsai-Hill failure criterion.

CSTRESS was used to check the initial design by examining the properties of the covers for the box beam under a loading condition that would occur for a 9000 pound load at the center of the beam. The design criteria used to judge adequacy is no lamina failure under anticipated loading conditions. This criterion is different than the one shown in Figure 3-3. The reason for using a different criterion than the one shown in Figure 3-3 is that a design is desired that has a low stress level in normal service in order to reduce creep and insure the ability to absorb overloads that commonly occur in highway service.

Buckling behavior also was examined. Laminated composite plates are often thin enough for buckling to be the primary mode of failure. In this application, the walls and cover plates for the box beam are very thin in comparison with the depth and width of the box beam. The result of this analysis using CSTRESS indicated that the design produced using the procedures of Chamis was adequate and could be used to produce the FRPC beam for pavement repair. The materials properties that were

used for the initial portion of the design were book values. Table III-1 contains the values used for preliminary design.

TABLE III-1 PROPERTIES FOR COMPOSITES

ASSUMED DESIGN VALUES

E_1 = 7,480,000 psi	X_t = 160,000 psi
E_2 = 3,060,000 psi	Y_t = 4,000 psi
ν_{12} = 0.23	S = 12,000 psi
ν_{21} = 0.09	X_c = 90,000 psi
G_{12} = 1,480,000 psi	Y_c = 20,000 psi

UNIDIRECTIONAL REINFORCEMENT - AS MANUFACTURED

E_1 = 3,890,000 psi	X_t = 55,500 psi
E_2 = 377,000 psi	Y_t = 8,060 psi
ν_{12} = 0.24	S = 3,750 psi
ν_{21} = 0.045	X_c = not tested
G_{12} = 287,000 psi	Y_c = not tested

WOVEN REINFORCEMENT - AS MANUFACTURED

E_1 = 1,780,000 psi	X_t = 24,200 psi
E_2 = 1,780,000 psi	Y_t = 24,200 psi
ν_{12} = 0.06	S = 8,210 psi
ν_{21} = 0.06	X_c = not tested
G_{12} = 408,000 psi	Y_c = not tested

The materials selected to construct the FRPC member were commercially available products. The fiber reinforcement was style 7781 woven E-glass cloth with

a weight of 9 oz/sq.yd. The epoxy matrix was a thinned Shell EPON 8132 resin with an aliphatic curing agent.

A single test beam with one 14 ply layer was constructed according to the preliminary design. This beam was built using hand lay-up procedures with no consolidation other than that obtained with compaction rollers. A full discussion of construction procedures is contained in Appendix D. The beam was tested to failure in a 120,000 pound capacity universal test machine as a simply supported beam with the load placed at the midpoint of the beam. The design failure load was 9000 pounds. The observed failure load was 4,414 pounds. Buckling began at about 3500 pounds. This result was far below what was intended and indicated that the design values were not representative of what could be obtained using the proposed fabrication procedures. An estimate of the composite modulus was made by back-calculating the modulus from the deflection formula for a simply supported beam with a concentrated load. This was done for a load of 2000 pounds and a center-point deflection of 0.282 inches. The calculated modulus was 593,000 psi, which is less than 10 percent of the assumed design value.

A series of tensile test coupons were constructed subsequently with unidirectional E-glass reinforcement to determine what were the actual elastic characteristics and failure loads for the materials used to produce the first beam. These values are shown in Table III-1 under the sub-heading of unidirectional reinforcement. A comparison between the assumed design values and the

unidirectional reinforcement shows that the elastic and failure properties of the samples manufactured for this project are roughly one half as stiff or strong as those possible with the best materials and manufacturing techniques. After assessing the impact of these results, a second series of tensile test coupons were produced using woven E-glass cloth. These coupons were made to gage the effect woven reinforcement would have on the elastic and failure properties. The results from these tests show that the FRPC beams will have elastic properties that are about 25% of the design values and failure stresses that are about 15% of the design values. A more detailed discussion of the tensile tests and other related materials properties are contained in Appendix E.

Further study indicated that the design parameters obtained from book values were maximum values obtained using the best technique, materials, and mechanical compaction from vacuum and autoclave equipment. The test results indicated that the initial design was very optimistic. Therefore, a second test beam was produced using vacuum compaction to optimize the mechanical properties of the laminate and to see how close to the design values one could come with the equipment and materials used in this project..

The improved beam had the same section containing fourteen plys. This beam was loaded to failure using the same test conditions as the first beam. The improved beam had a failure load of 5,189 pounds and buckling began in this unit at a load of 2500 pounds. The lower load value for buckling is a result of a thinner wall section

due to compactive effort. Modulus was calculated in the same fashion as for the first test beam. The improved beam yielded a modulus of 2.61 x 10^6 psi for a load of 2100 pounds and a corresponding deflection of 0.142 inches. These results show that vacuum compaction produces a much stronger product and would have to be used to produce all components for the FRPC beams.

As construction of the box beam FRPC unit progressed, the inherent inefficiency of the manufacturing process chosen was noted and a search was made for a more efficient method of fabricating a FRPC beam. A search of the literature lead to the structural sandwich method of construction using honeycomb and FRPC covers (Bruene, 1977, and Osgood, 1966). Since three units were to be constructed, a decision was made to complete one box beam FRPC unit for installation in US-36 and build the other two units using the honeycomb structural sandwich approach.

The structural sandwich design using FRPC covers involves the use of an aluminum or fiberglass honeycomb core with bonded facing sheets of fiberglass and epoxy. A drawing of this design is shown in Figure 3-4. The fiberglass facing sheets are designed to carry the bending stresses for the structural unit. The honeycomb core acts as a light weight spacer for the fiberglass facing sheets and also carries the shear loads. The use of the honeycomb core eliminates the need for angle plys to carry the shear loads and also acts as a ready-made form on which to lay up the facing sheets. A notch is placed along one side of the honeycomb core in order to form a lip. The lip

section is intended to act like a dowel in the same manner as the sawtooth section for the box beam unit.

Two units for use in US-36 were constructed of commercial grade aluminum honeycomb with fiberglass and epoxy facing sheets. The facing sheets were constructed using the same materials as the FRPC box beam unit. The facing sheets each had 20 plys oriented in the 0/90 degree directions. The details of the design process for the structural sandwich using honeycomb are outlined in Appendix F. Details of the construction of the units are presented in Appendix D.

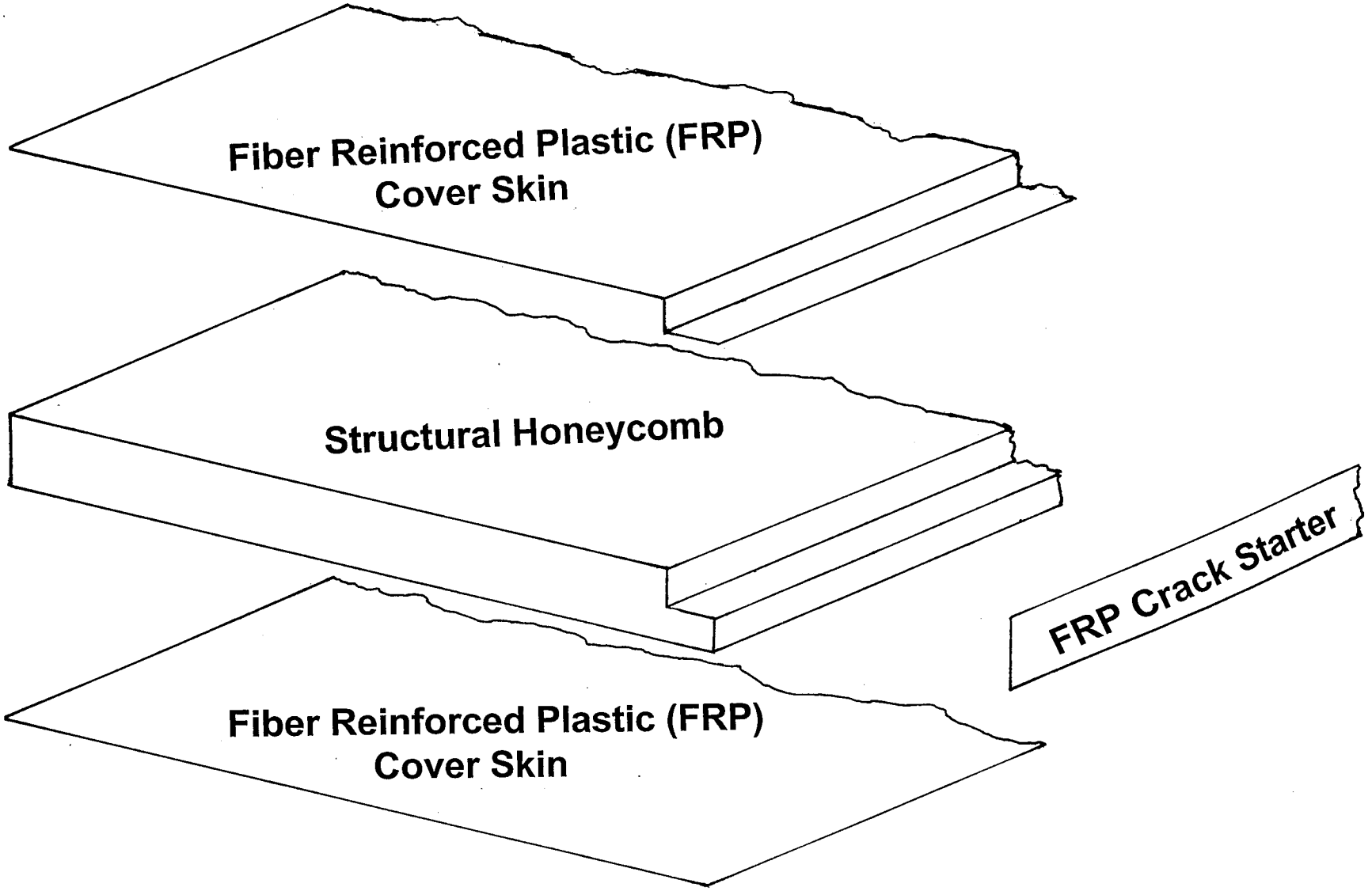

Figure 3-4. Configuration of the Honeycomb Sandwich Beam

Chapter 4

FIELD INSTALLATION

A location on US-36, 4 miles east of Hiawatha, Kansas was selected as the site for the installation of the three FRPC members manufactured from the designs described in the previous chapter. The procedures outlined in this chapter were used to install all three units. Maintenance personnel from the Horton, Kansas sub-area office installed the three units in August and September of 1997. Equipment used for installation consisted of a Bobcat loader equipped with a hydraulically powered pavement milling head, a small tractor mounted backhoe, a dump truck, a vibrating plate compactor, and standard hand tools.

After traffic control was set up, the first step in the installation of the FRPC units was milling a 5 inch deep slot in the pavement about 40 inches wide over the thermal crack. A photograph of the milling operation is shown in Figure 4-1. Because the milling head was small, two passes had to be made to achieve a 5 inch total depth. After completion of the milling, the slot was cleared of millings using the backhoe and shovels. The bottom surface of the milled slot was covered with a thin layer of compacted millings or sand to act as a bedding for the repair and to provide uniform support (Figure 4-2).

After grading and compacting the bedding, the FRPC unit was placed and centered over the thermal crack in the milled slot (Figure 4-3). At this time the

Figure 4-1. Milling a slot in the Pavement

Figure 4-2. Placement of bedding

Figure 4-3. Placement of the FRPC beam.

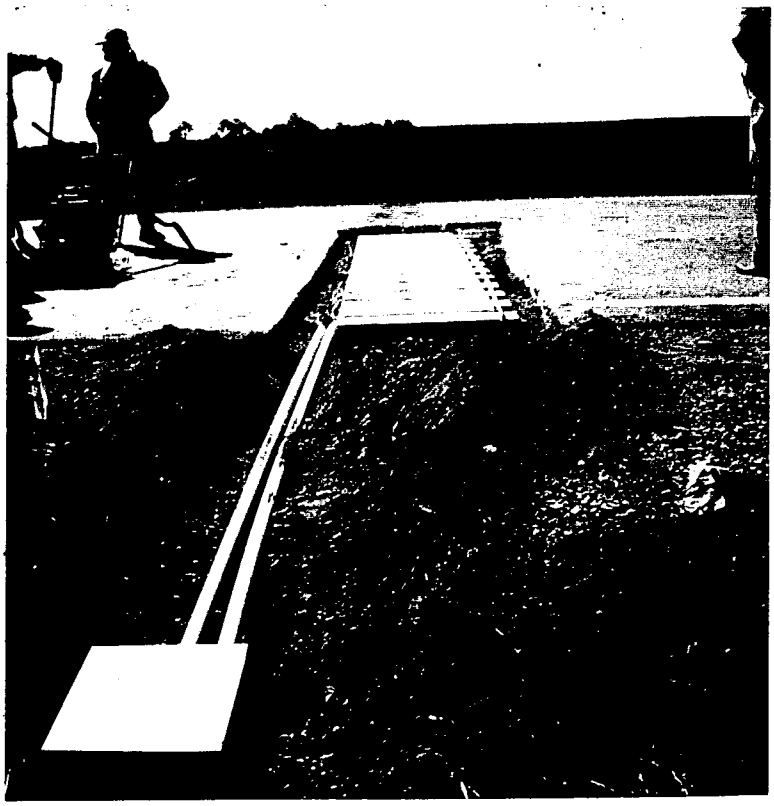

Figure 4-4. Placement of instrumentation cables and access box.

instrumentation cables and access box were laid out and set up (Figure 4-4). Sand, millings or hot mixed asphalt were placed in the space between the pavement and the FRPC unit sides and compacted. This provided a epoxy concrete fill around the unit and produced a bond with the pavement structure on one side of the FRPC unit. The millings or sand were bonded by pouring a low viscosity, quick setting epoxy (PRO-POXY 100) over the surface of the millings or sand and allowing it to penetrate the material and set up (Figure 4-5). A polymer concrete was produced in this way. After the epoxy had set, hot mixed asphalt was dumped on the repair, spread with hand tools, and compacted (Figures 4-6 to 4-8). The asphalt was allowed to cool for about one hour before the area was returned to service (Figure 4-9). Total elapsed time from the start of milling to return to service was three hours.

Figure 4-5. Embedment of FRPC beam.

Figure 4-6. Placement of hot mixed asphalt.

Figure 4-7. Spreading the hot mixed asphalt.

Figure 4-8. Compaction of the asphalt.

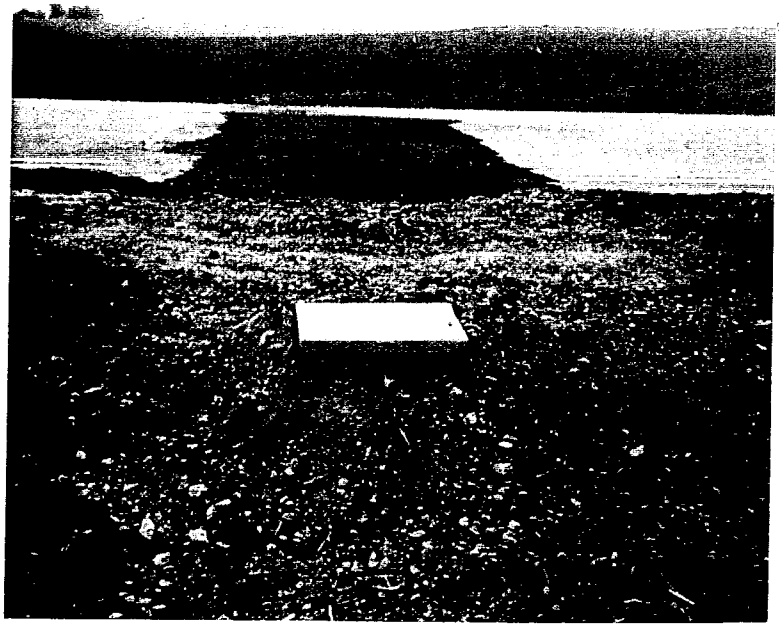

Figure 4-9. The completed repair.

Chapter 5

FIELD PERFORMANCE

The field performance of the FRPC members was evaluated through the use of two methods. The first is the use of the FWD and its ability to measure surface deformation. The FWD imparts an impact load to the pavement structure through the use of a falling weight impacting a loading plate set on the pavement. The FWD measures the deformation basin caused by the impact load. Two series of FWD tests have been performed on the three units since their installation. These tests were conducted on October 9 and November 25, 1997. Each test series consisted of an FWD test on undeteriorated pavement on each side of the repaired crack and one test directly over the center of the repaired crack. The results of these tests are contained in Table V-1.

TABLE V-1 - FWD MEASUREMENTS

Unit	Maximum Deflection (inches)		
	10-9-97	11-25-97	8-24-98
Undeteriorated Pavement	0.006	0.004	0.009
Honeycomb Sandwich #1	0.028	0.025	0.047
Honeycomb Sandwich #2	0.026	0.080	0.047
FRPC Box Beam	0.047	out of service	out of service

A new, full depth bituminous pavement usually has a maximum deflection of about 0.020 inches under a 9,000 pound load. The two honeycomb sandwich beams initially had deflections close to this target value. The box beam unit had more than twice the

desirable deflection on the first test. Analysis of the results of a subsequent static load test revealed that the most probable cause for the greater deflection was buckling in the upper skin of the box beam unit.

Deflection measurements have continued on a periodic basis since emplacement of the FRPC beams. After one year of service both honeycomb sandwich beams had identical deflection measurements and appear to be aging gracefully.

Another field test procedure is the application of static loads to the FRPC beams. This method uses a loaded maintenance dump truck to apply an approximate 18,000 pound axle load to each of the repaired thermal cracks. The load is applied at the leading edge of the FRPC beam, in the center, and at the trailing edge. The time required to apply and record the deformations is approximately one hour for each beam. Two sets of load tests were run. One test was run on August 19, 1997 on only one of the honeycomb sandwich units that had been installed in early August. The second load test was run on all three units on October 2, 1997. Appendix H contains a description of the instrumentation and location of the strain gages on each FRPC beam. Appendix I contains a record of the field observations and a discussion of the field test results is presented in Appendix J.

The strain gages on all three FRPC beams show that the stresses induced by wheel loads are less than 10 percent of the failure stress in tension. The maximum principal stresses on the lower and upper surfaces of each FRPC beam directly over

the thermal crack for an axle load of 24,160 pounds are presented in Table V-2 along with the predicted principal stresses from a finite element analysis (FEA). These results are for the load test run on October 2, 1997.

TABLE V-2 - PRINCIPAL STRESSES

Unit	Upper Surface Principal Stresses Major (psi)	Minor (psi)	Deviator Stress (psi)	Lower Surface Principal Stresses Major (psi)	Minor (psi)	Deviator Stress (psi)
Honeycomb FRPC #1	- 877	- 1671	794	1835	1068	767
Honeycomb FRPC #2	128	- 783	911	1170	478	692
FRPC Box Beam	256	- 1514	1770	1132	- 122	1254
FEA-Design (18K load)	-137	- 955	818	654	- 269	914
FEA-Load Test (12K)	- 90	- 542	632	387	- 200	587

The finite element analyses used as a comparison in the above table were plane strain analysis of a honeycomb sandwich beam using 714 CST elements. The materials properties used in the analysis were average pavement modulus values backcalculated from FWD tests, coupon tests for the FRP materials, laboratory unconfined compression tests on the BM-2 overlay materials, and manufacturer's design literature values for the aluminum honeycomb.

The finite element analysis conducted during the design phase indicated that the FRPC units placed over a two inch deteriorated crack with an 18,000 pound load should theoretically exhibit the maximum stress level shown in Table V-2 under the heading FEA-Design. This analysis was for a two inch wide crack with a softened

zone four inches on either side of the crack. The softened zone was modeled by reducing the pavement modulus to one half the undeteriorated value. The same modulus values were used to model the repair with a 12,080 pound load. The stresses predicted by this analysis are those shown under the heading FEA- Load Test.

The stresses predicted by the two finite element analyses are quite a bit lower than those observed under the load test. One would expect the results of the field load tests to fall in between the results for the 18,000 pound FEA design check and the 12,080 wheel load FEA run instead of being markedly higher than the analysis values. This discrepancy can be explained by noting one fundamental omission in the finite element analysis that would skew the results. That omission is the lack of any modeling of the granular bedding underneath the FRPC units. The bedding was placed during construction to reduce the stress concentration effects of milling irregularities. The bedding consisted of sand and epoxy cemented sand on the first honeycomb sandwich unit, asphalt millings and epoxy cemented asphalt millings on the second honeycomb sandwich unit, and only millings on the box beam unit. The granular backfill was irregular in material consistency and thickness for all three units and would be very difficult to model. The higher stress values observed from the strain gages in the field load test are indicative of a larger soft area being bridged by the units than assumed in the initial analyses.

For each structural unit under field load test, a comparison of the stress values between the upper and lower surfaces shows a difference in the stress levels between

the two surfaces. This is especially apparent in the box beam unit, where there is a 500 psi differential in the deviator stress. The upper surface has a stronger compressive stress when compared to the lower surface. This indicates a much larger deformation in the upper surface, which can be interpreted as a buckled condition.

The two honeycomb units show slightly higher stresses on the lower surface of the structural sandwich than on the upper surface. This differential can be traced to the influence of the overlay on the upper surface of the beam. Honeycomb FRPC #1 shows only a 27 psi differential in the deviator stress between the upper and lower skins but Honeycomb FRPC #2 has a 219 psi differential. The reason for the greater stress differential in one unit than the other can be traced to the bonding of the overlay to the fiberglass skin. On Honeycomb FRPC #1, the overlay was placed without a tack coat of emulsified asphalt, which would result in a poor bond between the asphalt overlay and the fiberglass skin of the structural sandwich. Honeycomb FRPC #2 had a generous tack coat of emulsified asphalt prior to placement of the overlay. This produces a good bond between the overlay and the fiberglass skin, allowing the overlay to carry some of the compressive stress, thereby reducing the stress in the fiberglass skin.

At the time of writing, two of the three FRPC units are still in service. Shortly after the first FWD test on the box beam unit on October 9, 1997, the 1.5 inch overlay over the top of the box beam ravelled and was patched many times over the next two weeks. This ravelling or shedding of the overlay occurred in the wheel paths of the

repaired area and resulted in the destruction of many of the instrumentation cables leading to the strain gages on the box beam unit. The continuous maintenance required to patch the overlay finally resulted in the removal of the box beam unit from service on October 20, 1997. The slot where the unit had been installed was filled with hot mixed bituminous concrete.

The cause of the ravelling on the box beam unit in one wheel path was due in part to excessive deformation in the silicone rubber protective coating applied over the top of the instrumentation cables. Some very minor ravelling due to the same cause has occurred in the overlays on the honeycomb units. However, this was not the cause of ravelling in the other wheel path since there is no silicone rubber in that area. The raveling and shedding of the overlay had to be caused by deflection of the upper surface of the box beam unit. Excessive deflection of the upper surface would cause cracking and debonding of the overlay and would result in the loss of the overlay through raveling. When the prototype box beam sections were load tested, buckling was first observed in the upper surface of the box section under load. Apparently, the polyurethane foam does not provide sufficient support to the upper surface of the box beam to limit deflections below that which would cause debonding of the overlay. This conclusion is supported by strain gage data from the field load test.

The two honeycomb sandwich units are still in service one year after installation and appear to be performing satisfactorily. There has been some settlement of the polymer concrete at the leading edge of the repaired cracks and

some limited raveling of the bituminous overlay in these areas as previously stated. These raveled areas have been repaired with maintenance pothole patch material and appear to be performing well. The access boxes for the strain gage cables were accidentally plowed out by maintenance snowplows in March 1998. The strain gage cables were cut and no additional measurements of surface strains on the honeycomb beams can be made. FWD data will be used as a performance measure for the remainder of the project.

Chapter 6

CONCLUSIONS AND RECOMMENDATIONS FOR IMPLEMENTATION

An investigation has been made into the development of a cost-effective long-term repair of thermal cracks in full depth bituminous pavements. The concept involves bridging the crack with a fiber reinforced plastic composite structural member. This concept is a totally new method of repair that has never been attempted.

Two types of structural members were designed and manufactured as part of the development process, a box beam based unit and two aluminum honeycomb sandwich units. These units met the design goals of bridging a deteriorated thermal crack with minimal deflection under truck loading. The units also met the design goal of being light enough to be handled by two men.

All three units structural members were instrumented with strain gages and installed over thermal cracks on US-36 east of Hiawatha, Kansas using KDOT maintenance personnel. Two sets of static load tests and and two sets of FWD deflection measurements have been conducted to date to measure the load-deformation behavior of the units. The units have also been subjected to continuous highway traffic over the last six months, including over 600 semi-trailer trucks daily. Of the three units, only the box beam unit had to be removed from service. The upper skin on the box beam unit buckled slightly under load and caused raveling of the overlay. The two honeycomb units are still in service and performing adequately.

The major accomplishments of the development process described in this report are as follows:

1) A fiber reinforced plastic composite (FRPC) structural member has been designed and manufactured that will successfully bridge a thermal crack. The structural member has an elastic response to load that is similar to and fully compatible with bituminous pavements. The unit is fully capable of supporting 18,000 pound axle loads and weighs less than 250 pounds. The structural unit is designed for ease of manufacture and the tooling exists in a number of firms in this country to mass produce these units economically.

2) The repair concept developed using the FRPC structural unit is tailor-made for maintenance use. The units can be installed over an existing crack by a five man crew of state, county, city, or township maintenance forces using tools the maintenance organization already owns or can rent locally. The units can be installed, overlaid with asphalt, and the repaired area opened to traffic within three hours.

3) The measured pavement performance of the units in actual service closely models the performance of a new asphalt overlay. A new asphalt overlay usually has a 0.020 inch deflection under a 9000 pound wheel load. Measured deflections for repaired cracks using the honeycomb sandwich units have been in the 0.020 to 0.030 inch range.

4) This process of pavement repair has resulted in a patent application for the FRPC structural units and the repair method which has been filed with the US Department of Commerce Office of Patents and Trademarks. Licensing negotiations are currently in progress with a composites manufacturer to begin commercial production of the FRPC units.

In summary, structural composites have the flexibility to be designed and manufactured to meet any pavement engineering requirement. If a thinner repair component had been necessary, the FRPC units could have been designed with high strength, high modulus fibers and epoxies. Glass fibers and low modulus epoxy were chosen for the designs described in this report because cost was the primary constraint.

The results of this investigation show that fiber reinforced plastic composites have a broader area of application in the transportation industry than simply a retrofit application for highway bridges. Structural composites and composites technology has a place in the relatively "low-tech" field of pavement maintenance and repair. The design methodology and fabrication techniques are now sufficiently developed to permit wide use in the field of civil engineering.

APPENDIX A

LITERATURE REVIEW

A smooth, safe pavement surface is the ultimate goal of all rehabilitative effort. One type of pavement distress that is common in full depth bituminous pavements in Kansas is that of low temperature transverse cracks. These cracks typically form when the temperature at the surface of the pavement drops to the point that the thermal induced tensile stress is greater than the tensile strength of the bituminous binder. A crack is then initiated in the surface of the pavement and propagates down through the pavement to the subgrade over the next several thermal cycles (Roberts, 1991). Wide transverse cracks usually allow the ingress of water into the pavement structure. This results in softening of the subgrade with concomitant loss of support and deterioration of the overlying bituminous concrete by means of stripping. This type of defect can deteriorate into a depression on either side of the crack which can result in considerable ride roughness.

The asphalt industry has developed a number of standard maintenance procedures to treat transverse cracks and preserve the surface and ride (Asphalt Institute, 1988 and ERES, 1982). Narrow cracks less than 1/8 inch wide can be filled with emulsified or cutback asphalt using a squeegee. Cracks wider than 1/4 inch are usually filled with an asphalt emulsion slurry or a mixture of fine sand and a light grade of cutback asphalt. For areas where there is depression of the pavement surface, the depressed areas and voids are filled with hot-mix asphalt and compacted to restore the surface profile.

State transportation departments have elaborated upon the Asphalt Institute recommended practices. Standard Kansas Department of Transportation (KDOT)

practice calls for initial sealing of small thermal cracks less than 3/8 inch wide with a low modulus crack sealant (KDOT, 1989). These cracks, if open and not depressed, are routed or sawed to provide a channel for the sealant. After routing, the crack is cleaned with a heat lance or compressed air to remove debris and the channel is filled with crack sealant.

Shallow cracks that are over 3/8 inch wide are normally filled with MC cutback asphalt, soft grades of asphalt cement with or without fibers, slurry crack pour asphalt, and fine graded cold or hot mix asphalt. Department policy states that deep cracks should be filled with aggregate to within 1/2 inch of the surface prior to filling the crack with asphalt. Any shallow depressions associated with thermal cracks are usually filled with a standard sand seal or emulsion based slurry.

Deep depressions in the pavement surface can be filled with slurry leveling mixes, cold mix, or hot mixed asphalt concrete. All cracks associated with the depression are sealed prior to placing the leveling course.

All of the above methods are aimed at sealing the surface to prevent the ingress of moisture and leveling the surface to provide an adequate ride. The maintenance treatments outlined above for deep depressions usually do not last more than a year or two due to the underlying deterioration. Therefore, the long term repair of badly deteriorated thermal cracks on full depth asphalt pavements is not normally undertaken by maintenance forces. The reason for this is that repairs of this type normally require equipment and time that is not readily available at the area or sub area maintenance level. Repair of badly deteriorated thermal cracks on KDOT facilities is normally done by contract maintenance.

Contract maintenance has allowed the development of many specialized techniques for the repair and treatment of transverse thermal cracks. Many of these

techniques require the use of specialized equipment that is not possessed by maintenance organizations. Methods of repair which have been attempted include the use of stress absorbing surface courses and interlayers, reinforcement of pavements and reinforcement interlayers, and crack arresters (Roberts, 1991).

Some of the earliest work which attempted to control cracking involved the use of steel mesh as a reinforcement for thermal stresses, much as it is used in Portland cement concrete. One attempt at wire reinforcement was a laboratory study by Tons and Krokosky (Tons, 1960) at MIT followed by field studies in Massachusetts . Similar studies were also undertaken in Ontario (Brownridge, 1964) and in California (Zube, 1956). These three studies showed that continuous welded wire reinforcement could reduce transverse cracking due to thermal effects. However, placement and control of the wire mesh was difficult under construction conditions and other studies indicate that the results of wire mesh reinforcement are unreliable (Button, 1983). Expanded wire mesh was used as a reinforcement by Vicelja in his studies but was abandoned because it did not reduce cracking and had a high cost (Vicelja, 1964).

Polymer grid reinforcement, a modern-day cousin of the welded wire grid reinforcement, has had some use in the last ten years (Brown, 1985). However, the results are not yet clear as to the benefits of this method of reinforcement and polymer grids do suffer from a fairly high installation cost at present which limits their use.

Bond breakers and interlayers intended to reduce and absorb stress are another method to attempt to control reflection cracking and thermal cracks. Vicelja thought bond breakers or other types of interlayers would work better than reinforcement (Vicelja, 1964). Materials which have been used as bond breakers are stone dust, metal films, paper, and plastic films. Bond breakers are rarely now because of

multiple cracking in the overlay, slippage, and construction problems associated with their use (Roberts, 1991).

Stress Absorbing Membrane Interlayers (SAMI) have succeeded bond breakers as a stress relief mechanism. Typical materials which are used as a SAMI include asphalt rubber, low viscosity asphalt cement, and rubberized chip seals (Sherman, 1982). The SAMI can be a very successful method for the reduction of thermal and reflection cracks (Kari, 1980 and Molenaar, 1986). However, field trials have yielded mixed results and at least in KDOT's experience, they have not proven to be worth their cost (Maag, 1995). The SAMI is difficult to design in a rational sense since there is no standard laboratory test that yields a mechanical parameter that can be used in a fracture analysis to determine the effective life of the treatment (Roberts, 1991).

Tensile reinforcement in the form of fiber or polymer additives to asphalt concrete have also been tried (Caltabiano, 1990). An early study at Clemson focused on the properties of oriented and random glass fiber reinforcement (Busching, 1968). This study showed that fiber reinforcement might be a practical way to add tensile strength to asphalt concrete. Mineral fibers such as asbestos and polymer fibers have been used to provide tensile reinforcement of asphalt concrete and seem to have worked fairly well. However, the use of mineral fibers like asbestos have been discontinued due to environmental concerns (Roberts, 1991). The KDOT has evaluated fiberglass reinforcement on test sections on US-54 in Kingman County (Parcells, 1990). This study reported that no apparent benefit was achieved in the reduction of reflection cracking by the use of fiberglass interlayers.

Polymer modified asphalts have been used extensively in recent years to control reflection and thermal cracking (Caltabiano, 1990). Rubber modified binders

have been used in Kansas with varying success (Fager, 1994). The most effective and expensive method is the wet process asphalt rubber with gap-graded mixes. This system has delayed the onset of reflective cracking by three years in KDOT First District usage. Dry or microfine additive rubber has not been quite as effective in First District usage. All in all, rubber modified binders have not yet proven to be cost effective as a crack control methodology. Several projects have been let in 1995 with the new SHRP binder specifications as an alternate. In Kansas, this would probably result in a polymer modified binder. The SHRP binders have not been selected by contractors due to the cost and relative scarcity of the product.

Fabrics have been tried extensively to reduce cracking in asphalt concrete with mixed success (Roberts, 1991). They are attractive because of their cost, availability, and ease of use when compared to some other treatments (Caltabiano,1990). Theoretically, fabric reinforcement can provide considerable benefit in reducing tensile stresses in overlays (Yandell, 1983). This has been borne out for areas with mild climates. However, in areas with wide seasonal temperature ranges fabrics have not been as effective, especially in controlling thermal cracks (Sherman, 1982). Another problem with the use of fabrics is that it is difficult to obtain physical measurements that can be used to model the effect that fabrics have on an actual pavement system (Roberts, 1991). One of the few devices that seems to simulate the effect of horizontal movement of underlying layers on the fabric-overlay system is the Texas Transportation Institute (TTI) overlay tester (Button, 1983). The main drawback of the TTI device is that the stress conditions do not directly relate to a standard fracture mechanics test. This makes the results difficult to use in a mechanistic analysis.

The KDOT experience with fabric treatments has not been promising. On the projects where fabrics have been used the benefit observed in reduced maintenance of reflection cracks has not offset the increased cost of the fabric and its installation (Maag, 1983).

APPENDIX B

DESIGN OF A LAMINATED COMPOSITE BEAM USING CHAMIS'S PROCEDURE

The structural component to be designed using this procedure is a simply supported box beam shown in schematic form in Figure B-1. The beam is designed for a static load of 4500 pounds at the midpoint. The factor of safety for the design is 2.0. The composite system to be used is glass fibers (E-glass) in an epoxy matrix with a fiber volume ratio of 0.6.

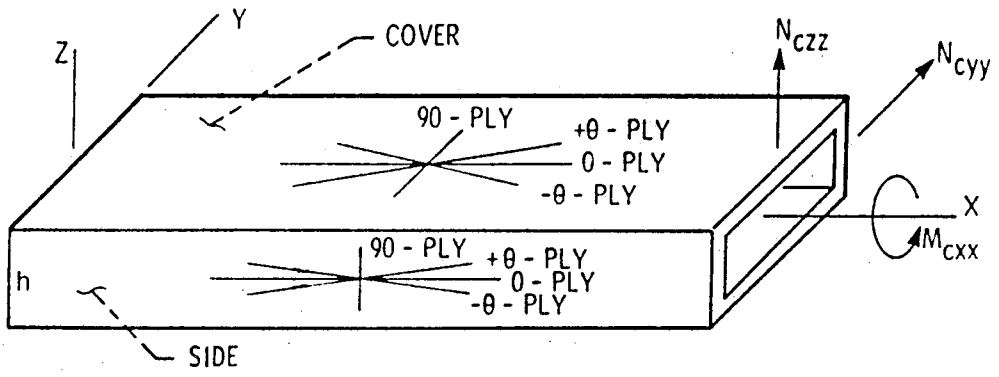

Figure B-1. Schematic of Box Beam (Chamis, 1985)

The design procedure requirements are that the box beam not exceed displacement limits of 0.020 inches when supported by an elastic foundation. The resulting laminate will not exceed the ply-fiber controlled strength at the design load or the ply matrix controlled strength at the specified loads. The composite panels in the beam will not exceed the load limits for combined stress buckling.

The design load for the beam is P_z = 4500 lbs, applied at the beam midpoint and the factored design load is $2P_z$ = 9000 lbs.

The assumed materials properties for design are:

TABLE B-1

$E_1 = 7.48 \times 10^6$ psi	S_{11t} = 160 ksi
$E_2 = 3.06 \times 10^6$ psi	S_{11C} = 78 ksi
$G_{12} = 1.48 \times 10^6$ psi	S_{22t} = 4 ksi
$\nu_{12} = 0.23$	S_{22C} = 20 ksi
$\nu_{21} = 0.09$	

and the ply thickness is assumed to be 0.006 in.

The preliminary design philosophy is to size the box beam covers for only vertical loads and add plys for combined loads such as lateral loads and twist moments. The design variables that must be determined are the number of plys, ply orientation, and the stacking sequence. In order to design the top and bottom covers and the side walls, the membrane loads must be obtained from the factored design load. The in-plane membrane design loads for bending and shear are calculated at the center of the beam by dividing the moment by the depth and width of the box beam section:

covers: $N_{cxx} = 2P_z / hw = 2(4500 \text{ lb})(18 \text{ in.})/(3 \text{ in.})(6 \text{ in.}) = \pm 9000$ lb/in.

$N_{cyy} = N_{cxy} = 0$ (Assume no transverse or shear loads on the covers)

walls : $N_{czx} = 2P_z / 2h_{sidewall} = 2(4500 \text{ lbs})/ 2(3 \text{ in.}) = 1500$ lb/in.

$N_{cyy} = N_{cxx} = 0$ (Assume no bending loads are carried by the side walls)

First, find the number of plys required for the bottom cover:

$$N_{l0} = \frac{N_{cxx}}{S_{l1T}\, t_l} = \frac{9000 \text{ lb/in}}{(160{,}000 \text{ psi})(0.006 \text{ in.})} = 9.3 \cong 10 \text{ plys}$$

$N_{l\pm45}$ = 2 plys (use this value for laminate integrity and buckling resistance)

N_{l90} = 2 plys (use this value for laminate integrity and buckling resistance)

Next, find the number of plys required for the top cover:

$$N_{l0} = \frac{N_{cxx}}{S_{l1C}\, t_l} = \frac{-9000 \text{ lb/in}}{(-78{,}000 \text{ psi})(0.006 \text{ in.})} = 19.2 \cong 20 \text{ plys}$$

$N_{l\pm45}$ = 2 plys (use this value for laminate integrity and buckling resistance)

N_{l90} = 2 plys (use this value for laminate integrity and buckling resistance)

Now determine the number of plys required for the side walls:

Because only shear loads act on the side walls, set $N_{l0} = 2$ and $N_{l90} = 2$ for laminate integrity. So

$$N_{l\pm45} = \frac{N_{cxy}\,(1/2)(E_{l11}/G_{\theta12})}{S_{l1C}\, t_l} = \frac{1500(1/2)(7.48 \times 10^6 \text{ psi} / 1.48 \times 10^6 \text{ psi})}{(79{,}000 \text{ psi})(0.006 \text{ in.})}$$

$N_{l\pm45} = 7.99 \cong 8$ plys

Because only shear loads act on the side walls, set $N_{l0} = 2$ and $N_{l90} = 2$ for laminate integrity.

The required laminate configuration is $N_{l0} = 20$ plys, $N_{l\pm45} = 8$ plys, and $N_{l90} =$ 2 plys or it may be written as $[\pm45_2/0_{10}/90]_s$. The laminate is thin, so buckling will

control. The total laminate thickness is t_l = (No. of plys)(ply thickness) = 30(0.006) = 0.18 in. In order to determine the resistance to buckling, the composite stresses must be determined. These are calculated by dividing the in-plane load by the laminate thickness.

The composite stresses are:

$$\sigma_{cxx} = N_{cxx} / t_l = 9000 \text{ lb/in} / 0.18 \text{ in} = 50{,}000 \text{ psi}$$

$$\sigma_{cxy} = 0$$

$$\sigma_{cxz} = N_{cxz} / t_l = 1500 \text{ lb/in} / 0.18 \text{ in} = 8{,}300 \text{ psi}$$

Next, the buckling stresses must be determined. In order to determine the buckling stresses, the elastic moduli for the laminate must be determined. The first step is to calculate the composite moduli using the ply volume fractions. The ply volume fractions are:

$$V_{P\theta} = 8/30 = 0.27$$

$$V_{P0} = 20/30 = 0.67$$

$$V_{P90} = 20/30 = 0.67$$

and the moduli and Poisson's ratios for each lamina are as listed in Table B-1. The ply stiffnesses are computed using the following equations:

$$Q_{11} = \frac{E_1}{1 - \nu_{12}\nu_{21}} = \frac{7.48 \times 10^6 \text{ psi}}{1 - (0.23)(0.09)} = 7.6 \times 10^6 \text{ psi}$$

$$Q_{12} = \frac{\nu_{12} E_2}{1 - \nu_{12} \nu_{21}} = \frac{(0.23)\ 3.06 \times 10^6 \text{ psi}}{1 - (0.23)(0.09)} = 0.72 \times 10^6 \text{ psi}$$

$$Q_{22} = \frac{E_2}{1 - \nu_{12} \nu_{21}} = \frac{(0.23)\ 7.48 \times 10^6 \text{ psi}}{1 - (0.23)(0.09)} = 3.12 \times 10^6 \text{ psi}$$

$$Q_{66} = G_{12} = 1.48 \times 10^6 \text{ psi}$$

Next, the stiffness for the angle plys must be determined using the following equations. For this design, the angle plys are oriented at $\theta = \pm 45$ degrees to the axis of the box beam. The stiffnesses have the values:

$$Q_{\theta 11} = Q_{11} \cos^4 45 + 2(Q_{12} + 2Q_{66}) \sin^2 45 \cos^2 45 + Q_{22} \sin^4 45$$

$$Q_{\theta 11} = 7.6 \times 10^6 (0.25) + 2(0.72 \times 10^6 + 2(1.48 \times 10^6))(0.5)(0.5) + 3.12 \times 10^6 (0.25)$$

$$Q_{\theta 11} = 4.5 \times 10^6 \text{ psi.}$$

$$Q_{\theta 12} = (Q_{11} + Q_{22} - 4Q_{66}) \sin^2 45 \cos^2 45 + Q_{12} (\sin^4 45 + \cos^4 45)$$

$$Q_{\theta 12} = (7.6 \times 10^6 + 3.12 \times 10^6 - 4(1.48 \times 10^6))(0.5)(0.5) + 0.72 \times 10^6 (0.25 + 0.25)$$

$$Q_{\theta 12} = 1.56 \times 10^6 \text{ psi.}$$

$$Q_{\theta 22} = Q_{11} \sin^4 45 + 2(Q_{12} + 2Q_{66}) \sin^2 45 \cos^2 45 + Q_{22} \cos^4 45$$

$$Q_{\theta 22} = (7.6 \times 10^6)(0.25) + 2(0.72 \times 10^6 + 2(1.48 \times 10^6))(0.5)(0.5) + (3.12 \times 10^6)(0.25)$$

$$Q_{\theta 22} = 4.5 \times 10^6 \text{ psi.}$$

$$Q_{\theta 66} = (Q_{11} + Q_{22} - 2Q_{12} - 2Q_{66}) \sin^2 45 \cos^2 45 + Q_{66} (\sin^4 45 + \cos^4 45)$$

$$Q_{\theta 66} = (7.6 \times 10^6 + 3.12 \times 10^6 - 2(0.72 \times 10^6) - 2(1.48 \times 10^6))(0.5)(0.5) + 1.48 \times 10^6 (0.25 + 0.25)$$

$$Q_{\theta 66} = 2.32 \times 10^6 \text{ psi.}$$

The reduced stiffnesses for the plys oriented at 0, 45, and 90 are summarized in Table B-2.

TABLE B-2

$\theta = 0°$	$\theta = \pm 45°$	$\theta = 90°$
$Q_{l11} = 7.6 \times 10^6$ psi	$Q_{\theta 11} = 4.5 \times 10^6$ psi	$Q_{l11} = 3.12 \times 10^6$ psi
$Q_{l22} = 3.12 \times 10^6$ psi	$Q_{\theta 22} = 4.5 \times 10^6$ psi	$Q_{l22} = 7.6 \times 10^6$ psi
$Q_{l12} = 0.72 \times 10^6$ psi	$Q_{\theta 12} = 1.56 \times 10^6$ psi	$Q_{l21} = 0.72 \times 10^6$ psi
$Q_{l66} = 1.48 \times 10^6$ psi	$Q_{\theta 66} = 2.32 \times 10^6$ psi	$Q_{l66} = 1.48 \times 10^6$ psi

Now that the reduced stiffnesses for the angle plys have been calculated, the reduced laminate stiffness coefficients can be determined. These are calculated using the following equations:

$$Q_{cxx} = V_{P\theta} Q_{\theta 11} + V_{P0} Q_{l11} + V_{P90} Q_{l22}$$

$$= (0.27)(4.5 \times 10^6) + (0.67)(7.6 \times 10^6) + (0.67)(7.6 \times 10^6)$$

$$Q_{cxx} = 6.8 \times 10^6 \text{ psi.}$$

$$Q_{cyy} = V_{P\theta} Q_{\theta 22} + V_{P0} Q_{l22} + V_{P90} Q_{l11}$$

$$Q_{cyy} = (0.27)(4.5 \times 10^6) + (0.67)(3.12 \times 10^6) + (0.67)(3.12 \times 10^6)$$

$$Q_{cyy} = 3.5 \times 10^6 \text{ psi.}$$

$$Q_{cxy} = V_{P\theta} Q_{\theta 12} + V_{P0} Q_{l12} + V_{P90} Q_{l21}$$

$$Q_{cxy} = (0.27)(1.56 \times 10^6) + (0.67)(0.72 \times 10^6) + (0.67)(0.72 \times 10^6)$$

$Q_{cxy} = 1.7 \times 10^6$ psi.

$G_{cxy} = V_{P\theta}Q_{\theta 66} + V_{P0}Q_{I66} + V_{P90}Q_{I66}$

$G_{cxy} = (0.27)(2.32 \times 10^6) + (0.67)(1.48 \times 10^6) + (0.67)(1.48 \times 10^6)$

$G_{cxy} = 1.7 \times 10^6$ psi.

Once the reduced laminate stiffnesses have been determined, the laminate elastic coefficients can be calculated using the following formulas:

$E_{cxx} = Q_{cxx} - Q^2_{cxy} / Q_{cxy}$

$E_{cxx} = 6.8 \times 10^6 - (1.7 \times 10^6)^2 / 3.5 \times 10^6$

$E_{cxx} = 5.9 \times 10^6$ psi.

$E_{cyy} = Q_{cyy} - Q^2_{cxy} / Q_{cxx}$

$E_{cyy} = 3.5 \times 10^6 - (1.7 \times 10^6)^2 / 6.8 \times 10^6$

$E_{cyy} = 3.1 \times 10^6$ psi.

$\nu_{cxy} = Q_{cxy} / Q_{cxy}$

$\nu_{cxy} = 1.7 \times 10^6 / 3.5 \times 10^6$

$\nu_{cxy} = 0.49$

$G_{cxy} = 1.7 \times 10^6$ psi

$\nu_{cyx} = \nu_{cxy} (E_{cyy} / E_{cxx})$

$\nu_{cyx} = (3.1 \times 10^6 / 5.9 \times 10^6)$

$\nu_{cyx} = 0.25$

Now the averaged elastic modulus for the entire laminate can be calculated. This value is determined using the following equation:

$$E = \sqrt[3]{4E_{cxx}\, E_{cyy}\, G_{cxy}}$$

$$E = \sqrt[3]{4\,(5.0 \times 10^6)(\,5.0 \times 10^6)(\,5.0 \times 10^6)}$$

$$E = 5.0 \times 10^6 \text{ psi.}$$

After determining the preceding values, buckling in the top cover can be checked. For this case $\sigma_{cxx} = 25{,}000$ psi, and $\sigma_{cxy} = 0$.

The following equation must be satisfied if bucking is to be avoided:

$$\frac{\sigma_{cxx}}{\sigma_{cxx}^{CR}} + \left[\frac{\sigma_{cxy}}{\sigma_{cxy}^{CR}}\right]^2 \leq 1 .$$

Calculate the critical buckling stress, σ_{cxx}^{CR}:

$$\sigma_{cxx}^{CR} = \frac{\pi^2\, t_c^{\,2}\, E}{12\, b^2\, (1 - \nu_{cxy}\, \nu_{cyx})} \left[\frac{a}{b} + \frac{b}{a}\right]^2$$

$$\sigma_{cxx}^{CR} = \frac{\pi^2\, (0.18)^2\, (5.0 \times 10^6)}{12\, (6)^2\, (1 - \nu_{cxy}\, \nu_{cyx})} \left[\frac{36}{6} + \frac{6}{36}\right]^2$$

$$\sigma_{cxx}^{CR} = (4{,}218)(38)$$

$$\sigma_{cxx}^{CR} = 160{,}000 \text{ psi}$$

$$\frac{\sigma_{cxx}}{\sigma_{cxx}^{CR}} + \left[\frac{\sigma_{cxy}}{\sigma_{cxx}^{CR}}\right]^2 = \frac{25{,}000}{160{,}000} + 0 = 0.16 \leq 1 \quad \therefore \text{ top cover buckling is OK.}$$

Check buckling on the sidewalls:

For this case $\sigma_{cxx} = 0$, and $\sigma_{cxy} = 8{,}300$ psi, and the same procedure is used.

$$\frac{\sigma_{cxx}}{\sigma_{cxx}^{CR}} + \left[\frac{\sigma_{cxy}}{\sigma_{cxy}^{CR}}\right]^2 \leq 1$$

Calculate the critical buckling stress for the side walls:

$$\sigma_{cxy}^{CR} = \frac{\pi^2 \, t_c^2 \, E}{12 \, b^2 \, (1 - \nu_{cxy} \, \nu_{cyx})} \left[\frac{a}{b} + \frac{b}{a}\right]^2$$

$$\sigma_{cxy}^{CR} = \frac{\pi^2 \, (0.18)^2 \, (5.0 \times 10^6)}{12 \, b^2 \, (1 - \nu_{cxy} \, \nu_{cyx})} \left[\frac{36}{3} + \frac{3}{36}\right]^2$$

$$\sigma_{cxy}^{CR} = (16{,}871)(12.08)^2$$

$$\sigma_{cxy}^{CR} = 2.5 \times 10^6$$

$$\frac{\sigma_{cxx}}{\sigma_{cxx}^{CR}} + \left[\frac{\sigma_{cxy}}{\sigma_{cxy}^{CR}}\right]^2 = 0 + \left[\frac{8.3 \times 10^3}{2.5 \times 10^6}\right]^2 = 0.003 \leq 1 \quad \therefore \text{ side wall buckling is OK.}$$

While the results from Chamis' procedure appear good, an independent check was desired. This check was done by using stiffness values contained in the A, B, and

D matrices calculated using the FORTRAN program CSTRESS and the buckling formulas presented in Mechanics of Composite Materials (Jones, 1975). The equation to calculate the compressive buckling load, N_x is:

$$\bar{N}_x = \pi^2 D_{11}\left(\frac{m}{a}\right)^2 + 2(D_{12} + D_{66}) \frac{1}{b^2} + D_{22} \frac{1}{b^4} \left(\frac{a}{m}\right)^2$$

where D_{11}, D_{12}, D_{22}, and D_{66} are the bending stiffnesses from CSTRESS, a is the length of the plate, b is the width of the plate, and m is the mode number. The bending stiffnesses are tabulated in Table B-3 and the critical loads in Table B-4. The results in Table B-4 confirm the adequacy of the buckling predictions using Chamis's method.

TABLE B-3 - Bending Stiffnesses

[D]:

0.16179E+05	0.33186E+04	0.46430E+02
0.33186E+04	0.15986E+05	0.46430E+02
0.46430E+02	0.46430E+02	0.56927E+04

TABLE B-4 - Buckling Loads for a Given Plate Size

Plate Size	Mode, m	N_x (pounds/in.)
a = 3 in., b = 3 in.	1	67,522
a = 36 in., b = 6 in.	6	16,880
a = 3 in., b = 36 in.	1	17,967

APPENDIX C

CSTRESS - A FORTRAN PROGRAM FOR CALCULATING STIFFNESS, STRESS, AND FAILURE IN A LAMINATED COMPOSITE PLATE

```
C
C  PROGRAM CSTRESS-A LAMINATED COMPOSITE PLATE STIFFNESS,
C  STRESS, AND FAILURE PROGRAM WRITTEN IN FORTRAN BY JEFFREY
C  FRANTZEN, DECEMBER 1995. THE PROGRAM OUTPUT FORMAT WAS
C  MODELED AFTER A SIMILAR PROGRAM WRITTEN BY DR J. LOCKE OF
C  THE DEPARTMENT OF AEROSPACE ENGINEERING AT THE UNIV.
C  OF KANSAS. THE MECHANICS OF THE PROGRAM ARE BASED
C  ON PRINCIPLES AND TECHNIQUES CONTAINED IN "MECHANICS OF
C  COMPOSITE MATERIALS" BY ROBERT M. JONES. THIS PROGRAMWAS
C  WRITTEN TO PERFORM COMPUTATIONS FOR PHD RESEARCH INTO
C  COMPOSITE BEAMS IN PAVEMENT STRUCTURES.
C
      CHARACTER*12 STIME,ETIME
      INTEGER I,J
      REAL NU12,NT,MT,KAPPA,MX,MY,MXY,NTX,NTY,NTXY,MTX,MTY,
     MTXY
      DIMENSION QB(3,3),A(3,3),B(3,3),D(3,3),Z(99),T(99)
      DIMENSION AS(3,3),X(3,3),BS(3,3),DUM(3,3),DS(3,3)
      DIMENSION THTA(99),E1(99),E2(99),G12(99),NU12(99),HS(3,3)
      DIMENSION AP(3,3),BP(3,3),HP(3,3),DP(3,3),DUMM(3,3)
      DIMENSION ALFA(3,99),NT(3),MT(3),TM(3,3),SOT(3),SOB(3)
      DIMENSION EPS(3),KAPPA(3),ST(3,99),SB(3,99),ET(3)
      DIMENSION EPSLT(3),EPSLB(3)
C
C     INITIALIZE MATRICES AND VARIABLES
C
      CALL TIME(STIME)
      DO 5 I=1,99
      DO 6 J=1,3
      ST(J,I)=0.0
    6 SB(J,I)=0.0
    5 CONTINUE
      DO 10 I=1,3
      DO 10 J=1,3
      QB(I,J)=0
      A(I,J)=0
      B(I,J)=0
   10 D(I,J)=0
      DO 9 J=1,3
      NT(J)=0.0
      MT(J)=0.0
      EPS(J)=0.0
    9 KAPPA(J)=0.0
```

```
C
C    READ IN THE LAMINATE DATA
C
     TOTT=0.0
     READ(5,999)NLAYER
     READ(5,997)FX,FY,FXY
     READ(5,997)MX,MY,MXY
     READ(5,998)TEMP
     DO 20 I=1,NLAYER
     READ(5,1000)T(I),THTA(I),E1(I),E2(I),G12(I),NU12(I),ALFA(1,I),
    1ALFA(2,I)
     ALFA(3,I)=0.0
  20 TOTT=TOTT+T(I)
     READ(5,1002)XT,XC,YT,YC,S
C
C    ECHO THE INPUT DATA
C
     WRITE(6,2016)
     WRITE(6,2017)
     WRITE(6,2016)
     WRITE(6,2001)
     WRITE(6,2013)FX,FY,FXY
     WRITE(6,2001)
     WRITE(6,2014)MX,MY,MXY
     WRITE(6,2001)
     WRITE(6,2015)TEMP
     WRITE(6,2001)
     WRITE(6,2012)
     WRITE(6,2009)
     DO 21 N=1,NLAYER
  21 WRITE(6,2019)N,T(N),THTA(N)
     WRITE(6,2001)
     WRITE(6,2010)
     WRITE(6,2011)
     DO 30 I=1,NLAYER
  30 WRITE(6,2026)I,E1(I),E2(I),G12(I),NU12(I),ALFA(1,I),ALFA(2,I)
     Z(1)=-TOTT/2
C
C    THIS SECTION CALCULATES THE Z VALUES FOR EACH LAYER
C    STARTING WITH Z(1) WHICH IS EQUAL TO A NEGATIVE ONE-HALF
C    OF THE TOTAL LAMINATE THICKNESS. THE LAMINATE PROPERTIES
C    ARE THEN CALCULATED FROM THE TOP DOWN TO THE BOTTOM
C   OF THE LAMINATE.
C
     DO 40 I=1,NLAYER
     ZA=Z(I)
     Z(I+1)=Z(I)+T(I)
     ZB=Z(I+1)
     THETA=THTA(I)
C
C    COMPUTE THE ORTHOTROPIC STIFFNESSES FOR EACH LAYER
```

```
C    ONE LAYER AT A TIME
C
     CALL ALST(THETA,NU12,E1,E2,G12,QB)
  40 CALL STMAT(QB,ZA,ZB,A,B,D)
     WRITE(6,2001)
     WRITE(6,2027)
     WRITE(6,2001)
     WRITE(6,2028)
     WRITE(6,2029)XT,XC,YT,YC,S
C
C    WRITE HEADERS AND PRINT THE A, B, AND, D MATRICES
C
     WRITE(6,2001)
     WRITE(6,2016)
     WRITE(6,2018)
     WRITE(6,2016)
     WRITE(6,2001)
     WRITE(6,2020)
     WRITE(6,2001)
     WRITE(6,2002)
     WRITE(6,2000)((A(I,J),I=1,3),J=1,3)
     WRITE(6,2001)
     WRITE(6,2003)
     WRITE(6,2000)((B(I,J),I=1,3),J=1,3)
     WRITE(6,2001)
     WRITE(6,2004)
     WRITE(6,2000)((D(I,J),I=1,3),J=1,3)
C
C    INVERT THE STIFFNESS MATRICES USING JONES' METHOD
C    TO GET THE A', B', D' AND H' MATRICES TO SOLVE FOR
C    THE MIDLAYER STRAINS AND CURVATURES
C
     J=1
     DO 50 I=1,3
  50 X(I,J)=0.0
     DO 51 I=1,3
     DO 52 J=1,3
  52 AS(I,J)=A(I,J)
  51 CONTINUE
C
C    CALCULATE A-STAR
C
     CALL GAUSSJ(AS,3,3,X,1,1)
     CN=-1.0
C
C    CALCULATE B-STAR
C
     CALL CNMULT(CN,AS,DUM)
     CALL MTMULT(DUM,B,BS)
C
C    CALCULATE H-STAR
```

```
C
      CALL MTMULT(B,AS,HS)
C
C     CALCULATE D-STAR
C
      CALL MTMULT(AS,B,DUM)
      CALL MTMULT(B,DUM,DUMM)
      CALL MATSUB(D,DUMM,DS)
C
C     CALCULATE D-PRIME
C
      DO 60 I=1,3
      DO 61 J=1,3
   61 DP(I,J)=DS(I,J)
   60 CONTINUE
      CALL GAUSSJ(DP,3,3,X,1,1)
C
C     CALCULATE B-PRIME
C
      CALL MTMULT(BS,DP,BP)
C
C     CALCULATE H-PRIME
C
      CALL CNMULT(CN,DP,DUMM)
      CALL MTMULT(DUMM,HS,HP)
C
C     CALCULATE A-PRIME
C
      CALL MTMULT(DP,HS,DUM)
      CALL MTMULT(BS,DUM,DUMM)
      CALL MATSUB(AS,DUMM,AP)
C
C     CALCULATE THE THERMAL FORCES AND MOMENTS FOR THE
C     ENTIRE LAMINATE
C     BY ADDING ONE LAYER AT A TIME
C
      ZT=-TOTT/2.0
      DO 70 I=1,NLAYER
      ZB=ZT+T(I)
      THETA=THTA(I)
C
C     CONVERT PRINCIPAL THERMAL COEFFICIENTS TO X, Y, AND XY
C     FORM USING
C     THE T MATRIX TRANSPOSE FOR EACH LAMINAE
C
      TETAD=(6.283185*THTA(I))/360.0
      CT=COS(TETAD)
      SNT=SIN(TETAD)
      CT2=CT*CT
      ST2=SNT*SNT
      SCT=SNT*CT
```

```
      AX=CT2*ALFA(1,I)+ST2*ALFA(2,I)
      AY=ST2*ALFA(1,I)+CT2*ALFA(2,I)
      AXY=SCT*(ALFA(1,I)-ALFA(2,I))
C     WRITE(6,2001)
C     WRITE(6,2000)AX,AY,AXY
C
C     CALCULATE THE THERMAL LOADS BY MULTIPLYING THE
C     LAMINAE THERMAL
C     X-Y STRESSES BY THE LAMINAE THICKNESS AND THE
C     Q-BAR MATRIX
C
      CALL ALST(THETA,NU12,E1,E2,G12,QB)
C     WRITE(6,2001)
C     WRITE(6,2000)((QB(II,JJ),II=1,3),JJ=1,3)
      NTX=(QB(1,1)*AX+QB(1,2)*AY+QB(1,3)*AXY)*T(I)*TEMP
      NTY=(QB(2,1)*AX+QB(2,2)*AY+QB(2,3)*AXY)*T(I)*TEMP
      NTXY=(QB(3,1)*AX+QB(3,2)*AY+QB(3,3)*AXY)*T(I)*TEMP
C     WRITE(6,2001)
C     WRITE(6,2000)NTX,NTY,NTXY
C
C     SUM THE THERMAL LOADS
C
      NT(1)=NT(1)+NTX
      NT(2)=NT(2)+NTY
      NT(3)=NT(3)+NTXY
C
C     CALCULATE THE THERMAL MOMENTS BY INTEGRATING THE
C     LAMINAE THERMAL STRESSES
C
      ZI=(ZT*ZT-ZB*ZB)/2.0
      MTX=(QB(1,1)*AX+QB(1,2)*AY+QB(1,3)*AXY)*ZI*TEMP
      MTY=(QB(2,1)*AX+QB(2,2)*AY+QB(2,3)*AXY)*ZI*TEMP
      MTXY=(QB(3,1)*AX+QB(3,2)*AY+QB(3,3)*AXY)*ZI*TEMP
      MT(1)=MT(1)+MTX
      MT(2)=MT(2)+MTY
      MT(3)=MT(3)+MTXY
      ZT=ZB
   70 CONTINUE
C
C     COMBINE THE EXTERNAL FORCES AND MOMENTS WITH THE
C     THERMAL FORCES
C
      NT(1)=NT(1)+FX
      NT(2)=NT(2)+FY
      NT(3)=NT(3)+FXY
      MT(1)=MT(1)+MX
      MT(2)=MT(2)+MY
      MT(3)=MT(3)+MXY
C     WRITE(6,2013)NT(1),NT(2),NT(3)
C     WRITE(6,2014)MT(1),MT(2),MT(3)
      WRITE(6,2001)
```

```
C
C    CALCULATE THE LAMINA STRAINS AND CURVATURES DUE TO THE
C    IMPOSED LOADS USING THE A', B', D', AND H' MATRICES
C
     DO 80 J=1,3
     DO 81 K=1,3
     EPS(J)=EPS(J)+AP(J,K)*NT(K)+BP(J,K)*MT(K)
  81 KAPPA(J)=KAPPA(J)+DP(J,K)*MT(K)+HP(J,K)*NT(K)
  80 CONTINUE
C
C    CALCULATE THE LAMINAE STRESSES FROM THE LAMINAE
C    STRAINS
C    MINUS THE THERMAL STRAINS USING THE Q-BAR MATRIX FOR
C    EACH LAYER
C
     DO 90 I=1,NLAYER
     ZA=Z(I)
     Z(I+1)=Z(I)+T(I)
     ZB=Z(I+1)
     THETA=THTA(I)
     CALL ALST(THETA,NU12,E1,E2,G12,QB)
     TETAD=(6.283185*THTA(I))/360.0
     CT=COS(TETAD)
     SNT=SIN(TETAD)
     CT2=CT*CT
     ST2=SNT*SNT
     SCT=SNT*CT
     AX=CT2*ALFA(1,I)+ST2*ALFA(2,I)
     AY=ST2*ALFA(1,I)+CT2*ALFA(2,I)
     AXY=SCT*(ALFA(1,I)-ALFA(2,I))
     ET(1)=AX*TEMP
     ET(2)=AY*TEMP
     ET(3)=AXY*TEMP
     DO 93 J=1,3
     EPSLT(J)=EPS(J)+ZA*KAPPA(J)
     EPSLB(J)=EPS(J)+ZB*KAPPA(J)
  93 CONTINUE
     DO 91 J=1,3
     DO 92 K=1,3
     EPT=EPSLT(K)-ET(K)
     ST(J,I)=ST(J,I)+QB(J,K)*EPT
     EPB=EPSLB(K)-ET(K)
  92 SB(J,I)=SB(J,I)+QB(J,K)*EPB
  91 CONTINUE
  90 CONTINUE
C
C    PRINT OUT THE A', B', D', AND H' MATRICES
C
     WRITE(6,2001)
     WRITE(6,2005)
     WRITE(6,2000)((AP(I,J),I=1,3),J=1,3)
```

```
      WRITE(6,2001)
      WRITE(6,2006)
      WRITE(6,2000)((BP(I,J),I=1,3),J=1,3)
      WRITE(6,2001)
      WRITE(6,2008)
      WRITE(6,2000)((DP(I,J),I=1,3),J=1,3)
      WRITE(6,2001)
      WRITE(6,2007)
      WRITE(6,2000)((HP(I,J),I=1,3),J=1,3)
      WRITE(6,2001)
C
C     PRINT OUT THE MIDDLE SURFACE STRAINS AND CURVATURES
C
      WRITE(6,2021)(EPS(I),I=1,3)
      WRITE(6,2001)
      WRITE(6,2022)(KAPPA(I),I=1,3)
      WRITE(6,2001)
      WRITE(6,2001)
      WRITE(6,2023)
      WRITE(6,2001)
      WRITE(6,2024)
C
C     PRINT OUT THE LAMINAE STRESSES AT THE TOP AND BOTTOM OF
C     EACH LAYER FOR EACH LAMINAE
C
      DO 100 NL=1,NLAYER
      WRITE(6,2025)NL,Z(NL),(ST(J,NL),J=1,3)
      WRITE(6,2025)NL,Z(NL+1),(SB(J,NL),J=1,3)
  100 WRITE(6,2001)
C
C     CHECK THE LAYER STRESSES FOR FAILURE USING THE TSAI-HILL
C     FAILURE CRITERION
C
      DO 110 I=1,NLAYER
      TETAD=(6.283185*THTA(I))/360.0
      CT=COS(TETAD)
      SNT=SIN(TETAD)
      CT2=CT*CT
      ST2=SNT*SNT
      SCT=SNT*CT
      TM(1,1)=CT2
      TM(1,2)=ST2
      TM(1,3)=2.0*SCT
      TM(2,1)=ST2
      TM(2,2)=CT2
      TM(2,3)=-2.0*SCT
      TM(3,1)=-1*SCT
      TM(3,2)=SCT
      TM(3,3)=CT2-ST2
C     WRITE(6,2001)
C     WRITE(6,2000)((TM(II,JJ),II=1,3),JJ=1,3)
```

```
      DO 111 J=1,3
      SOT(J)=0.0
      SOB(J)=0.0
      DO 112 K=1,3
      SOT(J)=SOT(J)+TM(J,K)*ST(K,I)
  112 SOB(J)=SOB(J)+TM(J,K)*SB(K,I)
  111 CONTINUE
      IF(SOT(1))120,120,121
  120 XFT=XC
      GO TO 122
  121 XFT=XT
  122 IF(SOT(2))123,123,124
  123 YFT=YC
      GO TO 125
  124 YFT=YT
  125 CONTINUE
      FA=(SOT(1)*SOT(1))/(XFT*XFT)
      FB=(SOT(1)*SOT(2))/(XFT*XFT)
      FC=(SOT(2)*SOT(2))/(YFT*YFT)
      FD=(SOT(3)*SOT(3))/(S*S)
      FAIL=FA-FB+FC+FD
C     WRITE(6,2001)
C     WRITE(6,2000)XFT,YFT,S
C     WRITE(6,2000)SOT(1),SOT(2),SOT(3)
C     WRITE(6,2029)FAIL,FA,FB,FC,FD
      IF(FAIL.LT.1)GO TO 115
      WRITE(6,2030)I,FAIL
  115 IF(SOB(1))126,126,127
  126 XFB=XC
      GO TO 128
  127 XFB=XT
  128 IF(SOB(2))129,129,130
  129 YFB=YC
      GO TO 131
  130 YFB=YT
  131 CONTINUE
      FA=(SOB(1)*SOB(1))/(XFB*XFB)
      FB=(SOB(1)*SOB(2))/(XFB*XFB)
      FC=(SOB(2)*SOB(2))/(YFB*YFB)
      FD=(SOB(3)*SOB(3))/(S*S)
      FAIL=FA-FB+FC+FD
      IF(FAIL.GE.1)GO TO 116
      GO TO 117
  116 WRITE(6,2031)I,FAIL
  117 CONTINUE
  110 CONTINUE
      CALL TIME(ETIME)
      WRITE(*,*)'START TIME =',STIME,'END TIME =',ETIME
C
  997 FORMAT(3D10.3)
  998 FORMAT(F10.3)
```

```
 999 FORMAT(I2)
1000 FORMAT(8F10.5)
1001 FORMAT(1X,I2,2X,4F12.2,2D12.2)
1002 FORMAT(5D10.5)
2000 FORMAT(1X,D12.5,5X,D12.5,5X,D12.5)
2001 FORMAT(1H0)
2002 FORMAT(22X,4H[A]:)
2003 FORMAT(22X,4H[B]:)
2004 FORMAT(22X,4H[D]:)
2005 FORMAT(22X,5H[A']:)
2006 FORMAT(22X,5H[B']:)
2007 FORMAT(22X,5H[H']:)
2008 FORMAT(22X,5H[D']:)
2009 FORMAT(1X,5HLAYER,9X,1HT,7X,5HTHETA)
2010 FORMAT(1X,19HMATERIAL PROPERTIES)
2011
FORMAT(1X,5HLAYER,5X,2HE1,11X,2HE2,10X,3HG12,6X,4HNU12,4X,6HALP
HA1
   1,6X,6HALPHA2)
2012 FORMAT(1X,17HLAMINATE GEOMETRY)
2013 FORMAT(1X,8HFORCES: ,1X,D12.5,3x,D12.5,3x,D12.5)
2014 FORMAT(1X,9HMOMENTS: ,1X,D12.5,3x,D12.5,3x,D12.5)
2015 FORMAT(1X,13HTEMPERATURE: ,1X,F12.2)
2016 FORMAT(1X,51H----------------------------------------------------)
2017 FORMAT(15X,18H--- INPUT DATA ---)
2018 FORMAT(15X,19H--- OUTPUT DATA ---)
2019 FORMAT(2X,I2,5X,F8.4,4X,F8.4)
2020 FORMAT(1X,20HLAMINATE STIFFNESSES)
2021 FORMAT(1X,21HMID-SURFACE STRAINS: ,D12.5,2X,D12.5,2X,D12.5)
2022 FORMAT(1X,24HMID-SURFACE CURVATURES:
,D12.5,2X,D12.5,2X,D12.5)
2023 FORMAT(1X,15HLAMINA STRESSES)
2024 FORMAT(1X,5HLAYER,7X,1HZ,10X,2HSX,10X,2HSY,10X,3HSXY)
2025 FORMAT(3X,I2,1X,4D12.5)
2026 FORMAT(1X,I2,2X,3D12.5,3X,F5.3,2D12.5)
2027 FORMAT(1X,16HFAILURE STRESSES)
2028 FORMAT(6X,3HX-T,7X,3HX-C,7X,3HY-T,8X,3HY-C,9X,1HS)
2029 FORMAT(1X,D10.4,1X,D10.4,1X,D10.4,1X,D10.4,1X,D10.4)
2030 FORMAT(1X,24HFAILURE AT TOP OF LAYER ,I2,2X,4HF = ,F10.5)
2031 FORMAT(1X,27HFAILURE AT BOTTOM OF LAYER ,I2,2X,4HF = ,F10.5)
      STOP
      END
C
      SUBROUTINE MTMULT(E,F,EF)
C
C     MATRIX MULTIPLICATION SUBROUTINE
C
      DIMENSION E(3,3),F(3,3),EF(3,3)
      DO 10 I=1,3
      DO 11 J=1,3
      EF(I,J)=0.0
```

```
      DO 12 K=1,3
   12 EF(I,J)=EF(I,J)+E(I,K)*F(K,J)
   11 CONTINUE
   10 CONTINUE
      RETURN
      END
C
      SUBROUTINE MATSUB(S,T,SMT)
C
C     MATRIX SUBTRACTION SUBROUTINE
C
      DIMENSION S(3,3),T(3,3),SMT(3,3)
      DO 10 I=1,3
      DO 11 J=1,3
   11 SMT(I,J)=S(I,J)-T(I,J)
   10 CONTINUE
      RETURN
      END
C
      SUBROUTINE MATADD(P,Q,PPQ)
C
C     MATRIX ADDITION SUBROUTINE
C
      DIMENSION P(3,3),Q(3,3),PPQ(3,3)
      DO 10 I=1,3
      DO 11 J=1,3
   11 PPQ(I,J)=P(I,J)+Q(I,J)
   10 CONTINUE
      RETURN
      END
C
      SUBROUTINE VECTAD(X,Y,XPY)
C
C     VECTOR ADDITION SUBROUTINE
C
      DIMENSION X(3),Y(3),XPY(3)
      DO 10 I=1,3
   10 XPY(I)=X(I)+Y(I)
      RETURN
      END
C
      SUBROUTINE CNMULT(CONST,G,GC)
C
C     MATRIX MULTIPLICATION BY A CONSTANT SUBROUTINE
C
      DIMENSION G(3,3),GC(3,3)
      DO 10 I=1,3
      DO 11 J=1,3
   11 GC(I,J)=CONST*G(I,J)
   10 CONTINUE
      RETURN
```

```
      END
C
      SUBROUTINE ALST(THETA,NU12,E1,E2,G12,QB)
      REAL NU,NU12,NU21
      DIMENSION QB(3,3)
C
C     PROGRAM LAMSTIFF-A LAMINATED COMPOSITE PLATE STIFFNESS,
C     STRESS,  AND FAILURE PROGRAM WRITTEN IN FORTRAN
C     initialize variables
C
      THTAl=(6.283185*THETA)/360
      SN=SIN(THTAl)
      SN2=SN*SN
      SN3=SN*SN2
      SN4=SN*SN3
      CS=COS(THTAl)
      CS2=CS*CS
      CS3=CS*CS2
      CS4=CS*CS3
      SNCS=SN4+CS4
C
C     compute reduced orthotropic stiffnesses
C
      NU21=(E2*NU12)/E1
      NU=(1-NU12*NU21)
      Q11=E1/NU
      Q12=(NU12*E2)/NU
      Q22=E2/NU
      Q66=G12
      QA=2*(Q12+2*Q66)
      QBT=Q11-Q12-2*Q66
      QC=Q12-Q22+2*Q66
C
C     compute transformed reduced stiffnesses Q-bar
C
      QB11=Q11*CS4+QA*SN2*CS2+Q22*SN4
      QB12=(Q11+Q22-4*Q66)*SN2*CS2+Q12*SNCS
      QB22=Q11*SN4+QA*SN2*CS2+Q22*CS4
      QB16=QBT*SN*CS3+QC*SN3*CS
      QB26=QBT*SN3*CS+QC*SN*CS3
      QB66=(Q11+Q22-2*Q12-2*Q66)*SN2*CS2+Q66*SNCS
      QB(1,1)=QB11
      QB(1,2)=QB12
      QB(1,3)=QB16
      QB(2,1)=QB12
      QB(2,2)=QB22
      QB(2,3)=QB26
      QB(3,1)=QB16
      QB(3,2)=QB26
      QB(3,3)=QB66
      RETURN
```

```
      END
C
      SUBROUTINE STMAT(QB,ZA,ZB,A,B,D)
      DIMENSION QB(3,3),A(3,3),B(3,3),D(3,3)
C
C     PROGRAM STIFFMAT-A LAMINATED COMPOSITE PLATE STIFFNESS,
C     STRESS, AND FAILURE PROGRAM WRITTEN IN MATLAB
C     generate extensional, coupling, and bending stiffness matrices
C
      Z1=ZB-ZA
      Z2=(ZB*ZB-ZA*ZA)/2
      Z3=(ZB*ZB*ZB-ZA*ZA*ZA)/3
      A(1,1)=A(1,1)+QB(1,1)*Z1
      B(1,1)=B(1,1)+QB(1,1)*Z2
      D(1,1)=D(1,1)+QB(1,1)*Z3
      A(1,2)=A(1,2)+QB(1,2)*Z1
      B(1,2)=B(1,2)+QB(1,2)*Z2
      D(1,2)=D(1,2)+QB(1,2)*Z3
      A(1,3)=A(1,3)+QB(1,3)*Z1
      B(1,3)=B(1,3)+QB(1,3)*Z2
      D(1,3)=D(1,3)+QB(1,3)*Z3
      A(2,1)=A(1,2)
      B(2,1)=B(1,2)
      D(2,1)=D(1,2)
      A(2,2)=A(2,2)+QB(2,2)*Z1
      B(2,2)=B(2,2)+QB(2,2)*Z2
      D(2,2)=D(2,2)+QB(2,2)*Z3
      A(2,3)=A(2,3)+QB(2,3)*Z1
      B(2,3)=B(2,3)+QB(2,3)*Z2
      D(2,3)=D(2,3)+QB(2,3)*Z3
      A(3,1)=A(1,3)
      B(3,1)=B(1,3)
      D(3,1)=D(1,3)
      A(3,2)=A(2,3)
      B(3,2)=B(2,3)
      D(3,2)=D(2,3)
      A(3,3)=A(3,3)+QB(3,3)*Z1
      B(3,3)=B(3,3)+QB(3,3)*Z2
      D(3,3)=D(3,3)+QB(3,3)*Z3
      RETURN
      END
C
      SUBROUTINE gaussj(a,n,np,b,m,mp)
C
C     MATRIX INVERSION SUBROUTINE USING GAUSS-JORDAN
C     PROCEDURE
C     THIS SUBROUTINE FROM NUMERICAL RECIPES PACKAGE
C
      INTEGER m,mp,n,np,NMAX
      REAL a(np,np),b(np,mp)
      PARAMETER (NMAX=50)
```

```
      INTEGER i,icol,irow,j,k,l,ll,indxc(NMAX),indxr(NMAX),ipiv(NMAX)
      REAL big,dum,pivinv
      do 11 j=1,n
        ipiv(j)=0
11    continue
      do 22 i=1,n
        big=0.
        do 13 j=1,n
          if(ipiv(j).ne.1)then
            do 12 k=1,n
              if (ipiv(k).eq.0) then
                if (abs(a(j,k)).ge.big)then
                  big=abs(a(j,k))
                  irow=j
                  icol=k
                endif
              else if (ipiv(k).gt.1) then
                pause 'singular matrix in gaussj'
              endif
12            continue
          endif
13        continue
        ipiv(icol)=ipiv(icol)+1
        if (irow.ne.icol) then
          do 14 l=1,n
            dum=a(irow,l)
            a(irow,l)=a(icol,l)
            a(icol,l)=dum
14          continue
          do 15 l=1,m
            dum=b(irow,l)
            b(irow,l)=b(icol,l)
            b(icol,l)=dum
15          continue
        endif
        indxr(i)=irow
        indxc(i)=icol
        if (a(icol,icol).eq.0.) pause 'singular matrix in gaussj'
        pivinv=1./a(icol,icol)
        a(icol,icol)=1.
        do 16 l=1,n
          a(icol,l)=a(icol,l)*pivinv
16        continue
        do 17 l=1,m
          b(icol,l)=b(icol,l)*pivinv
17        continue
        do 21 ll=1,n
          if(ll.ne.icol)then
            dum=a(ll,icol)
            a(ll,icol)=0.
            do 18 l=1,n
```

```
          a(ll,l)=a(ll,l)-a(icol,l)*dum
18        continue
          do 19 l=1,m
            b(ll,l)=b(ll,l)-b(icol,l)*dum
19        continue
        endif
21      continue
22    continue
      do 24 l=n,1,-1
        if(indxr(l).ne.indxc(l))then
          do 23 k=1,n
            dum=a(k,indxr(l))
            a(k,indxr(l))=a(k,indxc(l))
            a(k,indxc(l))=dum
23        continue
        endif
24    continue
      return
      END
C  (C) Copr. 1986-92 Numerical Recipes Software *%&&j9&ic:K.
```

SAMPLE OUTPUT FROM CSTRESS FOR AN FRPC PLATE WITH 24 PLYS OF E-GLASS CLOTH

--- INPUT DATA ---

FORCES: -0.90000E+04 0.00000E+00 0.00000E+00

MOMENTS: 0.00000E+00 0.00000E+00 0.00000E+00

TEMPERATURE: 0.00

LAMINATE GEOMETRY

LAYER	T	THETA
1	0.0060	45.0000
2	0.0060	-45.0000
3	0.0060	45.0000
4	0.0060	-45.0000
5	0.0060	0.0000
6	0.0060	90.0000
7	0.0060	0.0000
8	0.0060	90.0000
9	0.0060	0.0000
10	0.0060	90.0000
11	0.0060	0.0000
12	0.0060	90.0000
13	0.0060	0.0000
14	0.0060	90.0000
15	0.0060	90.0000
16	0.0060	0.0000
17	0.0060	90.0000
18	0.0060	0.0000
19	0.0060	90.0000
20	0.0060	0.0000
21	0.0060	90.0000
22	0.0060	0.0000
23	0.0060	90.0000
24	0.0060	0.0000
25	0.0060	-45.0000
26	0.0060	45.0000
27	0.0060	-45.0000
28	0.0060	45.0000
29	0.0060	45.0000
30	0.0060	-45.0000

31	0.0060	45.0000
32	0.0060	-45.0000
33	0.0060	0.0000
34	0.0060	90.0000
35	0.0060	0.0000
36	0.0060	90.0000
37	0.0060	0.0000
38	0.0060	90.0000
39	0.0060	0.0000
40	0.0060	90.0000
41	0.0060	0.0000
42	0.0060	90.0000
43	0.0060	90.0000
44	0.0060	0.0000
45	0.0060	90.0000
46	0.0060	0.0000
47	0.0060	90.0000
48	0.0060	0.0000
49	0.0060	90.0000
50	0.0060	0.0000
51	0.0060	90.0000
52	0.0060	0.0000
53	0.0060	-45.0000
54	0.0060	45.0000
55	0.0060	-45.0000
56	0.0060	45.0000

MATERIAL PROPERTIES

LAYER	E1	E2	G12	NU12	ALPHA1	ALPHA2
1	0.74800E+07	0.31000E+07	0.14800E+07	0.230	0.21000E-05	0.93000E-05
2	0.74800E+07	0.31000E+07	0.14800E+07	0.230	0.21000E-05	0.93000E-05
3	0.74800E+07	0.31000E+07	0.14800E+07	0.230	0.21000E-05	0.93000E-05
4	0.74800E+07	0.31000E+07	0.14800E+07	0.230	0.21000E-05	0.93000E-05
5	0.74800E+07	0.31000E+07	0.14800E+07	0.230	0.21000E-05	0.93000E-05
6	0.74800E+07	0.31000E+07	0.14800E+07	0.230	0.21000E-05	0.93000E-05
7	0.74800E+07	0.31000E+07	0.14800E+07	0.230	0.21000E-05	0.93000E-05
8	0.74800E+07	0.31000E+07	0.14800E+07	0.230	0.21000E-05	0.93000E-05
9	0.74800E+07	0.31000E+07	0.14800E+07	0.230	0.21000E-05	0.93000E-05
10	0.74800E+07	0.31000E+07	0.14800E+07	0.230	0.21000E-05	0.93000E-05
11	0.74800E+07	0.31000E+07	0.14800E+07	0.230	0.21000E-05	0.93000E-05
12	0.74800E+07	0.31000E+07	0.14800E+07	0.230	0.21000E-05	0.93000E-05
13	0.74800E+07	0.31000E+07	0.14800E+07	0.230	0.21000E-05	0.93000E-05
14	0.74800E+07	0.31000E+07	0.14800E+07	0.230	0.21000E-05	0.93000E-05
15	0.74800E+07	0.31000E+07	0.14800E+07	0.230	0.21000E-05	0.93000E-05
16	0.74800E+07	0.31000E+07	0.14800E+07	0.230	0.21000E-05	0.93000E-05
17	0.74800E+07	0.31000E+07	0.14800E+07	0.230	0.21000E-05	0.93000E-05
18	0.74800E+07	0.31000E+07	0.14800E+07	0.230	0.21000E-05	0.93000E-05
19	0.74800E+07	0.31000E+07	0.14800E+07	0.230	0.21000E-05	0.93000E-05
20	0.74800E+07	0.31000E+07	0.14800E+07	0.230	0.21000E-05	0.93000E-05
21	0.74800E+07	0.31000E+07	0.14800E+07	0.230	0.21000E-05	0.93000E-05

22	0.74800E+07	0.31000E+07	0.14800E+07	0.230	0.21000E-05	0.93000E-05
23	0.74800E+07	0.31000E+07	0.14800E+07	0.230	0.21000E-05	0.93000E-05
24	0.74800E+07	0.31000E+07	0.14800E+07	0.230	0.21000E-05	0.93000E-05
25	0.74800E+07	0.31000E+07	0.14800E+07	0.230	0.21000E-05	0.93000E-05
26	0.74800E+07	0.31000E+07	0.14800E+07	0.230	0.21000E-05	0.93000E-05
27	0.74800E+07	0.31000E+07	0.14800E+07	0.230	0.21000E-05	0.93000E-05
28	0.74800E+07	0.31000E+07	0.14800E+07	0.230	0.21000E-05	0.93000E-05
29	0.74800E+07	0.31000E+07	0.14800E+07	0.230	0.21000E-05	0.93000E-05
30	0.74800E+07	0.31000E+07	0.14800E+07	0.230	0.21000E-05	0.93000E-05
31	0.74800E+07	0.31000E+07	0.14800E+07	0.230	0.21000E-05	0.93000E-05
32	0.74800E+07	0.31000E+07	0.14800E+07	0.230	0.21000E-05	0.93000E-05
33	0.74800E+07	0.31000E+07	0.14800E+07	0.230	0.21000E-05	0.93000E-05
34	0.74800E+07	0.31000E+07	0.14800E+07	0.230	0.21000E-05	0.93000E-05
35	0.74800E+07	0.31000E+07	0.14800E+07	0.230	0.21000E-05	0.93000E-05
36	0.74800E+07	0.31000E+07	0.14800E+07	0.230	0.21000E-05	0.93000E-05
37	0.74800E+07	0.31000E+07	0.14800E+07	0.230	0.21000E-05	0.93000E-05
38	0.74800E+07	0.31000E+07	0.14800E+07	0.230	0.21000E-05	0.93000E-05
39	0.74800E+07	0.31000E+07	0.14800E+07	0.230	0.21000E-05	0.93000E-05
40	0.74800E+07	0.31000E+07	0.14800E+07	0.230	0.21000E-05	0.93000E-05
41	0.74800E+07	0.31000E+07	0.14800E+07	0.230	0.21000E-05	0.93000E-05
42	0.74800E+07	0.31000E+07	0.14800E+07	0.230	0.21000E-05	0.93000E-05
43	0.74800E+07	0.31000E+07	0.14800E+07	0.230	0.21000E-05	0.93000E-05
44	0.74800E+07	0.31000E+07	0.14800E+07	0.230	0.21000E-05	0.93000E-05
45	0.74800E+07	0.31000E+07	0.14800E+07	0.230	0.21000E-05	0.93000E-05
46	0.74800E+07	0.31000E+07	0.14800E+07	0.230	0.21000E-05	0.93000E-05
47	0.74800E+07	0.31000E+07	0.14800E+07	0.230	0.21000E-05	0.93000E-05
48	0.74800E+07	0.31000E+07	0.14800E+07	0.230	0.21000E-05	0.93000E-05
49	0.74800E+07	0.31000E+07	0.14800E+07	0.230	0.21000E-05	0.93000E-05
50	0.74800E+07	0.31000E+07	0.14800E+07	0.230	0.21000E-05	0.93000E-05
51	0.74800E+07	0.31000E+07	0.14800E+07	0.230	0.21000E-05	0.93000E-05
52	0.74800E+07	0.31000E+07	0.14800E+07	0.230	0.21000E-05	0.93000E-05
53	0.74800E+07	0.31000E+07	0.14800E+07	0.230	0.21000E-05	0.93000E-05
54	0.74800E+07	0.31000E+07	0.14800E+07	0.230	0.21000E-05	0.93000E-05
55	0.74800E+07	0.31000E+07	0.14800E+07	0.230	0.21000E-05	0.93000E-05
56	0.74800E+07	0.31000E+07	0.14800E+07	0.230	0.21000E-05	0.93000E-05

FAILURE STRESSES

X-T	X-C	Y-T	Y-C	S
0.1600E+06	0.9000E+05	0.4000E+04	0.2000E+05	0.1200E+05

--- OUTPUT DATA ---

LAMINATE STIFFNESSES

[A]:

0.17347E+07	0.32748E+06	0.46882E-02
0.32748E+06	0.17347E+07	0.35903E-01
0.46882E-02	0.35903E-01	0.57982E+06

[B]:

-0.19179E+00	-0.34695E-01	0.66881E-03
-0.34695E-01	-0.17616E+00	0.66545E-03
0.66881E-03	0.66545E-03	-0.57155E-01

[D]:

0.16179E+05	0.33186E+04	0.46430E+02
0.33186E+04	0.15986E+05	0.46430E+02
0.46430E+02	0.46430E+02	0.56927E+04

[A']:

0.59776E-06	-0.11284E-06	0.21540E-14
-0.11284E-06	0.59776E-06	-0.36101E-13
0.21540E-14	-0.36101E-13	0.17247E-05

[B']:

0.71369E-11	-0.14168E-11	-0.10021E-12
-0.14275E-11	0.66367E-11	-0.10129E-12
-0.10360E-12	-0.99193E-13	0.17318E-10

[D']:

0.64557E-04	-0.13401E-04	-0.41723E-06
-0.13401E-04	0.65338E-04	-0.42361E-06
-0.41723E-06	-0.42361E-06	0.17567E-03

[H']:

0.71369E-11	-0.14275E-11	-0.10360E-12
-0.14168E-11	0.66367E-11	-0.99193E-13
-0.10021E-12	-0.10129E-12	0.17318E-10

MID-SURFACE STRAINS: -0.53798E-02 0.10156E-02 -0.19386E-10

MID-SURFACE CURVATURES: -0.64232E-07 0.12847E-07 0.93243E-09

LAMINA STRESSES

LAYER	Z	SX	SY	SXY
1	-0.16800E+00	-0.22858E+05	-0.39277E+04	-0.48859E+04
1	-0.16200E+00	-0.22858E+05	-0.39277E+04	-0.48859E+04
2	-0.16200E+00	-0.22858E+05	-0.39277E+04	0.48859E+04
2	-0.15600E+00	-0.22858E+05	-0.39277E+04	0.48859E+04
3	-0.15600E+00	-0.22858E+05	-0.39277E+04	-0.48859E+04
3	-0.15000E+00	-0.22858E+05	-0.39277E+04	-0.48859E+04
4	-0.15000E+00	-0.22858E+05	-0.39277E+04	0.48859E+04
4	-0.14400E+00	-0.22858E+05	-0.39277E+04	0.48859E+04
5	-0.14400E+00	-0.40403E+05	-0.70291E+03	-0.22741E-03
5	-0.13800E+00	-0.40403E+05	-0.70291E+03	-0.21913E-03
6	-0.13800E+00	-0.16311E+05	0.38450E+04	-0.12660E-03
6	-0.13200E+00	-0.16311E+05	0.38450E+04	-0.11832E-03
7	-0.13200E+00	-0.40403E+05	-0.70291E+03	-0.21085E-03
7	-0.12600E+00	-0.40403E+05	-0.70291E+03	-0.20257E-03
8	-0.12600E+00	-0.16311E+05	0.38450E+04	-0.11004E-03
8	-0.12000E+00	-0.16311E+05	0.38450E+04	-0.10176E-03
9	-0.12000E+00	-0.40403E+05	-0.70291E+03	-0.19429E-03
9	-0.11400E+00	-0.40403E+05	-0.70291E+03	-0.18601E-03
10	-0.11400E+00	-0.16311E+05	0.38450E+04	-0.93483E-04
10	-0.10800E+00	-0.16311E+05	0.38450E+04	-0.85203E-04
11	-0.10800E+00	-0.40403E+05	-0.70291E+03	-0.17773E-03
11	-0.10200E+00	-0.40403E+05	-0.70291E+03	-0.16945E-03
12	-0.10200E+00	-0.16311E+05	0.38450E+04	-0.76923E-04

12 -0.96000E-01-0.16311E+05 0.38450E+04-0.68643E-04

13 -0.96000E-01-0.40403E+05-0.70291E+03-0.16117E-03
13 -0.90000E-01-0.40403E+05-0.70291E+03-0.15289E-03

14 -0.90000E-01-0.16311E+05 0.38450E+04-0.60363E-04
14 -0.84000E-01-0.16311E+05 0.38450E+04-0.52083E-04

15 -0.84000E-01-0.16311E+05 0.38450E+04-0.52083E-04
15 -0.78000E-01-0.16311E+05 0.38450E+04-0.43803E-04

16 -0.78000E-01-0.40403E+05-0.70291E+03-0.13633E-03
16 -0.72000E-01-0.40403E+05-0.70291E+03-0.12805E-03

17 -0.72000E-01-0.16311E+05 0.38450E+04-0.35523E-04
17 -0.66000E-01-0.16311E+05 0.38450E+04-0.27243E-04

18 -0.66000E-01-0.40403E+05-0.70291E+03-0.11977E-03
18 -0.60000E-01-0.40403E+05-0.70291E+03-0.11149E-03

19 -0.60000E-01-0.16311E+05 0.38450E+04-0.18963E-04
19 -0.54000E-01-0.16311E+05 0.38450E+04-0.10683E-04

20 -0.54000E-01-0.40403E+05-0.70291E+03-0.10321E-03
20 -0.48000E-01-0.40403E+05-0.70291E+03-0.94932E-04

21 -0.48000E-01-0.16311E+05 0.38450E+04-0.24028E-05
21 -0.42000E-01-0.16311E+05 0.38450E+04 0.58771E-05

22 -0.42000E-01-0.40403E+05-0.70291E+03-0.86652E-04
22 -0.36000E-01-0.40403E+05-0.70291E+03-0.78372E-04

23 -0.36000E-01-0.16311E+05 0.38450E+04 0.14157E-04
23 -0.30000E-01-0.16311E+05 0.38450E+04 0.22437E-04

24 -0.30000E-01-0.40403E+05-0.70291E+03-0.70092E-04
24 -0.24000E-01-0.40403E+05-0.70291E+03-0.61812E-04

25 -0.24000E-01-0.22858E+05-0.39277E+04 0.48860E+04
25 -0.18000E-01-0.22858E+05-0.39277E+04 0.48860E+04

26 -0.18000E-01-0.22858E+05-0.39277E+04-0.48860E+04
26 -0.12000E-01-0.22858E+05-0.39277E+04-0.48860E+04

27 -0.12000E-01-0.22858E+05-0.39277E+04 0.48860E+04
27 -0.60001E-02-0.22858E+05-0.39277E+04 0.48860E+04

28 -0.60001E-02-0.22858E+05-0.39277E+04-0.48860E+04
28 -0.95926E-07-0.22858E+05-0.39277E+04-0.48860E+04

29 -0.95926E-07-0.22858E+05-0.39277E+04-0.48860E+04
29 0.59999E-02-0.22858E+05-0.39277E+04-0.48860E+04

30 0.59999E-02-0.22858E+05-0.39277E+04 0.48860E+04
30 0.12000E-01-0.22858E+05-0.39277E+04 0.48860E+04

31 0.12000E-01-0.22858E+05-0.39277E+04-0.48860E+04
31 0.18000E-01-0.22858E+05-0.39277E+04-0.48860E+04

32 0.18000E-01-0.22858E+05-0.39277E+04 0.48860E+04
32 0.24000E-01-0.22858E+05-0.39277E+04 0.48860E+04

33 0.24000E-01-0.40403E+05-0.70291E+03 0.44278E-05
33 0.30000E-01-0.40403E+05-0.70291E+03 0.12708E-04

34 0.30000E-01-0.16311E+05 0.38450E+04 0.10524E-03
34 0.36000E-01-0.16311E+05 0.38450E+04 0.11352E-03

35 0.36000E-01-0.40403E+05-0.70291E+03 0.20988E-04
35 0.42000E-01-0.40403E+05-0.70291E+03 0.29268E-04

36 0.42000E-01-0.16311E+05 0.38450E+04 0.12180E-03
36 0.48000E-01-0.16311E+05 0.38450E+04 0.13008E-03

37 0.48000E-01-0.40403E+05-0.70291E+03 0.37548E-04
37 0.54000E-01-0.40403E+05-0.70291E+03 0.45828E-04

38 0.54000E-01-0.16311E+05 0.38450E+04 0.13836E-03
38 0.60000E-01-0.16311E+05 0.38450E+04 0.14664E-03

39 0.60000E-01-0.40403E+05-0.70291E+03 0.54108E-04
39 0.66000E-01-0.40403E+05-0.70291E+03 0.62388E-04

40 0.66000E-01-0.16311E+05 0.38450E+04 0.15492E-03
40 0.72000E-01-0.16311E+05 0.38451E+04 0.16320E-03

41 0.72000E-01-0.40403E+05-0.70291E+03 0.70668E-04
41 0.78000E-01-0.40403E+05-0.70291E+03 0.78948E-04

42 0.78000E-01-0.16311E+05 0.38451E+04 0.17148E-03
42 0.84000E-01-0.16311E+05 0.38451E+04 0.17976E-03

43 0.84000E-01-0.16311E+05 0.38451E+04 0.17976E-03
43 0.90000E-01-0.16311E+05 0.38451E+04 0.18804E-03

44 0.90000E-01-0.40403E+05-0.70291E+03 0.95507E-04
44 0.96000E-01-0.40403E+05-0.70291E+03 0.10379E-03

45 0.96000E-01-0.16311E+05 0.38451E+04 0.19632E-03
45 0.10200E+00-0.16311E+05 0.38451E+04 0.20460E-03

46 0.10200E+00-0.40403E+05-0.70291E+03 0.11207E-03
46 0.10800E+00-0.40403E+05-0.70291E+03 0.12035E-03

47 0.10800E+00-0.16311E+05 0.38451E+04 0.21288E-03
47 0.11400E+00-0.16311E+05 0.38451E+04 0.22116E-03

48 0.11400E+00-0.40403E+05-0.70291E+03 0.12863E-03
48 0.12000E+00-0.40403E+05-0.70291E+03 0.13691E-03

49 0.12000E+00-0.16311E+05 0.38451E+04 0.22944E-03
49 0.12600E+00-0.16311E+05 0.38451E+04 0.23772E-03

50 0.12600E+00-0.40403E+05-0.70291E+03 0.14519E-03
50 0.13200E+00-0.40403E+05-0.70291E+03 0.15347E-03

51 0.13200E+00-0.16311E+05 0.38451E+04 0.24600E-03
51 0.13800E+00-0.16311E+05 0.38451E+04 0.25428E-03

52 0.13800E+00-0.40403E+05-0.70291E+03 0.16175E-03
52 0.14400E+00-0.40403E+05-0.70291E+03 0.17003E-03

53 0.14400E+00-0.22858E+05-0.39277E+04 0.48860E+04
53 0.15000E+00-0.22858E+05-0.39277E+04 0.48860E+04

54 0.15000E+00-0.22858E+05-0.39277E+04-0.48860E+04
54 0.15600E+00-0.22858E+05-0.39277E+04-0.48860E+04

55 0.15600E+00-0.22858E+05-0.39277E+04 0.48860E+04
55 0.16200E+00-0.22858E+05-0.39277E+04 0.48860E+04

56 0.16200E+00-0.22858E+05-0.39277E+04-0.48860E+04
56 0.16800E+00-0.22858E+05-0.39277E+04-0.48860E+04

START TIME =17:50:32.89 END TIME =17:50:40.19

APPENDIX D

CONSTRUCTION OF THE FIBER REINFORCED COMPOSITE BEAMS

Construction of the FRPC beams focused on using materials and technology that could be used by any number of manufacturers and would be easy to implement or commonly available. Materials used in the construction of the FRPC beams were 7781 woven E-glass cloth as the fiber reinforcement and Fiber Glast Developments #88 low modulus epoxy as the matrix. The epoxy is a thinned Shell EPON 8132 resin cured with Shell EPI-CURE 3282 aliphatic amine curing agent. Hand lay-up techniques were used to construct the beams. The glass cloth was cut to the appropriate size and orientation by hand. Epoxy was applied by hand using rollers and brushes. Consolidation of the lay-up was obtained by using saturation rollers to work the epoxy into the glass fabric. After completing lay-up of the part, the part was covered with release film, bleeder and breather layers and placed inside a polyethylene vacuum bag. A vacuum of 24 psi was applied to the bag to complete the consolidation of the part and was maintained until polymerization of the epoxy was completed.

Construction of the box beam sections was accomplished by building up the sections on a removable mold pictured in Figure D-1. The mold was constructed of sheet steel with wood end plugs and interior bolsters. The mold was designed so that it could be extracted from the completed box beam by removing the end plugs and

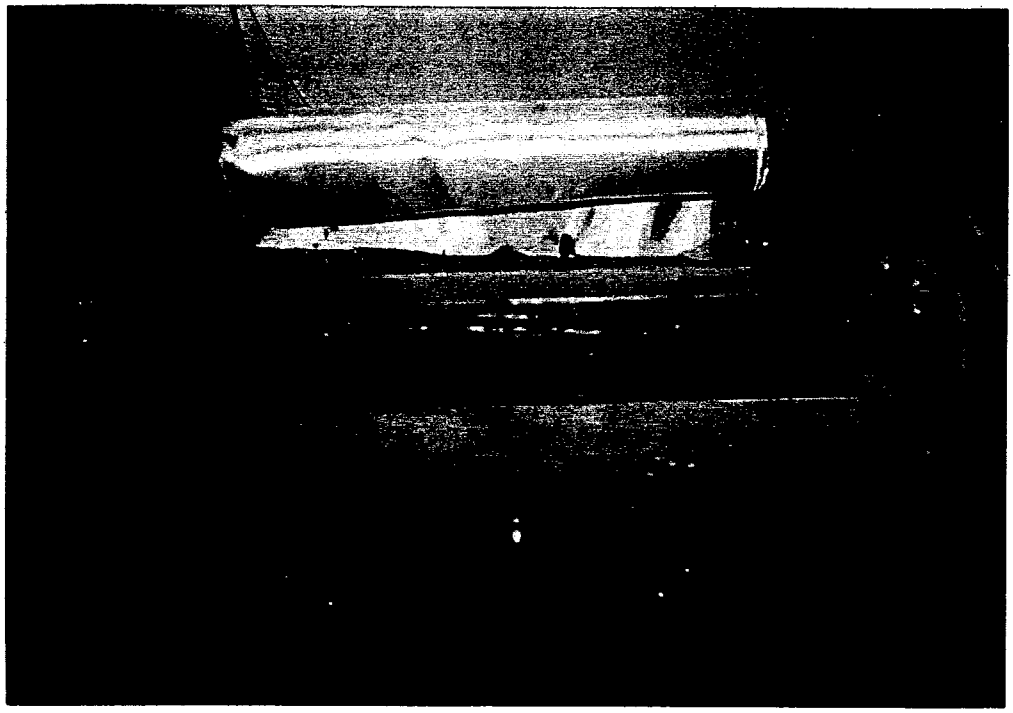

Figure D-1. FRPC box beam mold.

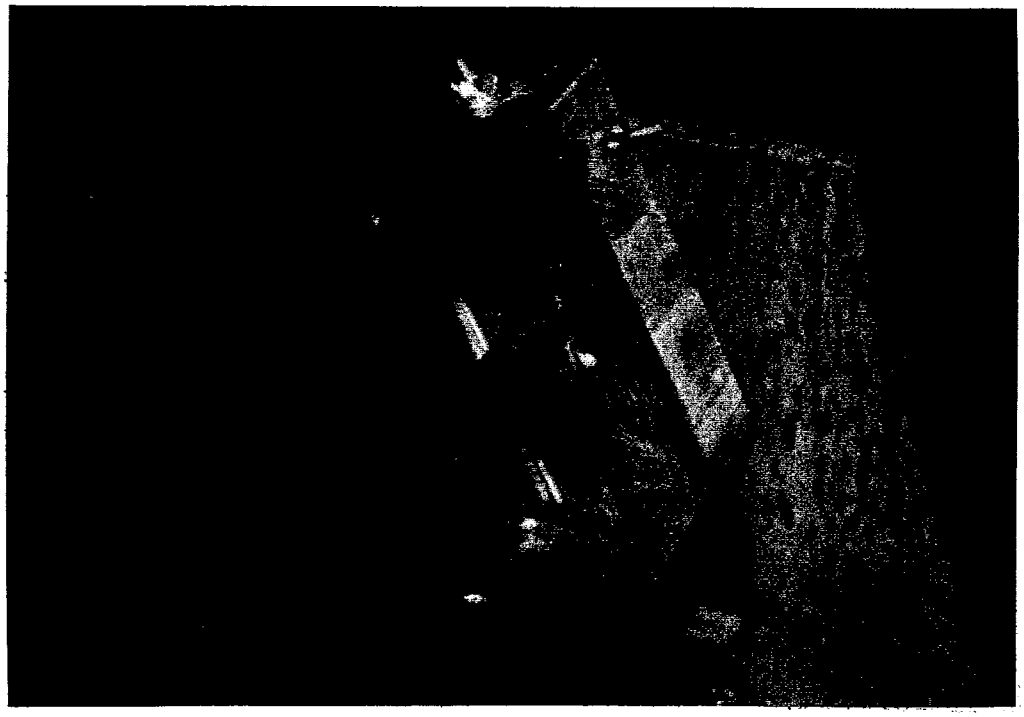

Figure D-2. Box beam mold end details.

bolsters and collapsing the sheet steel sides and withdrawing them from the completed box beam (Figure D-2).

The procedure for building a box beam consisted of placing a polyethylene release film over the mold and laying up the first two ±45° plys and the first 0°/90° ply with a spray contact adhesive. The epoxy matrix was applied next with a brush (Figure D-3) and worked into the fabric with a squeegee and saturation roller (Figure D-4 and 5). The form was then rotated about its long axis to wind the next 0°/90° layer onto the beam from the adjoining roll of E-glass cloth. Ten plys were built up in this fashion (Figure D-6). As the tenth ply was completed, the glass cloth was cut from the roll and two more ±45° plys were applied to the beam. When the final two bias plys were placed on the mold, a nylon release ply was placed over the laminate, followed by bleeder and breather layers of spun polyester (Figure D-7). After the breather layer was secured to the laminate with vinyl tape, the mold and laminate was removed from the support frame and placed inside a polyethylene vacuum bag. The vacuum bag was sealed and a vacuum of 20 to 28 inches of Hg was applied to the bag for a period of two hours to consolidate the laminate and extract excess epoxy before the epoxy sets (Figure D-8). After the epoxy had cured, the mold and laminate was removed from the vacuum bag, the bleeder and breather layers were removed (Figure D-9), and the mold was extracted from the box beam section (Figure D-10). The completed box beam section was trimmed to final length and set aside, ready for bonding into the FRPC beam.

The full FRPC beam is composed of twenty-four box sections that are bonded together with the epoxy used in the lamination procedure. Two lengths of box section are used in the assembly, 30 and 34 inches. These two lengths are alternately bonded together, resulting in a toothed pattern at one end. This configuration results in a structure that is about three inches thick and twelve feet wide. An exploded view of the FRPC beam is shown in Figure D-11. The arrangement of differing box lengths results in every other box section acting as a dowel to provide for load transfer and to allow for further contraction of the pavement sections.

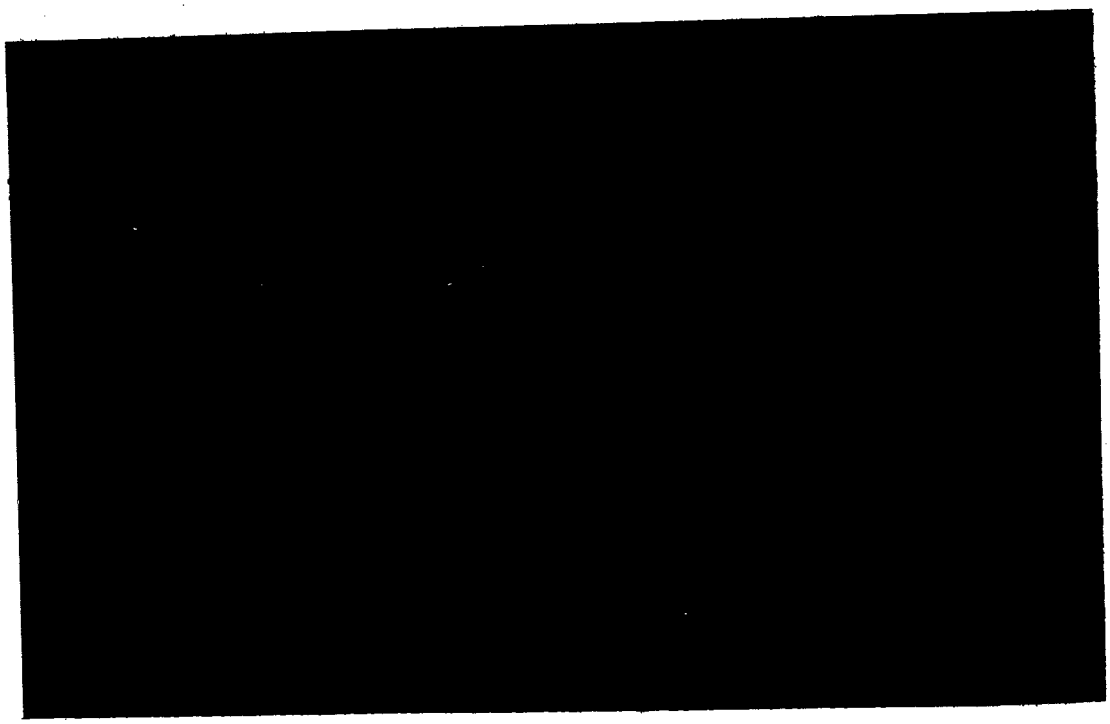

Figure D-3. Application of epoxy.

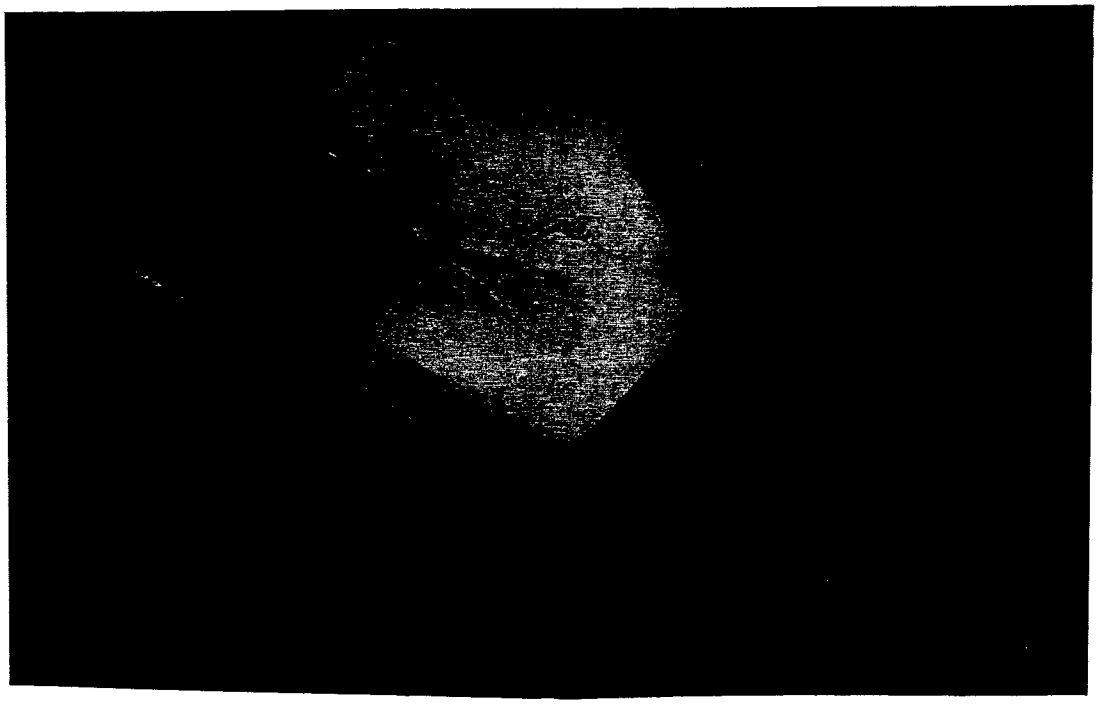

Figure D-4. Epoxy distribution.

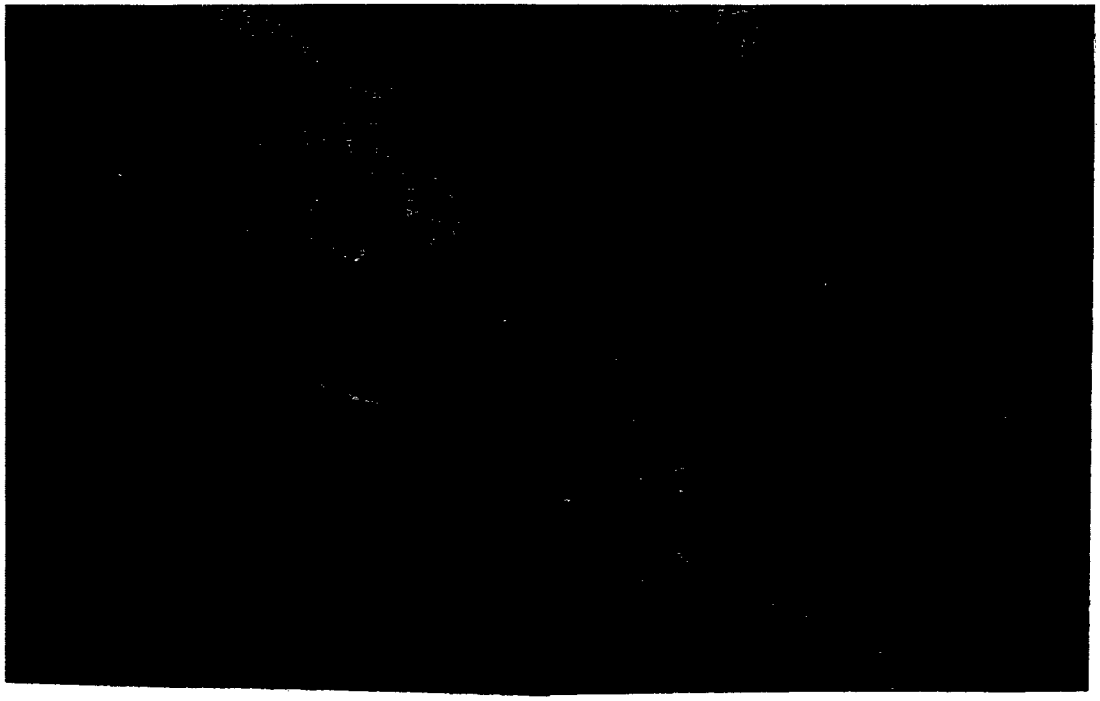

Figure D-5. Saturating the glass cloth.

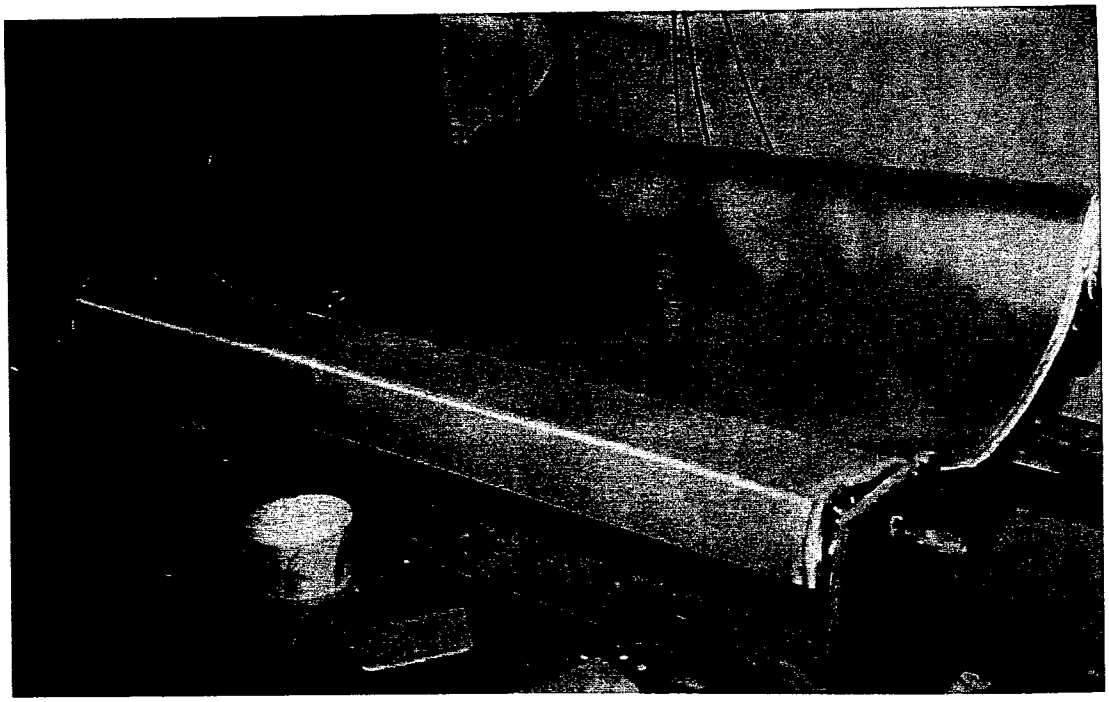

Figure D-6. Winding the cloth onto the form.

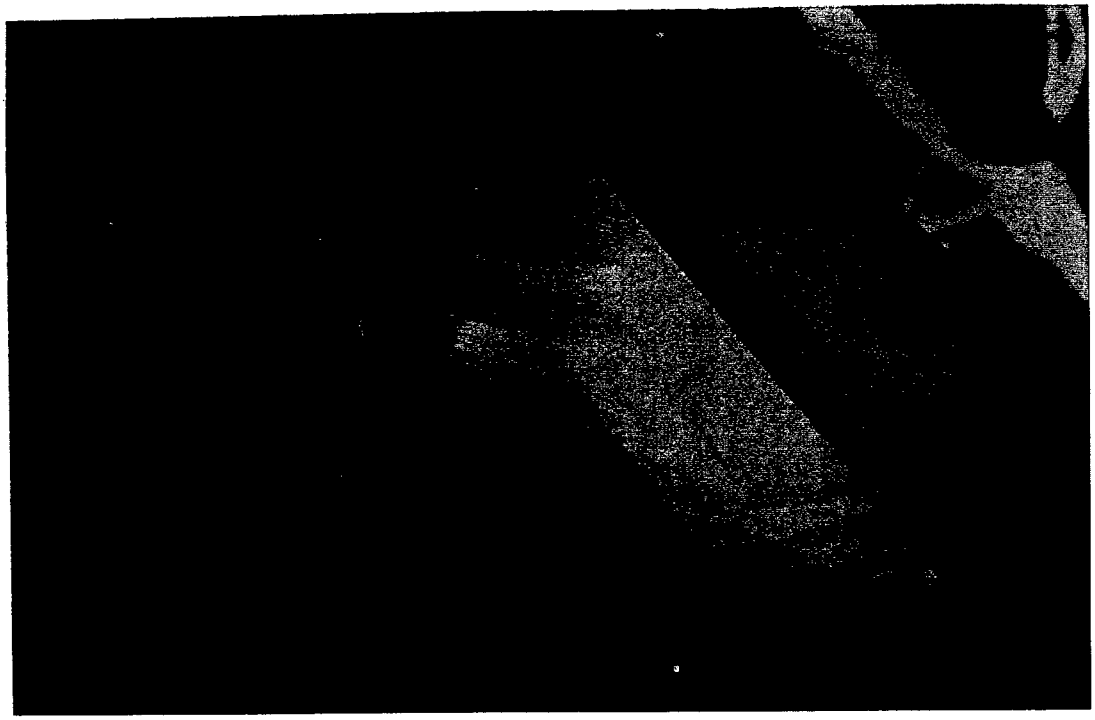

Figure D-7. Placing the release fabric layer.

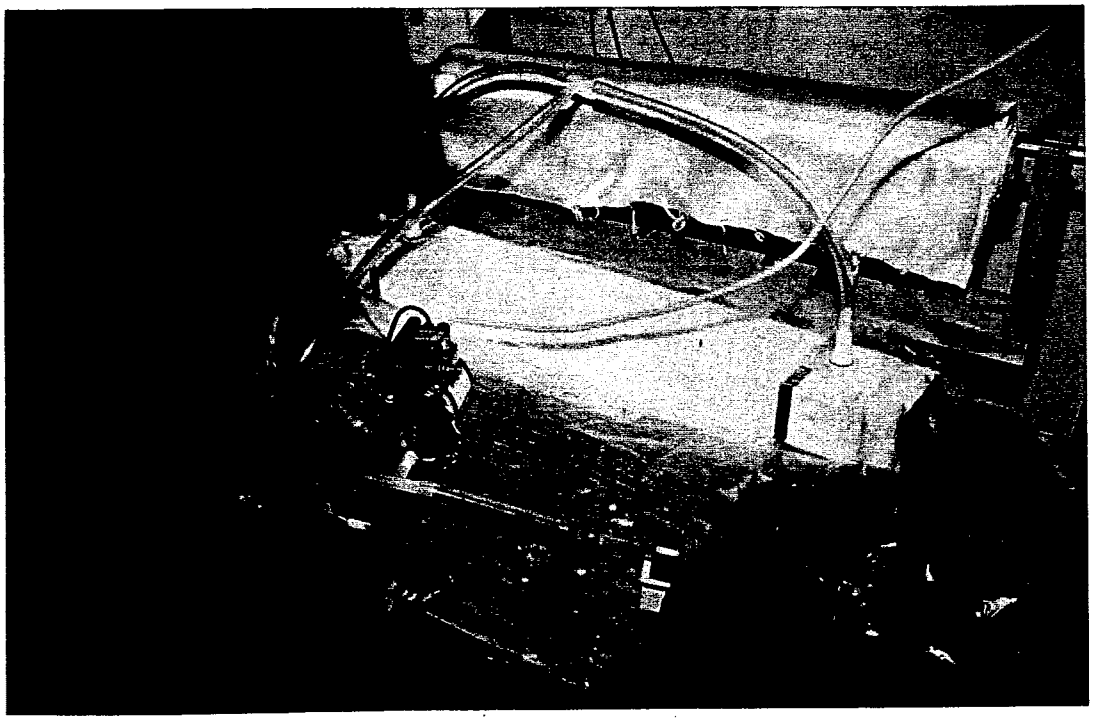

Figure D-8. Applying vacuum to the completed laminate.

Figure D-9. Removing the release film,bleeder, and breather layers.

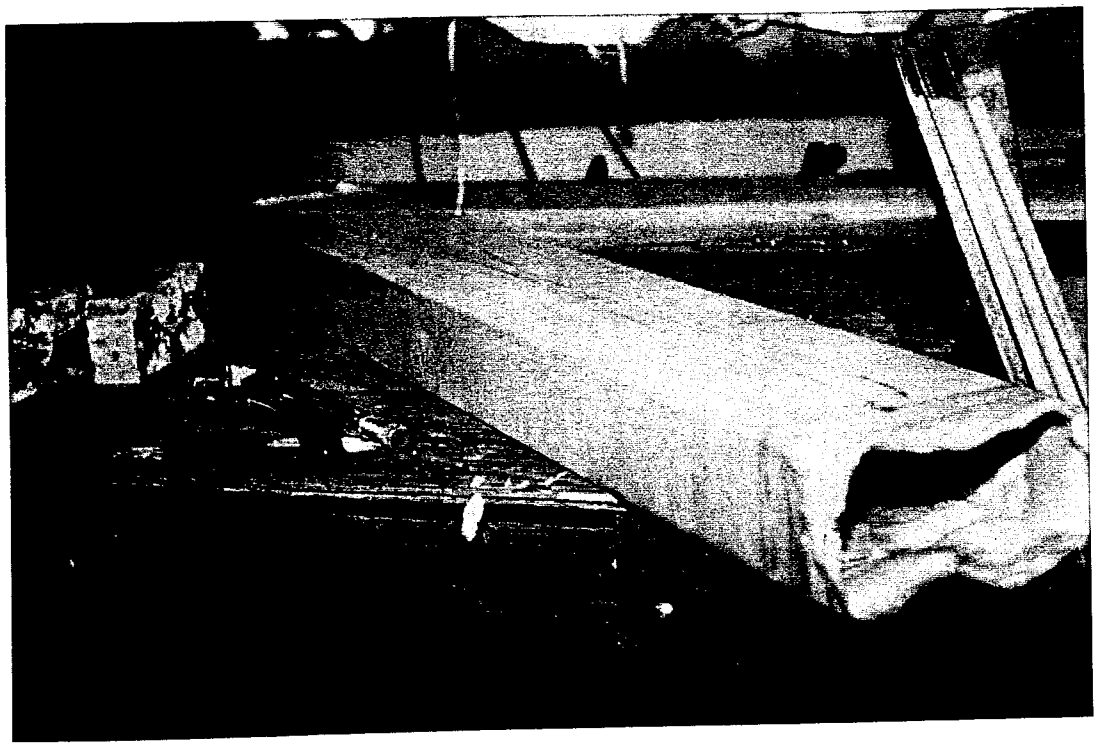

Figure D-10. Completed box beam, ready for trimming.

The top and bottom cover skins shown in Figure D-11 are composed of the same laminate configuration used in the box beam sections, $[\pm 45_2/(0/90)_{10}/\pm 45_2]$. This configuration results in a balanced laminate with the desired properties. The skins were laid up on the bonded box sections using the same hand lay up techniques as for the box sections (Figure D-12). One complete side was laid up and vacuum bagged at a time. The resulting product after removing the vacuum bag is shown in Figure D-13. The excess material around the edge of the unit was trimmed and the completed beam was then ready for filling with polyurethane foam and installation of instrumentation.

Production of the honeycomb sandwich beams used the same manufacturing techniques as the box beam unit. An exploded drawing of the unit is shown in Figure D-14. The aluminum honeycomb was delivered in 10 foot long by 3 foot wide sections. This required adhesive joining of two or three pieces of honeycomb for each sandwich beam. Each piece of honeycomb was laid on a single layer of epoxy saturated 7781 E-glass cloth and allowed to bond. The joints between the pieces of honeycomb were filled with a glass fiber impregnated epoxy paste adhesive to provide structural continuity between the honeycomb sections. At this time epoxy was poured into several rows of cells along the edge of the structural honeycomb sandwich to provide edge support for the honeycomb against end-on lateral loads. After the adhesive had set the unit was flipped over and set on another single layer of epoxy saturated glass cloth to provide a skin for each side of the honeycomb. The honeycomb sandwich at this point in production is shown in Figure D-15. The dark lines that can be seen on the unit are the areas of epoxy paste adhesive and the epoxy resin filled cells.

The honeycomb sandwich was then cut along one edge to develop the lip (Figure D-16) that would act as a dowel in the pavement. This photograph also shows the epoxy fill in the cells along the edge of the honeycomb sandwich. The remaining 19 plys of glass cloth were laid up using the techniques previously described. A photograph of the honeycomb structural sandwich inside the vacuum bag is presented

in Figure D-17. The completed unit ready for installation of instrumentation is shown in Figure D-18.

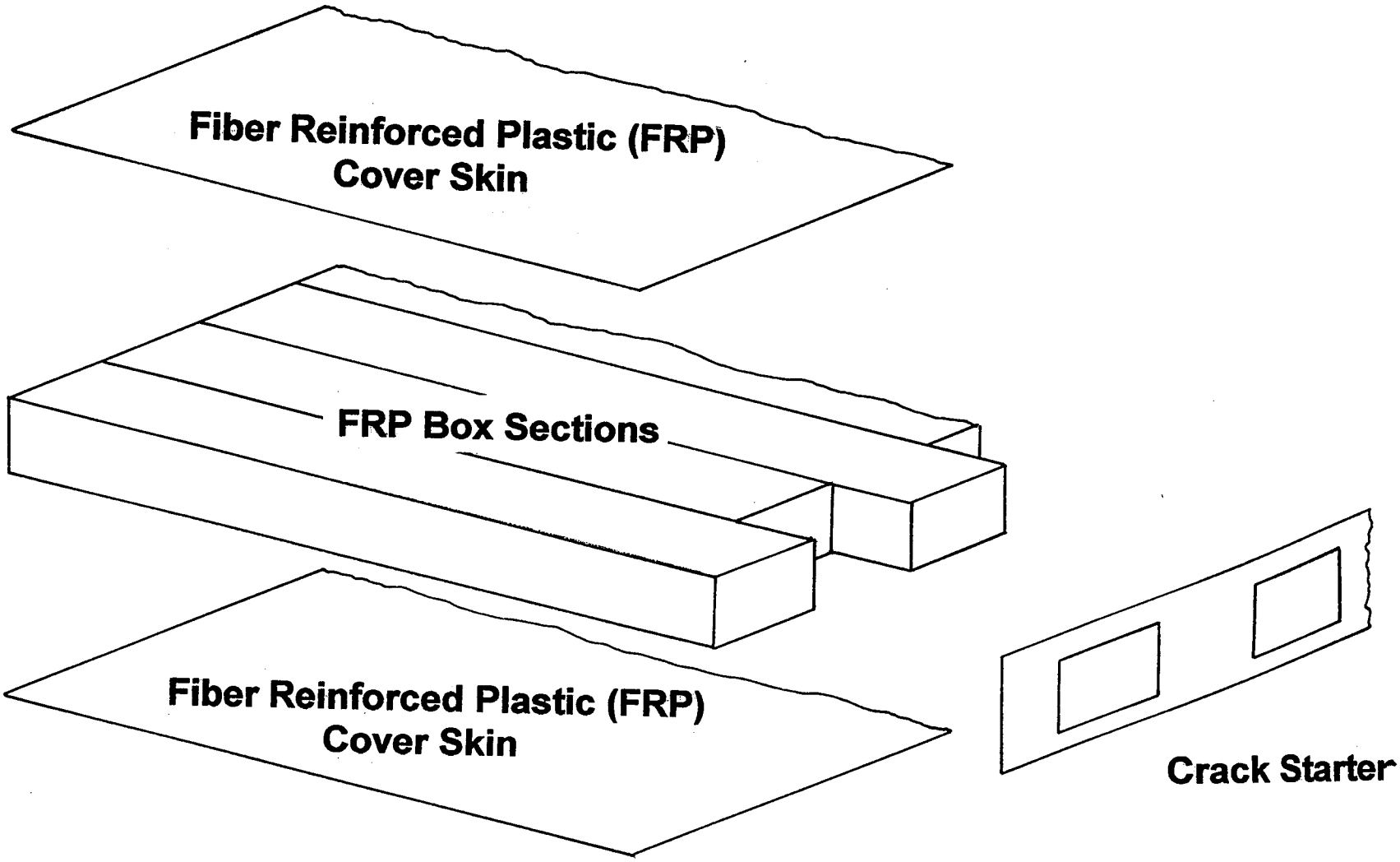

Figure D-11. Exploded view of the FRPC Beam

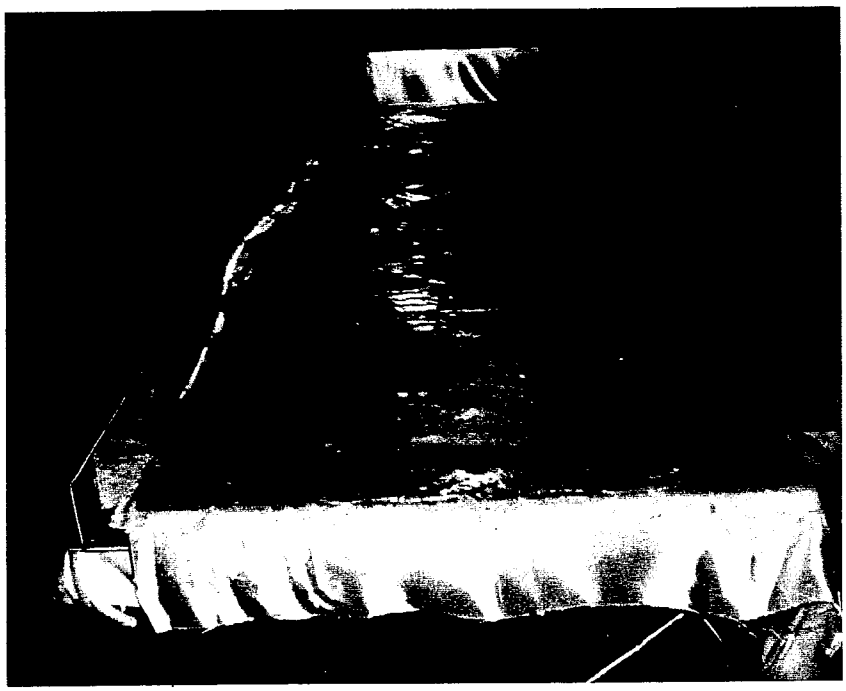

Figure D-12. Laying up the skin on the box beam unit.

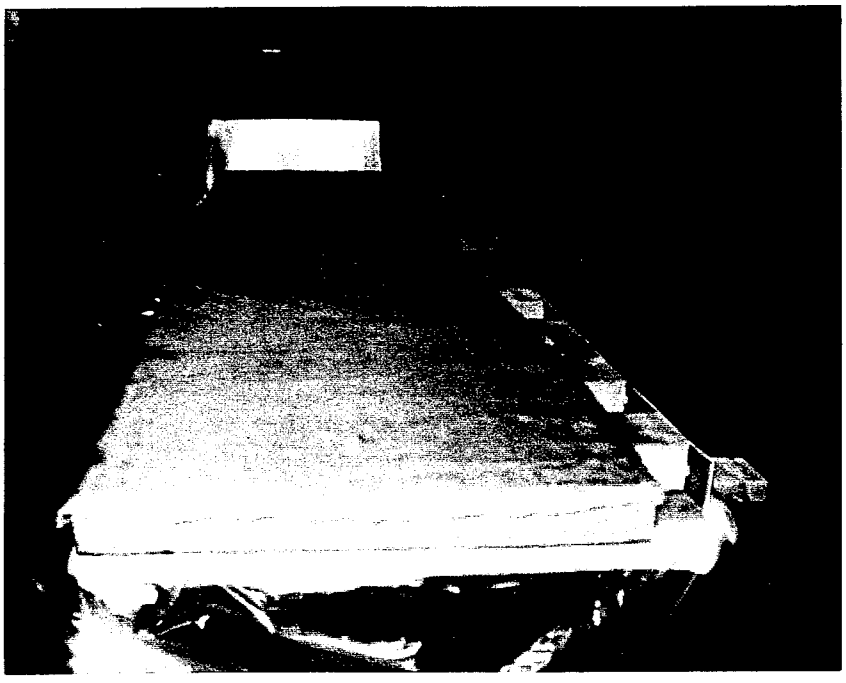

Figure D-13. Completed box beam unit, ready for trimming.

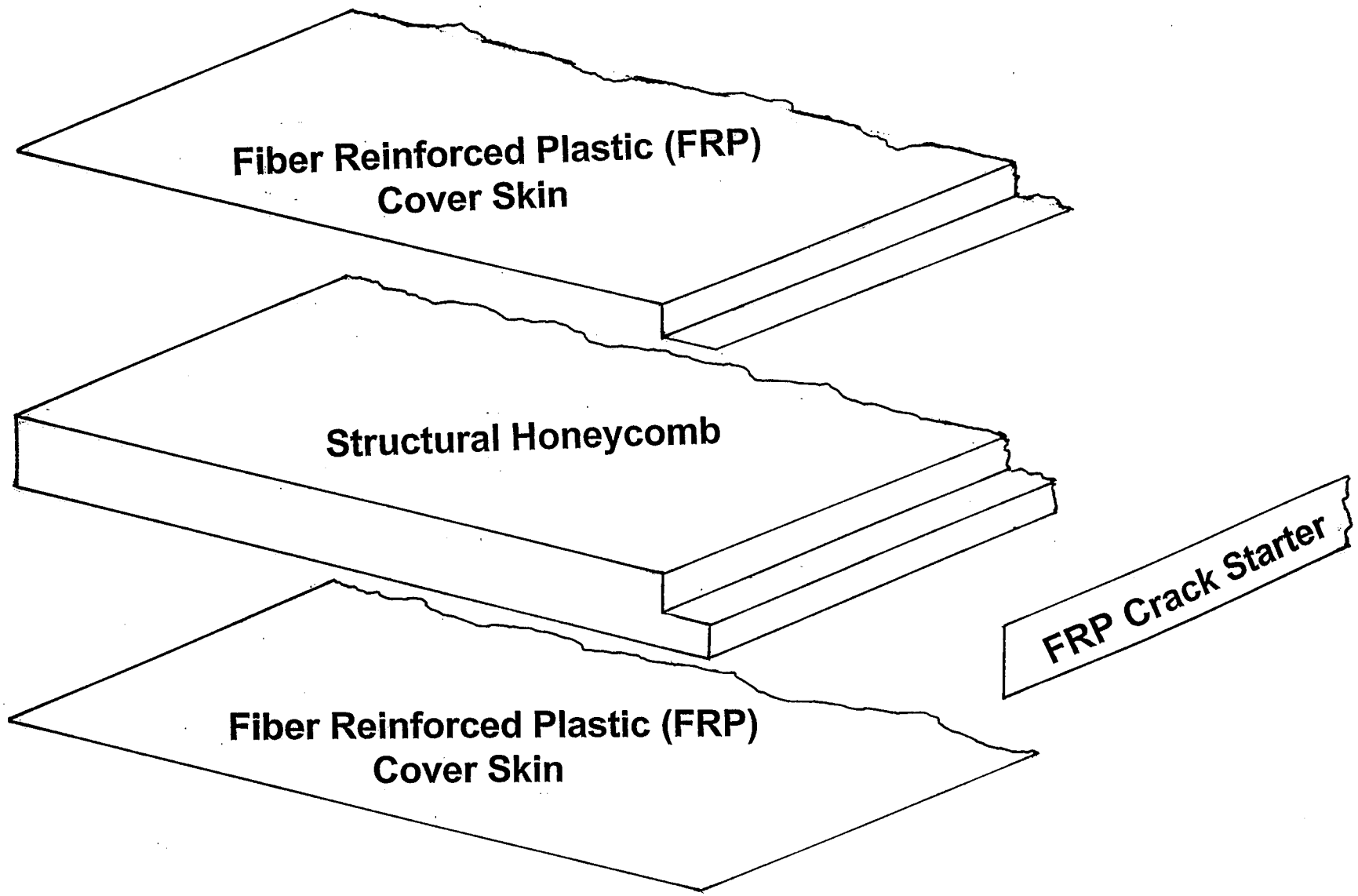

Figure D-14. Exploded view of the honeycomb structural sandwich

Figure D-15. Aluminum honeycomb with base ply.

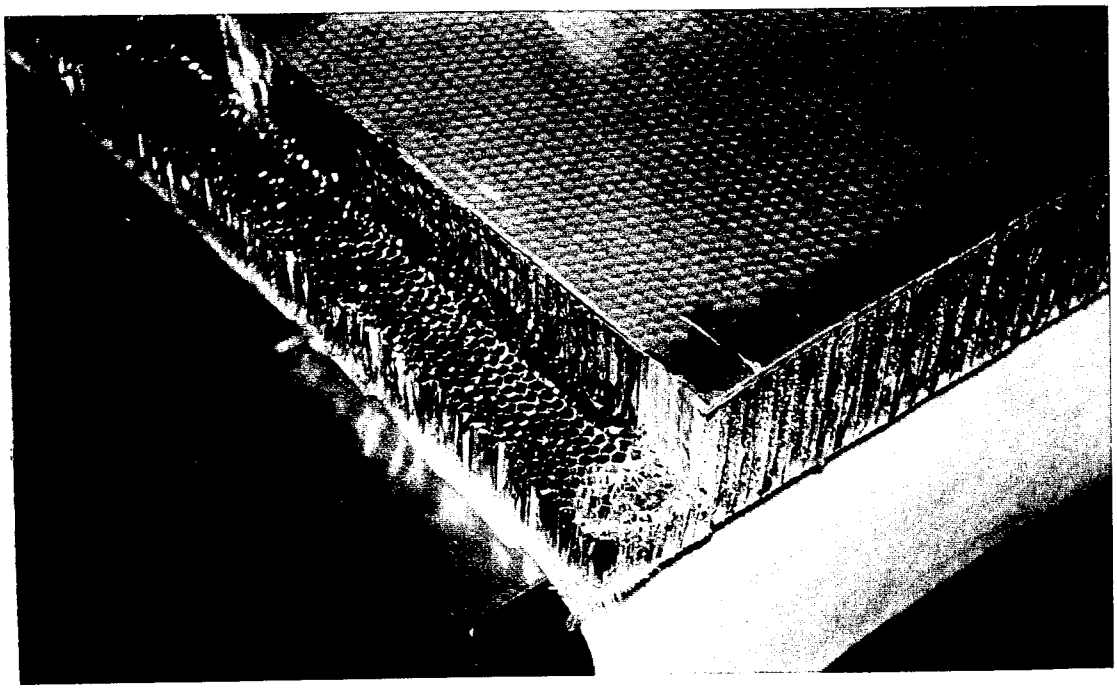

Figure D-16. Honeycomb with dowel lip cut.

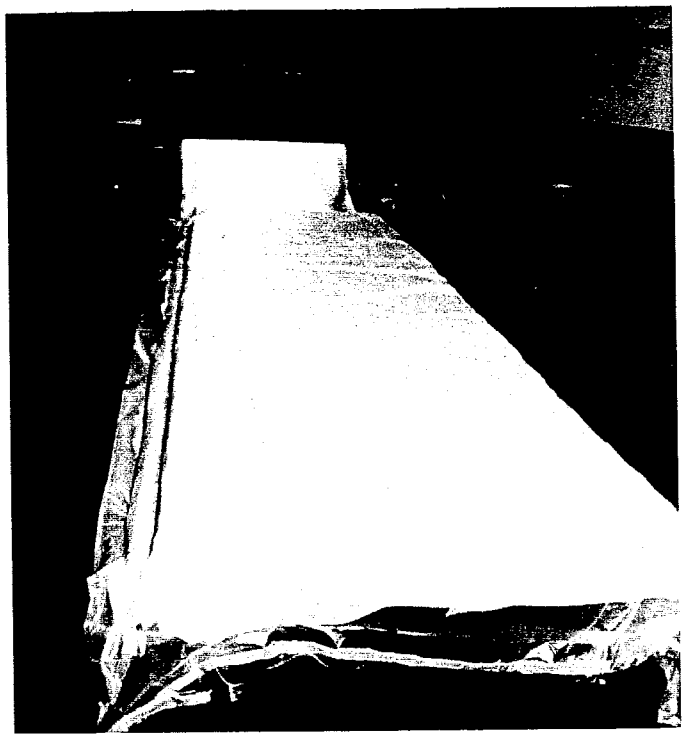

Figure D-17. Honeycomb structural sandwich in vacuum bag.

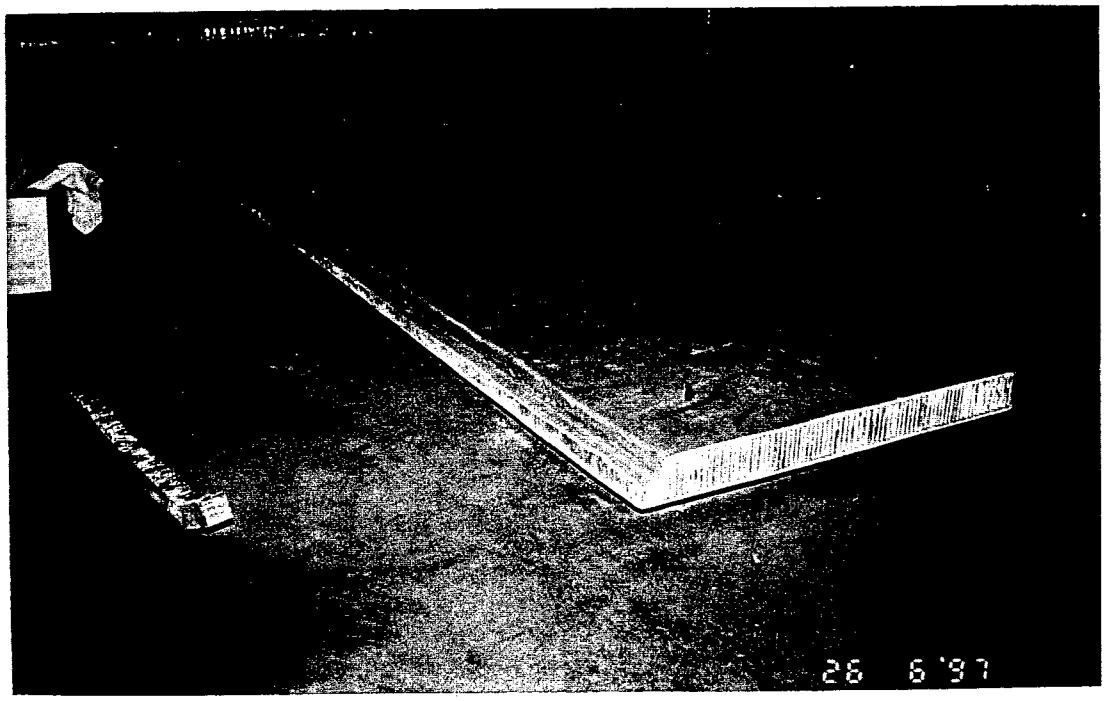

Figure D-18. Completed honeycomb structural sandwich ready for instrumentation installation.

APPENDIX E

MATERIALS PROPERTIES

Preliminary design of the FRPC beams used presumptive elastic and strength properties from the literature. A prototype beam was constructed using 7781 woven E-glass cloth and FiberGlast Developments 87/88 epoxy system. The configuration of the prototype followed the preliminary design developed in Appendix B. The prototype was set up as a simply supported beam and loaded to failure under controlled strain conditions in a 120,000 pound universal test machine. Load/deformation data was recorded throughout the test. Buckling was observed at a load of 2500 pounds and failure occurred at 4100 pounds. The elastic modulus of the beam was determined by back-calculation at a load level of 2000 pounds. At this load the beam had a calculated modulus of 593,000 psi. This data from the first prototype box beam load test indicated that the presumptive design values were very optimistic. Since good engineering properties are required for efficient design, a test program to develop engineering properties was undertaken.

The test program consisted of the determination of the elastic and strength properties of the composites through tensile testing of sample coupons. Elastic and strength properties were determined using the test procedures outlined in ASTM D 3039-76, Tensile Properties of Fiber-Resin Composites, and ASTM D 3518-91, In-Plane Shear Stress-Strain Response of Unidirectional Polymer Matrix Composites. A minimum of five samples were tested for each material property desired. All tensile test coupons were constructed with a minimum gage length of 8 inches. The tabs used for load transfer between the test machine grips and the tensile test specimen were constructed of a balanced 0/90 cross-ply made from unidirectional and woven E-glass fabric.

All tests were run on a 120,000 pound universal test machine located at the KDOT Materials and Research Center. This test machine has a load accuracy of 0.01 percent over the load range used in the tests. An 8 inch gage length extensometer was used to obtain longitudinal strain measurements. This extensometer has a certified accuracy of 0.05 percent over the range of use. Transverse strain measurements were made with 0.5 inch, 120 ohm or 350 ohm strain gages. Strain readings from the strain gages were taken with a BLH 120 strain indicator. The strain indicator is accurate to ± 2 microstrain over a range of ± 1000 microstrain. The cumulative effect of these instrument errors lead to an error in the estimate of elastic modulus and tensile strength of ± 2.5 percent.

Engineering properties that rely on transverse strain measurement with strain gages have a much greater error due to errors in alignment of the strain gage on the specimen during mounting. The error due to misalignment for measurements on composites with a 90 degree orientation can be up to - 20 percent. The error due to misalignment for ± 45 degree angle ply composites can range between + 40 and - 60 percent.

Several series of tests were run on both unidirectional and woven E-glass cloth with the FiberGlast Developments 87/88 epoxy system. The first set of tests were run on style 7672 unidirectional E-glass cloth. Three sets of test samples were fabricated. One set had the reinforcement oriented in the 0 degree direction (oriented in the direction of load). The second set of samples had the reinforcement oriented in the 90 degree direction (oriented transverse to the direction of load). The third set had the reinforcement oriented at +45 degrees. The results of the tests on the three sample sets are summarized in Table E-1.

Table E-1 - Properties for Unidirectional E-glass

Property	Average Value	Standard Deviation	Coefficient of Variation (percent)
E_1	3.89×10^6 psi	162×10^3 psi	4.2
ν_{12}	0.235	0.035	14.9
S_1	55.5×10^3 psi	4×10^3 psi	7.2
E_2	0.38×10^6 psi	63×10^3 psi	16.7
ν_{21}	0.045	0.024	52.9
S_2	8.06×10^3 psi	1×10^3 psi	12.7
G_{12}	0.29×10^6 psi	71×10^3 psi	24.7
S_{45}	3.75×10^3 psi	644 psi	17.2

The high coefficient of variation for measurements of Poisson's ratio and the shear modulus can be explained by alignment error in mounting the strain gages for transverse strain measurement. The coefficient of variation for the other engineering values under test have reasonable magnitudes that can be accounted for by manufacturing variability.

Comparing the results in Table E-1 to the presumptive design values listed in Appendix B shows that the as-constructed properties are between one-half and one-third the presumptive design values. This information was valuable, but was not really representative of the materials that would be used in construction. The beams were being manufactured using woven fabric rather than unidirectional fabrics. The resulting strengths and moduli should be somewhat less, but by how much? The only

way to answer this question was by running a set of tensile tests on coupons manufactured from woven fabric.

Two sets of samples were manufactured from style 7781 E-glass using the same epoxy resin system as the first series of tests. One set had the fabric oriented to 0/90 degrees and the other had the fabric oriented at ±45 degrees. These sets of samples were configured and run in the same manner as the first series of tests on the unidirectional materials. The results of these tests are presented in Table E-2. As expected, the values came in at about one-half of the unidirectional reinforcement results. The coefficient of variability of the results for the tests on the woven fabric can be attributed to error in gage alignment for the Poisson's and shear modulus values. Manufacturing variability accounts for the variation in the other engineering properties measured.

Table E-2 - Properties for Woven E-glass

Property	Average Value	Standard Deviation	Coefficient of Variation (percent)
E	1.78×10^6 psi	207×10^3 psi	11.7
ν_{12}	0.0627	0.013	21.0
S	24.2×10^3 psi	3.5×10^3 psi	14.5
G_{12}	0.41×10^6 psi	88×10^3 psi	22.0
S_{45}	8.21×10^3 psi	516 psi	6.3

APPENDIX F

DESIGN OF A COMPOSITE SANDWICH BEAM USING ALUMINUM HONEYCOMB

The honeycomb sandwich for the FRPC pavement repair was designed using the Hexcel, Inc. design guide, TSB 124, Bonded Honeycomb Sandwich Construction. The panel, Figure F-1, was to be designed using the following material properties:

Core: Aluminum Commercial Grade, ACG-1/4-4.8
σ_c = 630 psi, E_c = 148 ksi, τ_l = 365 psi, G_l = 70 ksi
τ_w = 215 psi, G_w = 38 ksi.

Facings: GFRP, $1 = 1-\mu^2 = 1-(0.06)^2 = 0.997$
$E_f = 1.78 \times 10^6$ psi
F_{cy} = 24.2 ksi

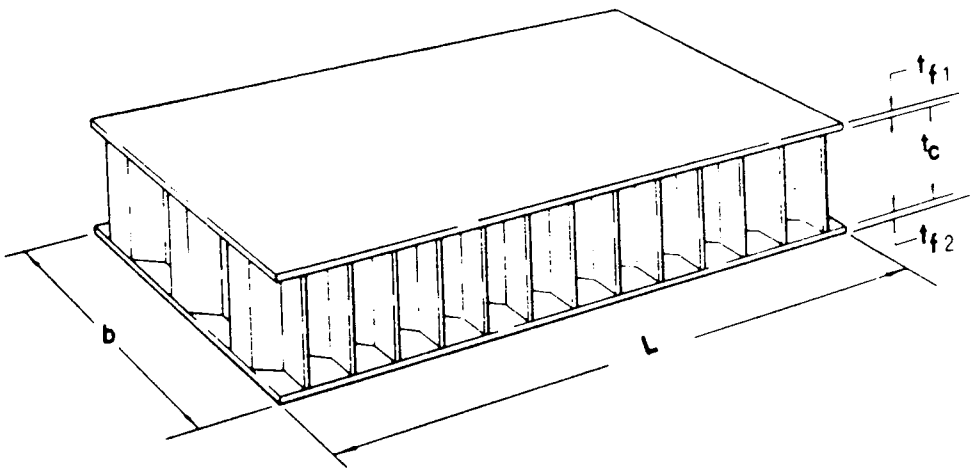

Figure F-1. Configuration of Honeycomb Sandwich (Hexcel, 1993)

The panel will be assumed to be simply supported for design purposes.

The dimensions of the plate to be designed are:

Height of the plate, $h = t_{f1} + t_{f2} + t_c = 0.24 + 0.24 + 3.0 = 3.48$ in.

Width of the plate, b= 12 in.

Plate span, L = 34 in.

Cell size, s = 0.25 in.

The imposed loads are:

P = 18,000 lb., applied at the center of the plate.

M = 0.25PL = 0.25(18000)(34) = 153000 in-lb.

V = 9000 lb

1. Check face yielding in the GFRP face sheets:

$$\sigma_c = \frac{M}{t_f hb} = \frac{153000}{(0.48)(3.48)(12)} = 7.6 \text{ ksi} < 28 \text{ ksi}$$

$\therefore$ yield stress OK.

2. Check the core stress due to shear loads:

$$\tau_c = \frac{V}{hb} = \frac{9000}{(3.48)(12)} = 215 \text{ psi} \leq 215 \text{ psi}$$

just adequate, $\therefore$ OK.

3. Check the beam deflection:

$$\Delta = \frac{2K_bPL^3}{E_ft_fh^2b} + \frac{K_sPL}{hG_wb}$$

$$\Delta = \frac{2(.02083)(18000)(34)^3(.996)}{1.78 \times 10^6(0.48)(3.28)^2(12)} + \frac{.25(18000)(34)}{3.48(38 \times 10^3)(12)}$$

$$\Delta = 0.266 + 0.096$$

$$\Delta = 0.363 \text{ in.}$$

4. Check face dimpling:

$$\sigma_{cr} = \frac{2E_f}{\lambda}\left(\frac{t_f}{s}\right)^2 = \frac{2(5 \times 10^6)}{0.88}\left(\frac{0.28}{0.25}\right)^2 = 13.2 \times 10^6 > 28 \text{ ksi}, \therefore \text{not critical}$$

5. Check face wrinkling:

$$\sigma_{cr} = 0.82E_f\frac{E_ct_f}{E_ft_c} = 0.82(1.78 \times 10^6)\frac{(148 \times 10^3)(0.28)}{(1.78 \times 10^6)(3)}$$

$$\sigma_{cr} = 129 \text{ ksi} > 28 \text{ ksi}, \therefore \text{not critical.}$$

The above design satisfies all of the design criteria for a honeycomb panel, therefore, aluminum commercial grade core, ACG-1/4-4.8 can be used in this design.

APPENDIX G

DESIGN REFINEMENT

The result of the materials tests has raised the question of adequacy in the initial design. The materials used to construct the FRPC units have moduli that are one quarter and tensile strengths that are one sixth of the design values. Is this reduction in stiffness and strength detrimental to the intended purpose?

The intent of the design is to bridge a deteriorated thermal crack. The initial design assumed that the cracked area to be spanned by the FRPC unit would be about 34 inches wide. In actual use, the ability to span a crack this wide will not be required. The pavement cracks themselves are not more than three or four inches wide. However, there is a zone of deteriorated pavement that can extend up to twelve inches on either side of the crack. This deteriorated zone is an area of lessened support so that the FRPC unit must carry a portion of the load and act as a stiffener in the deteriorated area of the pavement.

Adequacy of the design with as-manufactured material properties for these less stringent requirements was evaluated using finite element analysis. The program used for analysis was the same as that used for pavement properties validation and initial design studies. An axisymmetric and a plane strain analysis using constant strain triangle elements was run to evaluate the stresses in the FRPC units. Crack

widths of 0.5 inches up to 4 inches were simulated by assigning very low modulus values to elements in the area of the crack. Softening of the adjoining asphalt pavement due to stripping was modeled by gradually increasing the modulus values of the elements as one moves away from the crack. The results of the axisymmetric analysis are presented in tabular form in Table G-1.

Table G-1 - Stress Level in Composite Skin, Axisymmetric Analysis

Crack Width (in.)	Softened Zone Width (in.)	Surface Deflection	Averaged Stress Level, σ_θ	
			Upper Skin (psi)	Lower Skin (psi)
0.0	0.0	- 0.0120	84.1	55.0
1.0	0.0	- 0.0121	83.8	66.1
2.0	0.0	- 0.0128	82.0	69.7
4.0	0.0	- 0.0147	77.0	67.2
8.0	0.0	- 0.0266	65.9	79.9
2.0	1.0	- 0.0135	80.1	68.4
2.0	2.0	- 0.0145	78.4	69.9
2.0	3.0	- 0.0162	77.7	70.8
2.0	4.0	- 0.0188	78.7	71.2

The results tabulated for the axisymmetric analysis indicate that the reduced materials properties should not have an adverse effect on the surface deflection of the

pavement under the factored design load. Only the theta stress from the finite element analysis was listed in the table. This stress value was the largest of the four stresses generated.

The stress values from the axisymmetric analysis are difficult to interpret and appear to be lower than expected. As a comparison, a plane strain analysis was run in order to obtain stresses that would be easier to interpret. The results from this set of analyses are presented in Table G-2.

Table G-2 - Stress Level in Composite Skin, Plane Strain Analysis

Crack Width (in.)	Softened Zone Width (in.)	Surface Deflection (in.)	Principal Stresses Upper Skin σ_{max} (psi)	Upper Skin σ_{min} (psi)	Lower Skin σ_{max} (psi)	Lower Skin σ_{min} (psi)
0.0	0.0	- 0.229	- 1.62	- 137	- 11.5	- 135
1.0	0.0	- 0.266	- 133	- 270	496	- 397
2.0	0.0	- 0.333	- 135	- 639	505	- 343
4.0	0.0	- 0.438	- 136	- 1183	706	- 181
8.0	0.0	- 0.985	- 142	- 1870	1497	- 147
2.0	2.0	- 0.375	- 137	- 859	569	- 273
2.0	4.0	- 0.422	- 137	- 955	654	- 269
2.0	6.0	- 0.479	- 137	- 936	679	- 281
2.0	8.0	- 0.550	- 137	- 828	633	- 301

The results tabulated above show a very large surface deformation for the factored design load. The reason for this result is a plane strain analysis assumes an infinite expanse in the z-direction, which means that both the model and the loading extend infinitely in the z-direction. This assumption is not true for this situation. The loaded area is circular in shape and limited in extent to a radius of 6 inches around the point of application. For this application, a plane strain analysis will overestimate the stress and surface deformation. This does not invalidate the results of the analysis. The results can be used to set an upper bound on the stress values that could be expected under the factored design load.

Examination of the stress levels for the different pavement conditions indicates that all maximum values for the principal stresses are less than 8 percent of the tensile strength for the woven cloth. The maximum shear stress values are also less than 21 percent of the ±45 angle ply tensile strength.

The conclusion that may be drawn from this set of analyses is that the proposed design configuration may be built with woven E-glass cloth. The design will satisfy the deflection requirements for the repair and the stress levels in the glass fiber skins are low enough that a five year service life can be expected.

APPENDIX H

INSTRUMENTATION

Performance of the three FRPC units had to be monitored in order to determine the adequacy of the concept under field conditions. Two methods were selected to determine the performance. The first method was evaluation by the Falling Weight Deflectometer. This procedure would determine the deflection characteristics of the repaired area and permit a comparison with an undamaged asphalt pavement. The second method involved mounting strain gages on the glass fiber skins of the FRPC units and monitoring the surface strains under load. This method would measure the mechanical strain in the glass fiber skins and yield an estimate of the stress level in the skins.

Selection of the strain gage type to be used is a straightforward process. Since fiber reinforced plastics are anisotropic, a single gage or two gage rosette is not sufficient to determine the true strain state of the point under study. The effect of gage misalignment can induce considerable errors in the measurement of strain. Misalignment can be compensated for by using a three gage rosette. The three gage rosette yields three independent measurements of strain, which can be used to determine the major and minor principal strains and their directions.

The strain gage rosette selected for use on the FRPC units was the Measurements Group CEA-06-250UR-350 rectangular strain gage rosette. This gage

was selected because the 350 ohm resistance would reduce heating effects and the rectangular arrangement of the gages would facilitate alignment.

Temperature compensation of the gages was achieved by mounting a temperature sensor on the top skin of the FRPC units. The temperature sensor, a Measurements Group ETG-50B resistance sensor, was selected because it is compatible with the strain indicator units used to read the strain gages and would reduce the instrumentation required. Thermal compensation through the use of a dummy gage was not considered because of the difficulty of finding an unstrained portion of the FRPC unit that could be used as a mount for the dummy gage.

The temperature/strain relationship was obtained by mounting a rosette and a temperature gage on a piece of glass fiber composite skin from the production run. The skin with the mounted gages was placed in a laboratory oven and freezer and subjected to a temperature range of -7 degrees C to +80 degrees C. The thermal strains recorded by the rosette and the output of the temperature sensor were recorded and a correction factor chart was developed. This chart was used to correct the indicated strain results from field measurements for temperature induced strains.

A set of eleven gage rosettes were mounted on the honeycomb sandwich FRPC units and nine gage rosettes were mounted on the box beam unit. The gage configurations for each type of unit are shown in Figures H-1 and H-2 for the honeycomb sandwich units and Figures H-3 and H-4 for the box beam unit. The

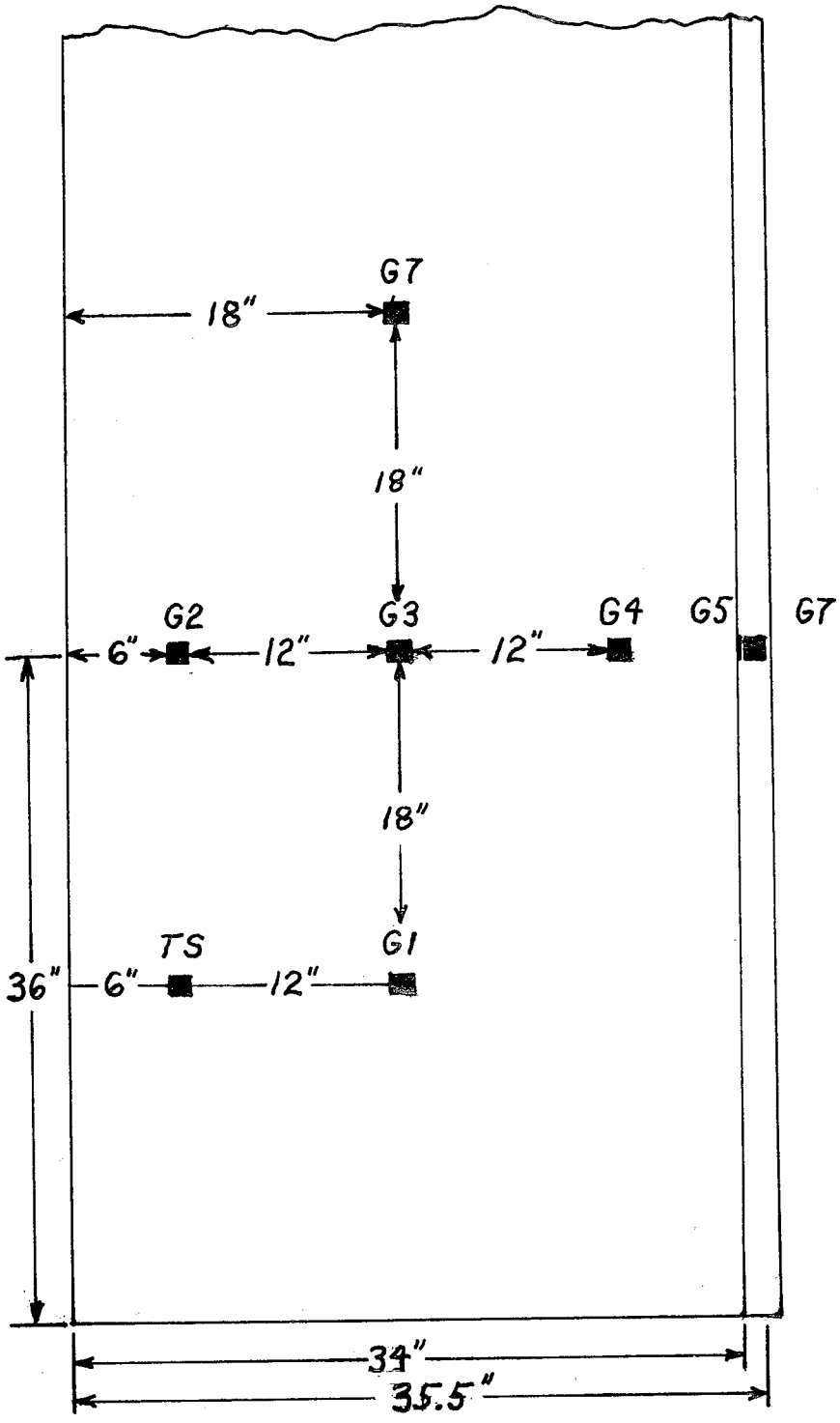

Figure H-1. Strain Gage Configuration for Honeycomb Sandwich Units, Upper Surface

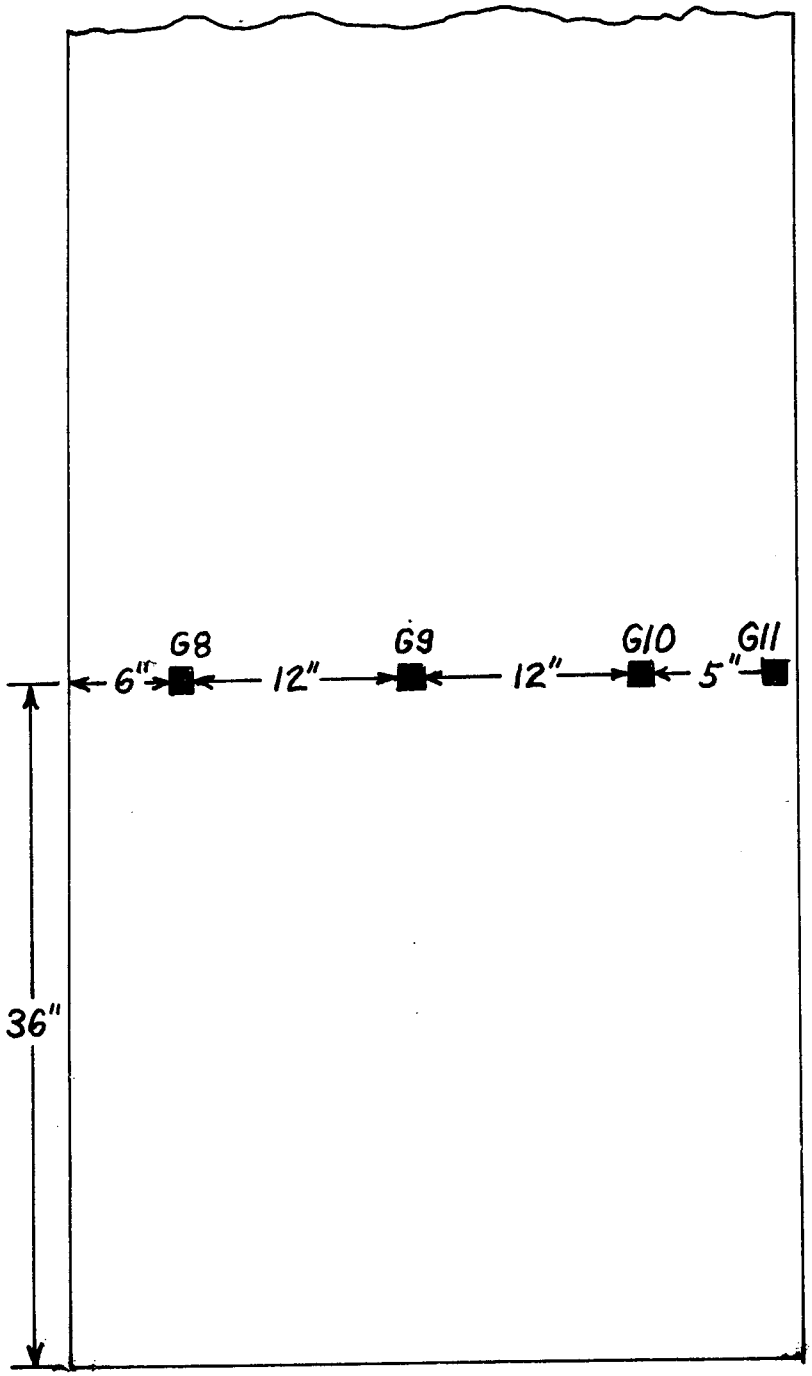

Figure H-2. Strain Gage Configuration for Honeycomb Sandwich Units, Lower Surface

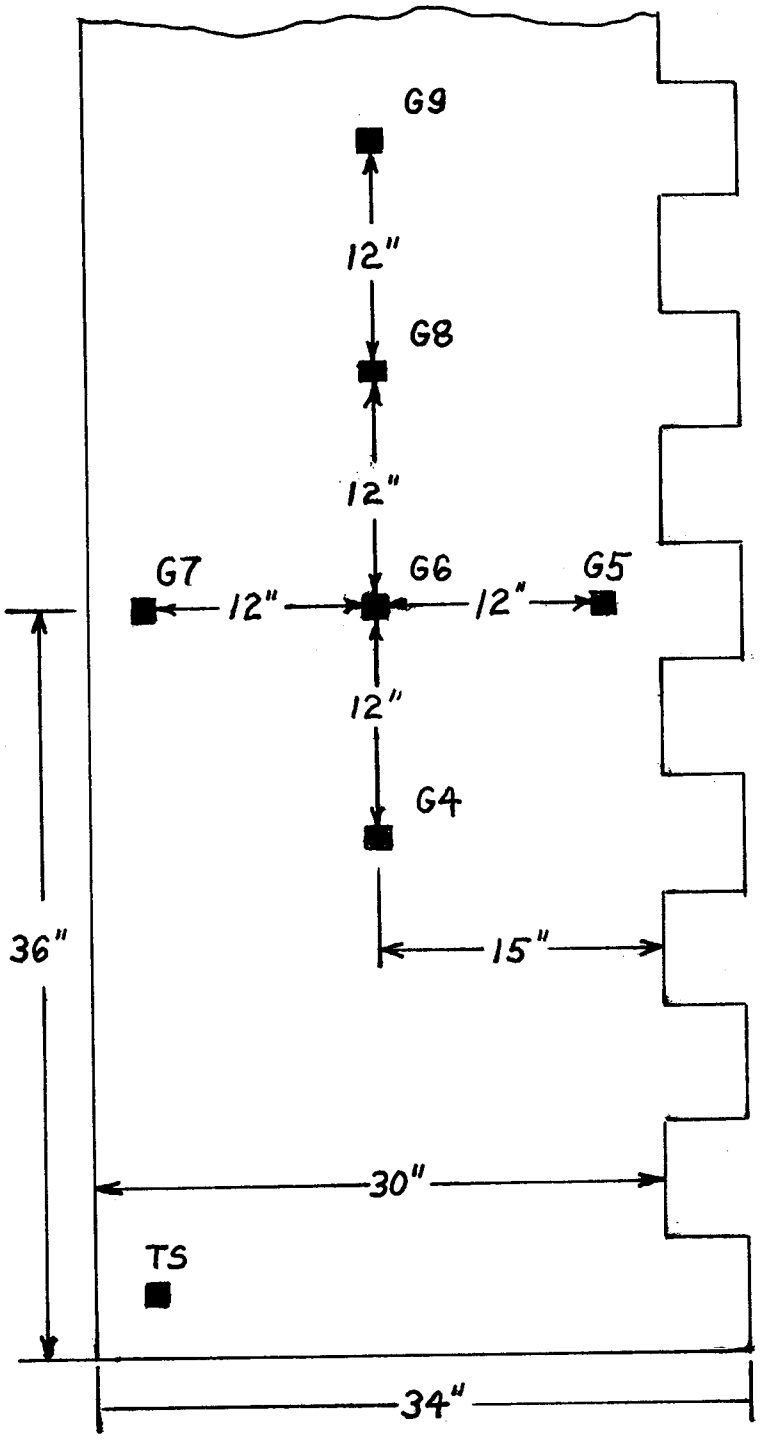

Figure H-3. Strain Gage Configuration for FRPC Box Beam Unit, Upper Surface

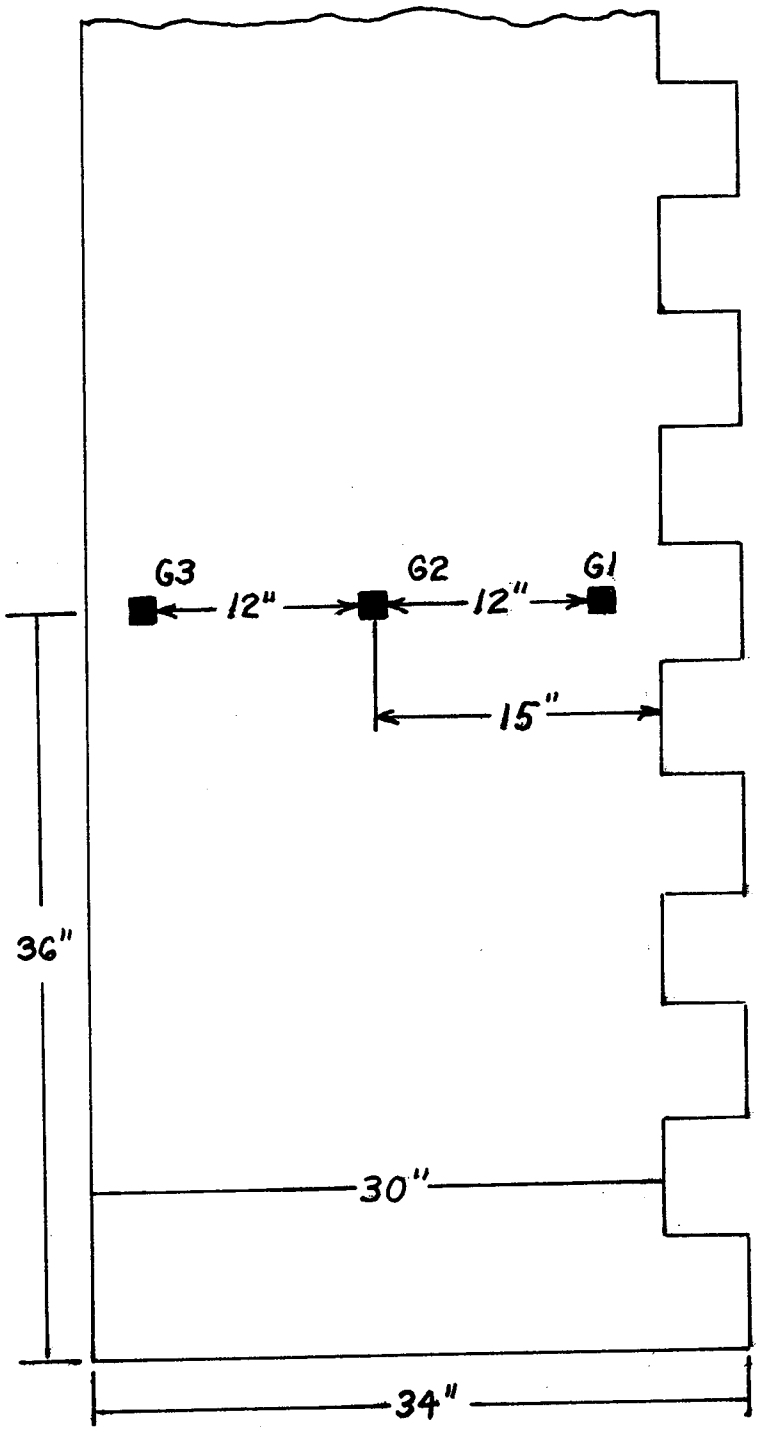

Figure H-4. Strain Gage Configuration for FRPC Box Beam Unit, Upper Surface

rosettes are arranged on the upper and lower surfaces of a wheel path so as to pick up the bending strains induced by loads traversing the repaired crack. The upper skin on each unit carries the temperature sensor and additional gages located 18 inches on either side of the wheel track to detect the amount of load sharing done by portions of the FRPC units outside the loaded area. Gages are also mounted on the dowel lip of the two honeycomb units to determine the load transmitted to the dowel section by a wheel load.

The strain gages were wired with vinyl insulated three conductor cable. Each rosette was wired with three cables, one for each gage. Two of the conductors were doubled up on one side of the gage to compensate for cable resistance. The cable runs for the gages were between 24 and 36 feet in length and terminated in a steel box set in the soil two feet beyond the outside edge of the shoulder. Approximately 1,000 feet of three conductor cable was required to instrument each FRPC unit.

In addition to the strain gage instrumentation, bending beam linear strain detectors were constructed and placed and bolted onto each of the FRPC units. The purpose of these detectors was to indicate if the expansion joint at the dowel end of the unit was functioning as intended. These detectors were constructed of 22 gauge steel bent into a square wave shape as shown in Figure H-5. Each detector was instrumented with four strain gages wired in a full bridge arrangement. Two three conductor cables were used to connect the strain detectors to the strain indicator. The sensitivity of these units were 65 microstrains for a movement of 0.001 inches. The

bending beam strain detectors were calibrated for thermal output in the same fashion as the strain gage rosettes.

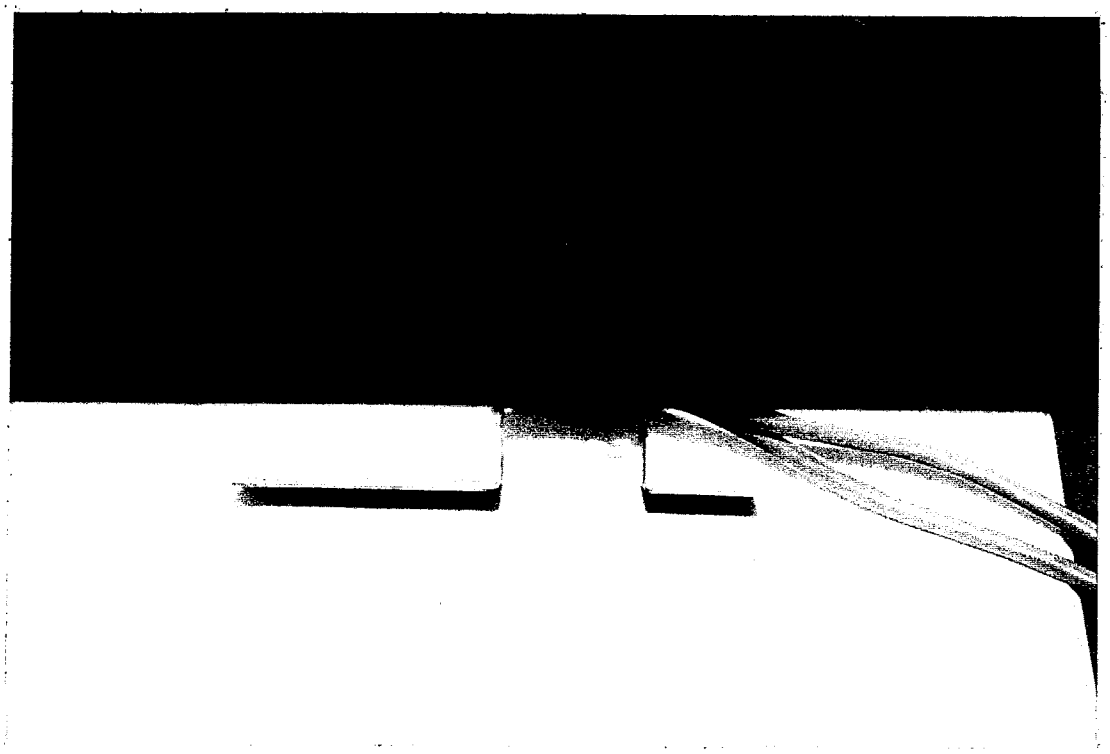

Figure H-5. Bending Beam Linear Strain Detector

APPENDIX I

FIELD OBSERVATIONS

After the FRPC units had been installed by the KDOT Area One maintenance forces, a program of field evaluation was begun. This program consisted of taking measurements of the surface deflection characteristics of the repaired cracks with the FWD and a series of static load tests on each of the units. The FWD measurements were taken with the KDOT FWD equipment using the KDOT standard 9000 pound impact load. A description of the equipment and procedure is presented in Chapter 2 of this report.

Deflection basin measurements on the units were taken on October 9, 1987 and November 25, 1987. A sample of the output data from the FWD is presented in Figure I-1. This figure shows a series of four deflection measurements. The first two measurements are on undamaged pavement just in front of the first honeycomb sandwich unit. The third measurement is on the center of the repaired crack and the fourth is on the undeteriorated pavement just beyond the repaired crack. The maximum deflection under the applied load ranges between 27.95 and 28.04 mils (0.001 in. = 1 mil) for the three load applications.

```
R80   53   9710090360031136F20
701053008002-122301961  03211  8
150 0   305 610 914 121915241829 5.9   0    12   24   36   48   60   72
A:\                  .FWD
03600311

KDOT STANDARD.(FEET).....
*
S     0WB       20 15 I61044   68  58  Heights .....
578 123 104  88  73  59  47  37  9188  4.83  4.10  3.48  2.89  2.31  1.83  1.44
580 122 105  88  73  59  46  36  9212  4.82  4.13  3.47  2.88  2.31  1.83  1.41
577 122 105  88  73  58  46  36  9169  4.78  4.12  3.45  2.86  2.29  1.80  1.41
S     54WB      21 15 I61045   69  58  Heights .....
575 130 112  95  80  68  53  39  9141  5.11  4.42  3.74  3.15  2.66  2.08  1.52
575 125 108  91  76  63  49  36  9141  4.94  4.26  3.57  2.98  2.48  1.93  1.41
575 129 112  95  80  67  52  39  9141  5.08  4.41  3.73  3.14  2.65  2.06  1.52
S     57WB      20 15 I61045   68  58  Heights .....
538 710 328 112  85  64  46  36  8541 27.95 12.91  4.41  3.34  2.50  1.81  1.42
536 711 329 113  85  64  47  35  8517 28.00 12.94  4.45  3.36  2.52  1.85  1.37
536 712 330 113  85  64  46  37  8521 28.04 12.98  4.46  3.36  2.51  1.81  1.44
S     59WB      20 15 I61047   68  58  Heights .....
576 129 110  92  75  60  47  36  9149  5.09  4.33  3.64  2.97  2.37  1.87  1.41
575 131 111  94  77  62  48  38  9129  5.15  4.37  3.69  3.02  2.43  1.89  1.50
574 127 108  90  73  58  45  36  9121  5.00  4.26  3.55  2.89  2.30  1.76  1.40
 EOF
```

Figure I-1. Sample FWD Data

A second phase to the field evaluation of the FRPC members was a static field load test. The load test consisted of applying an approximate 18,000 pound axle load to each of the FRPC units and measuring the strains on the fiberglass skins of the units.

Instrumentation for the load test consisted of Measurements Group SB-1 switch and balance units and a BLH 120 Strain Indicator. The strain gage cables were connected to the strain indicator through the SB-1 switch and balance units.

Appendix H described the location and placement of the strain gages on each of the FRPC members. The temperature sensor installed on each unit was read using the strain indicator through a resistive bridge adapter unit.

The loading system used for these tests was a KDOT maintenance truck with a single dual rear axle. The bed of the truck was loaded with sufficient sand to produce an axle load in the range of 18,000 to 25,000 pounds. The load carried by the truck was determined through weight measurement at a certified scale. The load was applied to the units in a stepwise fashion. A set of strain gage readings were taken prior to application of the load to provide a baseline point. Next, the load was applied to a point approximately 6 inches onto the unit under test. Each of the strain gages were read for this load location. The load was then moved to the center of the unit and the strain gage readings were repeated. The load was then applied at a point approximately 6 inches from the end of the FRPC unit and the strain gages were read again. Finally, the load was run off of the unit and readings were taken for a no-load condition.

After the load test was completed, the recorded readings were brought back and reduced. Reduction of the readings consisted of adjusting the readings for thermal effects. This was done by subtracting the apparent strain due to temperature obtained

from the calibration runs discussed in Appendix H. The corrected strain readings for each gage was then converted into principal strains by means of a computer program written for the purpose. The principal strains for the stain gages from the two load tests are presented at the end of this Appendix.

load test 1 beam 1 gage 1
CORRECTED GAGE OUTPUT IN MICROSTRAINS

LOAD	GAGE A	GAGE B	GAGE C
2680.000	-244.285	-124.471	-108.897
26800.000	-381.690	-523.549	-717.652
2680.000	-234.336	-284.740	-98.949
0.000	-99.888	-39.858	0.400

PRINCIPAL STRAINS AND ANGLE

LOAD	EPSILON-1	EPSILON-2	BETA (WRT GAGE A)
2680.000	-91.157	-262.025	-18.797
26800.000	-379.672	-719.671	4.420
2680.000	-30.519	-302.766	30.089
0.000	1.365	-100.853	-5.577

load test 1 beam 1 gage 2
CORRECTED GAGE OUTPUT IN MICROSTRAINS

LOAD	GAGE A	GAGE B	GAGE C
2680.000	-357.578	-353.784	-502.994
26800.000	-487.431	-263.396	-502.475
2680.000	-189.307	25.654	-119.106
0.000	-69.582	-29.734	-84.625

PRINCIPAL STRAINS AND ANGLE

LOAD	EPSILON-1	EPSILON-2	BETA (WRT GAGE A)
2680.000	-324.744	-535.827	23.228
26800.000	-263.274	-726.632	44.070
2680.000	29.047	-337.460	-39.479
0.000	-29.141	-125.066	40.489

load test 1 beam 1 gage 3
CORRECTED GAGE OUTPUT IN MICROSTRAINS

LOAD	GAGE A	GAGE B	GAGE C
2680.000	-244.505	-199.688	-53.959
26800.000	-510.725	-803.282	-921.903
2680.000	-324.695	-129.568	16.282
0.000	-69.801	-54.879	-29.687

PRINCIPAL STRAINS AND ANGLE

LOAD	EPSILON-1	EPSILON-2	BETA (WRT GAGE A)
2680.000	-41.423	-257.041	13.953
26800.00 0	-493.087	-939.541	-11.465
2680.000	18.053	-326.466	-4.112
0.000	-29.040	-70.448	7.181

load test 1 beam 1 gage 4
CORRECTED GAGE OUTPUT IN MICROSTRAINS

LOAD	GAGE A	GAGE B	GAGE C
2680.000	-109.776	-94.867	-24.532
26800.000	-369.225	-369.613	-88.421
2680.000	-558.891	-374.182	-117.628
0.000	-69.761	-69.881	-39.675

PRINCIPAL STRAINS AND ANGLE

LOAD	EPSILON-1	EPSILON-2	BETA (WRT GAGE A)
2680.000	-16.315	-117.994	16.516
26800.000	-29.989	-427.656	22.540
2680.000	-114.722	-561.796	4.624
0.000	-33.360	-76.077	22.613

load test 1 beam 1 gage 5
CORRECTED GAGE OUTPUT IN MICROSTRAINS

LOAD	GAGE A	GAGE B	GAGE C
2680.000	25.072	-40.057	-25.072
26800.000	-114.971	-135.014	25.431
2680.000	-215.797	-235.426	260.567
0.000	-14.983	-50.042	0.060

PRINCIPAL STRAINS AND ANGLE

LOAD	EPSILON-1	EPSILON-2	BETA (WRT GAGE A)
2680.000	47.257	-47.257	-28.979
26800.000	69.564	-159.103	26.060
2680.000	373.380	-328.610	23.633
0.000	35.778	-50.701	39.991

load test 1 beam 1 gage 6
CORRECTED GAGE OUTPUT IN MICROSTRAINS

LOAD	GAGE A	GAGE B	GAGE C
2680.000	59.933	-50.191	-0.240
26800.000	120.245	-165.286	-95.373
2680.000	-25.012	-205.264	10.089
0.000	209.784	-145.616	-5.833

PRINCIPAL STRAINS AND ANGLE

LOAD	EPSILON-1	EPSILON-2	BETA (WRT GAGE A)
2680.000	115.352	-55.659	-34.700
26800.000	220.301	-195.429	-29.379
2680.000	191.118	-206.041	42.465
0.000	372.020	-168.070	-33.235

load test 1 beam 1 gage 7
CORRECTED GAGE OUTPUT IN MICROSTRAINS

LOAD	GAGE A	GAGE B	GAGE C
2680.000	95.732	-84.893	-210.144
26800.000	252.236	-89.371	-630.291
2680.000	100.667	150.404	-195.180
0.000	10.089	-9.984	-25.012

PRINCIPAL STRAINS AND ANGLE

LOAD	EPSILON-1	EPSILON-2	BETA (WRT GAGE A)
2680.000	98.218	-212.629	-5.131
26800.000	263.349	-641.404	6.363
2680.000	199.626	-294.140	26.595
0.000	10.269	-25.192	-4.090

load test 1 beam 1 gage 8
CORRECTED GAGE OUTPUT IN MICROSTRAINS

LOAD	GAGE A	GAGE B	GAGE C
2680.000	469.372	-41.044	23.094
26800.000	508.987	209.065	107.839
2680.000	175.223	89.989	-105.581
0.000	10.288	5.137	-74.956

PRINCIPAL STRAINS AND ANGLE

LOAD	EPSILON-1	EPSILON-2	BETA (WRT GAGE A)
2680.000	609.990	-117.524	-26.081
26800.000	532.244	84.582	-13.175
2680.000	185.673	-116.031	10.726
0.000	24.417	-89.085	20.660

load test 1 beam 1 gage 9
CORRECTED GAGE OUTPUT IN MICROSTRAINS

LOAD	GAGE A	GAGE B	GAGE C
2680.000	249.939	-110.546	-55.937
26800.000	635.285	697.733	996.319
2680.000	310.131	189.893	-121.104
0.000	8.954	19.993	8.954

PRINCIPAL STRAINS AND ANGLE

LOAD	EPSILON-1	EPSILON-2	BETA (WRT GAGE A)
2680.000	354.811	-160.809	-26.807
26800.000	1031.502	600.102	16.594
2680.000	330.285	-141.258	11.931

load test 1 beam 1 gage 10
CORRECTED GAGE OUTPUT IN MICROSTRAINS

LOAD	GAGE A	GAGE B	GAGE C
2680.000	150.031	-70.300	-50.543
26800.000	410.138	69.582	-151.470
2680.000	629.871	279.434	-147.354
0.000	30.106	-30.033	-35.081

PRINCIPAL STRAINS AND ANGLE

LOAD	EPSILON-1	EPSILON-2	BETA (WRT GAGE A)
2680.000	206.167	-106.678	-25.062
26800.000	416.426	-157.757	-6.006
2680.000	631.742	-149.225	2.805
0.000	40.187	-45.162	-20.101

load test 1 beam 1 gage 11
CORRECTED GAGE OUTPUT IN MICROSTRAINS

LOAD	GAGE A	GAGE B	GAGE C
2680.000	164.954	89.870	-35.620
26800.000	354.721	199.639	-31.385
2680.000	609.454	419.455	-37.398
0.000	5.054	15.041	-15.003

PRINCIPAL STRAINS AND ANGLE

LOAD	EPSILON-1	EPSILON-2	BETA (WRT GAGE A)
2680.000	168.073	-38.738	7.053
26800.000	358.419	-35.083	5.564
2680.000	635.896	-63.839	11.209
0.000	17.413	-27.362	31.694

load test 2 beam 1 gage 1
CORRECTED GAGE OUTPUT IN MICROSTRAINS

LOAD	GAGE A	GAGE B	GAGE C
2416.000	-9.709	-9.855	-69.881
24160.000	21.336	-179.620	-339.698
2416.000	-39.715	-99.944	-59.773
0.000	-29.966	-9.955	0.120

PRINCIPAL STRAINS AND ANGLE

LOAD	EPSILON-1	EPSILON-2	BETA (WRT GAGE A)
2416.000	2.650	-82.241	22.431
24160.000	22.489	-340.851	-3.230
2416.000	1.448	-100.936	-39.351
0.000	0.919	-30.766	-9.139

load test 2 beam 1 gage 2
CORRECTED GAGE OUTPUT IN MICROSTRAINS

LOAD	GAGE A	GAGE B	GAGE C
2416.000	-268.937	-339.570	-188.708
24160.000	-339.538	-259.655	-18.619
2416.000	-90.179	10.054	70.281
0.000	-30.166	40.017	50.064

PRINCIPAL STRAINS AND ANGLE

LOAD	EPSILON-1	EPSILON-2	BETA (WRT GAGE A)
2416.000	-111.034	-346.611	35.044
24160.000	0.476	-358.633	13.332
2416.000	72.737	-92.635	-7.000
0.000	60.082	-40.184	-18.427

load test 2 beam 1 gage 4
CORRECTED GAGE OUTPUT IN MICROSTRAINS

LOAD	GAGE A	GAGE B	GAGE C
2416.000	-20.137	-10.054	40.035
24160.000	-299.503	-169.566	-38.756
2416.000	-349.327	-319.621	-68.523
0.000	-19.978	-30.003	0.080

PRINCIPAL STRAINS AND ANGLE

LOAD	EPSILON-1	EPSILON-2	BETA (WRT GAGE A)
2416.000	46.078	-26.180	16.809
24160.000	-38.756	-299.504	0.096
2416.000	-30.133	-387.716	19.127
0.000	12.473	-32.371	31.716

load test 2 beam 1 gage 5
CORRECTED GAGE OUTPUT IN MICROSTRAINS

LOAD	GAGE A	GAGE B	GAGE C
2416.000	19.938	39.998	9.909
24160.000	-99.928	-119.993	10.388
2416.000	-140.961	49.793	280.245
0.000	-19.978	-9.974	0.080

PRINCIPAL STRAINS AND ANGLE

LOAD	EPSILON-1	EPSILON-2	BETA (WRT GAGE A)
2416.000	40.494	-10.648	39.346
24160.000	48.509	-138.048	26.875
2416.000	281.178	-141.895	2.692
0.000	0.080	-19.978	0.073

load test 2 beam 1 gage 6
CORRECTED GAGE OUTPUT IN MICROSTRAINS

LOAD	GAGE A	GAGE B	GAGE C
2416.000	-119.705	-159.910	-39.476
24160.000	1699.128	2170.238	-266.500
2416.000	1458.798	2060.260	-115.710
0.000	1468.627	2230.404	-75.795

PRINCIPAL STRAINS AND ANGLE

LOAD	EPSILON-1	EPSILON-2	BETA (WRT GAGE A)
2416.000	10.190	-169.371	31.730
24160.000	2471.255	-1038.627	27.971
2416.000	2267.884	-924.795	30.226
0.000	2413.806	-1020.974	31.640

load test 2 beam 1 gage 7
CORRECTED GAGE OUTPUT IN MICROSTRAINS

LOAD	GAGE A	GAGE B	GAGE C
2416.000	-79.311	-179.799	-149.512
24160.000	-77.433	-208.905	-618.983
2416.000	-79.710	20.288	-49.624
0.000	-39.915	-49.972	-9.829

PRINCIPAL STRAINS AND ANGLE

LOAD	EPSILON-1	EPSILON-2	BETA (WRT GAGE A)
2416.000	-40.198	-188.625	-30.887
24160.000	-43.701	-652.715	13.612
2416.000	21.609	-150.944	-39.979
0.000	4.391	-54.135	29.532

load test 2 beam 1 gage 8
CORRECTED GAGE OUTPUT IN MICROSTRAINS

LOAD	GAGE A	GAGE B	GAGE C
2416.000	379.453	159.412	28.448
24160.000	330.188	129.807	-141.161
2416.000	119.945	39.858	-20.457
0.000	299.663	19.431	-1.199

PRINCIPAL STRAINS AND ANGLE

LOAD	EPSILON-1	EPSILON-2	BETA (WRT GAGE A)
2416.000	385.016	22.885	-7.120
24160.000	332.817	-143.789	4.259
2416.000	120.638	-21.150	-4.008
0.000	347.922	-49.458	-20.395

load test 2 beam 1 gage 9

CORRECTED GAGE OUTPUT IN MICROSTRAINS

LOAD	GAGE A	GAGE B	GAGE C
2416.000	229.821	209.882	-20.896
24160.000	486.213	678.382	807.132
2416.000	209.964	59.767	-50.783
0.000	39.875	29.923	19.818

PRINCIPAL STRAINS AND ANGLE

LOAD	EPSILON-1	EPSILON-2	BETA (WRT GAGE A)
2416.000	268.256	-59.331	20.031
24160.000	810.235	483.110	-5.589
2416.000	211.462	-52.281	-4.323
0.000	39.875	19.817	0.220

load test 2 beam 1 gage 10

CORRECTED GAGE OUTPUT IN MICROSTRAINS

LOAD	GAGE A	GAGE B	GAGE C
2416.000	100.087	100.044	-50.343
24160.000	299.703	219.737	-11.187
2416.000	339.778	119.574	-41.314
0.000	-10.069	-10.034	20.017

PRINCIPAL STRAINS AND ANGLE

LOAD	EPSILON-1	EPSILON-2	BETA (WRT GAGE A)
2416.000	131.212	-81.468	22.492
24160.000	317.059	-28.544	12.950
2416.000	342.072	-43.608	-4.424
0.000	26.224	-16.275	22.467

load test 2 beam 1 gage 11

CORRECTED GAGE OUTPUT IN MICROSTRAINS

LOAD	GAGE A	GAGE B	GAGE C
2416.000	139.763	149.896	19.418
24160.000	129.734	209.982	29.447
2416.000	349.407	229.532	48.545
0.000	9.909	19.969	19.938

PRINCIPAL STRAINS AND ANGLE

LOAD	EPSILON-1	EPSILON-2	BETA (WRT GAGE A)
2416.000	172.130	-12.949	24.721
24160.000	219.291	-60.110	34.483
2416.000	352.479	45.473	5.741
0.000	22.037	7.810	-22.589

load test 2 beam2 gage 1

CORRECTED GAGE OUTPUT IN MICROSTRAINS

LOAD	GAGE A	GAGE B	GAGE C
2416.000	-100.275	-120.106	120.198
24160.000	0.270	-59.953	-89.924
2416.000	-29.915	20.064	-19.893
0.000	-10.051	40.019	20.013

PRINCIPAL STRAINS AND ANGLE

LOAD	EPSILON-1	EPSILON-2	BETA (WRT GAGE A)
2416.000	180.460	-160.537	24.859
24160.000	2.739	-92.393	-9.271
2416.000	20.342	-70.150	-41.821
0.000	43.107	-33.146	-33.390

load test 2 beam 2 gage 2
CORRECTED GAGE OUTPUT IN MICROSTRAINS

LOAD	GAGE A	GAGE B	GAGE C
2416.000	-209.463	130.422	-119.269
24160.000	-259.450	60.412	-109.128
2416.000	-50.078	70.060	40.116
0.000	-10.022	-50.036	10.022

PRINCIPAL STRAINS AND ANGLE

LOAD	EPSILON-1	EPSILON-2	BETA (WRT GAGE A)
2416.000	133.852	-462.583	-40.651
24160.000	71.695	-440.273	-36.463
2416.000	82.568	-92.530	-29.498
0.000	51.030	-51.030	39.337

load test 2 beam 2 gage 4
CORRECTED GAGE OUTPUT IN MICROSTRAINS

LOAD	GAGE A	GAGE B	GAGE C
2416.000	48.849	119.667	369.537
24160.000	-158.726	-149.569	-379.199
2416.000	-269.862	-39.789	30.784
0.000	-50.108	-10.007	50.108

PRINCIPAL STRAINS AND ANGLE

LOAD	EPSILON-1	EPSILON-2	BETA (WRT GAGE A)
2416.000	392.837	25.549	14.588
24160.000	-106.460	-431.464	23.642
2416.000	50.628	-289.706	-13.974
0.000	51.097	-51.097	5.647

load test 2 beam 2 gage 5
CORRECTED GAGE OUTPUT IN MICROSTRAINS

LOAD	GAGE A	GAGE B	GAGE C
2416.000	49.778	109.969	59.799
24160.000	-120.258	-110.079	120.258
2416.000	-259.870	-199.914	30.754
0.000	-20.043	-20.014	20.043

PRINCIPAL STRAINS AND ANGLE

LOAD	EPSILON-1	EPSILON-2	BETA (WRT GAGE A)
2416.000	110.196	-0.619	-42.406
24160.000	163.032	-163.032	21.235
2416.000	53.968	-283.084	15.215
0.000	28.325	-28.325	22.480

load test 2 beam 2 gage 6
CORRECTED GAGE OUTPUT IN MICROSTRAINS

LOAD	GAGE A	GAGE B	GAGE C
2416.000	109.967	59.953	-20.313
24160.000	100.125	140.070	-70.241
2416.000	219.934	310.042	-40.626
0.000	69.971	29.962	-10.201

PRINCIPAL STRAINS AND ANGLE

LOAD	EPSILON-1	EPSILON-2	BETA (WRT GAGE A)
2416.000	111.700	-22.046	6.537
24160.000	166.313	-136.428	27.877
2416.000	345.669	-166.361	29.706
0.000	69.971	-10.201	0.055

load test 2 beam 2 gage 7
CORRECTED GAGE OUTPUT IN MICROSTRAINS

LOAD	GAGE A	GAGE B	GAGE C
2416.000	50.377	150.197	-140.031
24160.000	201.090	130.312	-420.244
2416.000	120.018	39.949	-40.326
0.000	9.992	9.997	-0.030

PRINCIPAL STRAINS AND ANGLE

LOAD	EPSILON-1	EPSILON-2	BETA (WRT GAGE A)
2416.000	172.194	-261.848	31.990
24160.000	282.929	-502.083	18.837
2416.000	120.018	-40.326	0.037
0.000	12.071	-2.109	22.516

load test 2 beam 2 gage 8
CORRECTED GAGE OUTPUT IN MICROSTRAINS

LOAD	GAGE A	GAGE B	GAGE C
2416.000	179.638	470.087	69.401
24160.000	232.503	350.919	-899.928
2416.000	80.022	90.015	-30.214
0.000	29.945	100.032	9.902

PRINCIPAL STRAINS AND ANGLE

LOAD	EPSILON-1	EPSILON-2	BETA (WRT GAGE A)
2416.000	474.455	-225.416	40.469
24160.000	554.724	-1222.149	25.204
2416.000	110.212	-60.404	24.876
0.000	100.656	-60.810	41.435

load test 2 beam 2 gage 9
CORRECTED GAGE OUTPUT IN MICROSTRAINS

LOAD	GAGE A	GAGE B	GAGE C
2416.000	200.310	170.082	-160.464
24160.000	287.836	379.345	638.589
2416.000	230.375	49.996	-190.529
0.000	69.971	49.976	-10.201

PRINCIPAL STRAINS AND ANGLE

LOAD	EPSILON-1	EPSILON-2	BETA (WRT GAGE A)
2416.000	254.630	-214.783	19.887
24160.000	657.611	268.814	12.779
2416.000	232.513	-192.666	4.066
0.000	74.724	-14.954	13.310

load test 2 beam 2 gage 10
CORRECTED GAGE OUTPUT IN MICROSTRAINS

LOAD	GAGE A	GAGE B	GAGE C
2416.000	50.018	39.999	-20.133
24160.000	239.197	199.704	199.111
2416.000	309.768	209.851	-10.921
0.000	59.949	49.976	-0.180

PRINCIPAL STRAINS AND ANGLE

LOAD	EPSILON-1	EPSILON-2	BETA (WRT GAGE A)
2416.000	58.048	-28.163	17.770
24160.000	247.083	191.225	-22.070
2416.000	320.776	-21.929	10.325
0.000	66.045	-6.275	16.877

load test 2 beam 2 gage 11
CORRECTED GAGE OUTPUT IN MICROSTRAINS

LOAD	GAGE A	GAGE B	GAGE C
2416.000	9.932	39.999	19.953
24160.000	319.639	239.823	29.015
2416.000	649.300	489.653	48.009
0.000	89.864	59.933	19.713

PRINCIPAL STRAINS AND ANGLE

LOAD	EPSILON-1	EPSILON-2	BETA (WRT GAGE A)
2416.000	40.495	-10.610	-39.346
24160.000	333.717	14.937	12.131
2416.000	680.721	16.588	12.563
0.000	90.239	19.338	4.172

load test 2 beam 3 gage 1
CORRECTED GAGE OUTPUT IN MICROSTRAINS

LOAD	GAGE A	GAGE B	GAGE C
2416.000	-587.373	-659.176	-707.631
24160.000	-896.601	-458.554	-876.558
2416.000	-149.813	10.177	-19.533
0.000	-89.834	-39.909	-29.705

PRINCIPAL STRAINS AND ANGLE

LOAD	EPSILON-1	EPSILON-2	BETA (WRT GAGE A)
2416.000	-586.250	-708.754	-5.494
24160.000	-458.437	-1314.722	-44.330
2416.000	30.391	-199.737	-27.760
0.000	-23.737	-95.801	-16.724

load test 2 beam 3 gage 2
CORRECTED GAGE OUTPUT IN MICROSTRAINS

LOAD	GAGE A	GAGE B	GAGE C
2416.000	120.108	44.982	-70.300
24160.000	509.389	554.829	58.421
2416.000	20.133	-65.017	-50.018
0.000	30.065	-35.025	-30.065

PRINCIPAL STRAINS AND ANGLE

LOAD	EPSILON-1	EPSILON-2	BETA (WRT GAGE A)
2416.000	122.203	-72.395	5.955
24160.000	636.386	-68.577	25.115
2416.000	46.194	-76.079	-27.495
0.000	46.159	-46.159	-24.679

load test 2 beam 3 gage 8
CORRECTED GAGE OUTPUT IN MICROSTRAINS

LOAD	GAGE A	GAGE B	GAGE C
2416.000	-305.027	-69.841	95.834
24160.000	-629.227	60.751	-78.044
2416.000	20.043	10.007	-20.043
0.000	29.945	-0.040	9.902

PRINCIPAL STRAINS AND ANGLE

LOAD	EPSILON-1	EPSILON-2	BETA (WRT GAGE A)
2416.000	98.825	-308.018	-4.919
24160.000	144.026	-851.297	-28.187
2416.000	22.402	-22.402	13.266
0.000	42.260	-2.414	-31.672

APPENDIX J

ANALYSIS OF FIELD TEST RESULTS

The deflection data recovered from the FWD is used as input to the MATCH program to compute the modulus values for the repaired section. This has been done for each of the repaired sections. Two series of FWD tests have been performed on the three units since their installation. These tests were conducted on October 9 and November 25, 1997. Each test series consisted of an FWD test on undeteriorated pavement on each side of the repaired crack and one test directly over the center of the repaired crack. The results of these tests are presented in Table J-1.

TABLE J-1 - FWD MEASUREMENTS

Unit	Maximum Deflection (inches)		
	10-9-97	11-25-97	8-24-98
Undeteriorated Pavement	0.006	0.004	0.009
Honeycomb Sandwich #1	0.028	0.025	0.047
Honeycomb Sandwich #2	0.026	0.080	0.047
FRPC Box Beam	0.047	out of service	out of service

A new, full depth bituminous pavement usually has a maximum deflection of about 0.020 inches under a 9,000 pound load. The two honeycomb sandwich beams initially had deflections close to this target value. The box beam unit had more than twice the desirable deflection on the first test. Analysis of the results of a subsequent static load

test revealed that the most probable cause for the greater deflection was buckling in the upper skin of the box beam unit.

The strain gages on all three FRPC beams show that the stresses induced by wheel loads are less than 10 percent of the failure stress in tension. The maximum principal stresses on the lower and upper surfaces of each FRPC beam directly over the thermal crack for an axle load of 24,160 pounds are presented in Table V-2 along with the predicted principal stresses from a finite element analysis (FEA). These results are for the load test run on October 2, 1997.

TABLE J-2 - PRINCIPAL STRESSES

Unit	Upper Surface Principal Stresses Major (psi)	Minor (psi)	Deviator Stress (psi)	Lower Surface Principal Stresses Major (psi)	Minor (psi)	Deviator Stress (psi)
Honeycomb FRPC #1	- 877	- 1671	794	1835	1068	767
Honeycomb FRPC #2	128	- 783	911	1170	478	692
FRPC Box Beam	256	- 1514	1770	1132	- 122	1254
FEA-Design (18K load)	-137	- 955	818	654	- 269	914
FEA-Load Test (12K)	- 90	- 542	632	387	- 200	587

The finite element analyses used as a comparison in the above table were plane strain analysis of a honeycomb sandwich beam using 714 CST elements. The results from the plane strain analysis can be used as a comparison if one assumes that the state of stress is uniform through the thickness of the FRP skin. The materials properties used in the analysis were average pavement modulus values backcalculated

from FWD tests, coupon tests for the FRP materials, laboratory unconfined compression tests on the BM-2 overlay materials, and manufacturer's design literature values for the aluminum honeycomb.

The finite element analysis conducted during the design phase indicated that the FRPC units placed over a two inch deteriorated crack with an 18,000 pound load should theoretically exhibit the maximum stress level shown in Table V-2 under the heading FEA-Design. This analysis was for a two inch wide crack with a softened zone four inches on either side of the crack. The softened zone was modeled by reducing the pavement modulus to one half the undeteriorated value. The same modulus values were used to model the repair with a 12,080 pound load. The stresses predicted by this analysis are those shown under the heading FEA- Load Test.

The stresses predicted by the two finite element analyses are quite a bit lower than those observed under the load test. One would expect the results of the field load tests to fall in between the results for the 18,000 pound FEA design check and the 12,080 wheel load FEA run instead of being markedly higher than the analysis values. This discrepancy can be explained by noting one fundamental omission in the finite element analysis that would skew the results. That omission is the lack of any modeling of the granular bedding underneath the FRPC units. The bedding was placed during construction to reduce the stress concentration effects of milling irregularities. The bedding consisted of sand and epoxy cemented sand on the first honeycomb sandwich unit, asphalt millings and epoxy cemented asphalt millings on

the second honeycomb sandwich unit, and only millings on the box beam unit. The granular backfill was irregular in material consistency and thickness for all three units and would be very difficult to model. The higher stress values observed from the strain gages in the field load test are indicative of a larger soft area being bridged by the units than assumed in the initial analyses.

For each structural unit under field load test, a comparison of the stress values between the upper and lower surfaces shows a difference in the stress levels between the two surfaces. This is especially apparent in the box beam unit, where there is a 500 psi differential in the deviator stress. The upper surface has a stronger compressive stress when compared to the lower surface. This indicates a much larger deformation in the upper surface, which can be interpreted as a buckled condition.

The two honeycomb units show slightly higher stresses on the lower surface of the structural sandwich than on the upper surface. This differential can be traced to the influence of the overlay on the upper surface of the beam. Honeycomb FRPC #1 shows only a 27 psi differential in the deviator stress between the upper and lower skins but Honeycomb FRPC #2 has a 219 psi differential. The reason for the greater stress differential in one unit than the other can be traced to the bonding of the overlay to the fiberglass skin. On Honeycomb FRPC #1, the overlay was placed without a tack coat of emulsified asphalt, which would result in a poor bond between the asphalt overlay and the fiberglass skin of the structural sandwich. Honeycomb FRPC #2 had a generous tack coat of emulsified asphalt prior to placement of the overlay.

This produces a good bond between the overlay and the fiberglass skin, allowing the overlay to carry some of the compressive stress, thereby reducing the stress in the fiberglass skin.

The cause of the raveling on the box beam unit in one wheel path was due in part to excessive deformation in the silicone rubber protective coating applied over the top of the instrumentation cables. Some very minor raveling due to the same cause has occurred in the overlays on the honeycomb units. However, this was not the cause of raveling in the other wheel path since there is no silicone rubber in that area. The raveling and shedding of the overlay had to be caused by deflection of the upper surface of the box beam unit. Excessive deflection of the upper surface would cause cracking and debonding of the overlay and would result in the loss of the overlay through raveling. When the prototype box beam sections were load tested, buckling was first observed in the upper surface of the box section under load. Apparently, the polyurethane foam does not provide sufficient support to the upper surface of the box beam to limit deflections below that which would cause debonding of the overlay. This conclusion is supported by strain gage data from the field load test.

APPENDIX K

RECOMMENDATIONS FOR FURTHER RESEARCH AND DEVELOPMENT

The use of FRPC structural units by internal maintenance forces to repair thermal cracks shows promise. The units are easy to install within a time period of three hours with standard maintenance tools and can bridge the cracked pavement area with a performance equal to undeteriorated asphalt pavement. The sandwich method of construction for the FRPC beams using structural honeycomb with glass fiber cover sheets appears to be the most cost-effective method of construction and the easiest to mechanize for large scale production.

While the concept shows promise, several areas of performance need to be improved. The first of these is the matter of the mechanics and interaction of the bituminous overlay with the FRPC beam. Shallow emplacement with a thin overlay is preferred but field results to date seem to indicate a deeper burial is needed to reduce the stresses in the overlay.

Another item that needs further work is the method of anchoring the FRPC beam within the existing pavement. The mechanics of interaction between the FRPC beam and the existing pavement is not understood. This question must be answered if a rapid and permanent method of installation is to be perfected.

Selection of the optimum polymer matrix for the glass fiber cover skins and adhesive for bonding to the honeycomb core remains as an obstacle to full

exploitation of this technology. The units must retain a reasonable measure of their load-carrying capacity throughout their design life. The effect of the environment on FRPC mechanical properties in this application has not been studied. The two honeycomb sandwich units currently in service can only deliver a qualitative indicator of performance and were not emplaced in the manner which good experimental design requires.

REFERENCES

AGARD (1995). **Composite Repair of Military Aircraft Structures,** AGARD Conference Proceedings 550, North Atlantic Treaty Organization, Neuilly-Sur-Seine, France.

Asphalt Institute (1988). **The Asphalt Handbook**, Asphalt Institute, Lexington, KY.

Borek, R. W. (1981). **Practical Aspects of Instrumentation System Installation**, AGARD, North Atlantic Treaty Organization, Neuilly-Sur-Seine, France.

Brown, S. F., J. M. Brunton, D. A. B. Hughes, and B. V. Brodrick (1985). "Polymer Grid Reinforcement of Asphalt," **Proceedings of the Association of Asphalt Paving Technologists**, Volume 54, pp. 18-44.

Brownridge, F. C. (1964). "An Evaluation of Continuous Wire Mesh Reinforcement in Bituminous Resurfacing", **Association of Asphalt Paving technologists**, Volume 33, pp.459-501.

Busching, H. W., and J. D. Antrim (1968). "Fiber Reinforcement of Bituminous Mixtures", **Proceedings of the Association of Asphalt Paving Technologists**, Volume 37, pp. 629-659.

Button, Joe W., Jon E. Epps, and Robert L. Lytton (1983). **Laboratory Evaluation of Fabrics for Reducing Reflection Cracking**, Texas Transportation Institute, College Station, TX.

Caltabiano, M. A., and J. M. Brunton (1991). "Reflection Cracking in Overlays", **Proceedings of the Association of Asphalt Paving Technologists**, Volume 60, pp. 310-332.

Chamis, Christos C. (1981). **Prediction of Composite Thermal Behavior Made Simple**, NASA Technical Memorandum 81618, National Aeronautics and Space Administration, Washington, DC.

Chamis, Christos C. (1982). **Designing With Fiber-Reinforced Plastics (Planar Random Composites)**, NASA Technical Memorandum 82812, National Aeronautics and Space Administration, Washington, DC.

Chamis, Christos C. (1983). **Design Procedures for Fiber Composite Structural Components: Rods, Columns, and Beam Columns**, NASA Technical Memorandum 83321, National Aeronautics and Space Administration, Washington, DC.

Chamis, Christos C. (1983). **Simplified Composite Micromechanics Equations for Strength, Fracture toughness, Impact Resistance and Environmental Effects**,

NASA Technical Memorandum 83696, National Aeronautics and Space Administration, Washington, DC.

Chamis, Christos C. (1985). **Design Procedures for Fiber Composite Structural Components: Panels Subjected to combined In-Plane Loads**, NASA Technical Memorandum 86909, National Aeronautics and Space Administration, Washington, DC.

Chamis, Christos C. and J. H. Sinclair (1982). **Prediction of Composite Hygral Behavior Made Simple**, NASA Technical Memorandum 82780, National Aeronautics and Space Administration, Washington, DC.

Chamis, Christos C. and P. L. N. Murthy (1989). **Simplified Procedures for Designing Adhesively Bonded Composite Joints**, NASA Technical Memorandum 102120, National Aeronautics and Space Administration, Washington, DC.

Christensen, R. M. (1979). **Mechanics of Composite Materials**, John Wiley and Sons, Inc., New York.

Civil Engineering Research Foundation (CERF) (1994). **Materials for Tomorrow's Infrastructure: A Ten Year Plan for Deploying High Performance Construction Materials and Systems**, CERF Report #94-5011, Civil Engineering Research Foundation, Washington, D.C.

Drickey, Donald C. (1995). Private Communication.

ERES Consultants (1982). **Techniques for Pavement Rehabilitation**, National Highway Institute, Federal Highway Administration, Washington, D.C.

Fager, Glenn A. (1994). "Use of Rubber in Asphalt Pavements: Kansas Experience", **Transportation Research Record 1436**, Transportation Research Board, Washington, D.C.

Frantzen, Jeffrey A. (1994). **Fracture Mechanics as Applied to Fiber Reinforced Composites for Civil Engineering Pavement Applications**. Department of Civil Engineering, University of Kansas, Lawrence, KS.

Frantzen, Jeffrey A. (1998). **A Fiber Reinforced Composite Structure for the Repair of Thermally Cracked Bituminous Pavements**, PhD Dissertation, Department of Civil Engineering, University of Kansas, Lawrence, KS.

Gisi, Andrew J. (1995). Private Communication.

Hoskin, Brian C., and Alan A. Baker (1986). **Composite Materials for Aircraft Structures**, American Institute of Aeronautics and Astronautics, New York.

Huhtala, Matti, Risto Alkio, Jari Pihljamaki, Markku Pienimaki, and Pakka Halonan (1993). "Behavior of Bituminous Materials Under Moving Wheel Loads", **Proceedings of the Association of Asphalt Paving Technologists**, Volume 62, pp. 422-442.

Jang, Bor Z. (1994). **Advanced Polymer Composites**, ASM International, Materials Park, OH.

Jones, A. (1962). "Tables of Stresses in Three-Layer Elastic Systems," **Highway Research Board Bulletin 342**, National Academy of Sciences, National Research Council, Washington, D.C.

Jones, F. R. (1994). **Handbook of Polymer-Fiber Composites,** Longman Scientific and Technical, Longman House, Burnt Mill, Harlow, Essex, England.

Jones, Robert M. (1975). **Mechanics of Composite Materials**, Hemisphere Publishing Corp., New York.

Kari, William J. (1980). "Symposium on Prevention and Control of Reflective Cracking", **Proceedings of the Association of Asphalt Paving Technologists**, Volume 49, pp.266-368.

Kansas Department of Transportation (1989). **Highway Maintenance Manual**, Kansas Department of Transportation, Topeka, KS.

Kottkamp, E., H. Wilhelm, and D. Kohl (1976). **Strain Gauge Measurements on Aircraft**, AGARD, North Atlantic Treaty Organization, Neuilly-Sur-Seine, France.

Krone, Norris J. (1974). **Divergence Elimination with Advanced Composites**, PhD Dissertation, University of Maryland, College Park, MD.

Locke, James E. (1995). Private Communication.

Maag, Rodney G. (1995). Private Communication.

Maag, Rodney G., James A. Thissen, and Robert F. Heinen (1983). **Petromat Performance on Flexible and Composite Pavements**, Bureau of Materials and Research, Kansas Department of Transportation, Topeka, KS.

Middleton, D. H. (1990). **Composite Materials in Aircraft Structures**, Longman Scientific and Technical, Longman House, Burnt Mill, Harlow, Essex, England.

Molenaar, A. A. A., J. C. P. Heerkens, and J. H. M. Verhoeven (1986). "Effects of Stress Absorbing Membrane Interlayers", **Proceedings of the Association of Asphalt Paving Technologists**, Volume 55, pp. 453-481.

Osgood, Carl C. (1966). **Spacecraft Structures**, Prentice-Hall, Inc., Englewood Cliffs, NJ.

Parcells, William H. (1990). **Crack Repair Using Fiberglass - 1989 Annual Report**, Bureau of Materials and Research, Kansas Department of Transportation, Topeka, KS.

Pendleton, Richard L., and Mark E. Tuttle (1989). **Manual on Experimental Methods for Mechanical Testing of Composites**, Society for Experimental Mechanics, Inc., Bethel, CN.

Reddy, J. N., and A. V. Krishna Murty (1992). **Composite Structures - Testing, Analysis, and Design**, Springer-Verlag, New York.

Roberts, Freddy L., Prithvi S. Kandhal, E. Ray Brown, Dah-Yinn Lee, and Thomas W. Kennedy (1991). **Hot Mix Asphalt Materials, Mixture Design, and Construction**, NAPA Education Foundation, Lanham, MD.

Schwartz Mel M. (1994). **Joining of Composite-Matrix Materials,** ASM International, Materials Park, OH.

Sherman, George (1982). "Minimizing Reflection Cracking of Pavement Overlays", **NCHRP Synthesis 92**, Transportation Research Board, Washington, D.C.

Tons, Egons, and Edward M. Krokosky (1960). "A Study of Welded Wire Fabric Strip Reinforcement in Bituminous Concrete Resurfacing", **Proceedings of the Association of Asphalt Paving Technologists**, Volume 29, pp.43-80.

Vicelja, (1963). "Methods to Eliminate Reflection Cracking in Asphalt Concrete Resurfacing over Portland Cement Concrete", **Proceedings of the Association of Asphalt Paving Technologists**, Volume 32, pp. 200-237.

Yandell, W. O., and J. I. Curiskis (1983). "Fabric Reinforcement to Extend Pavement Life", **Proceedings of the Association of Asphalt Paving Technologists**, Volume 52, pp. 585-600.

Zagainov, G. I., and G. E. Lozino-Lozinski (1996). **Composite Materials in Aerospace Design**, Chapman & Hall USA, New York, NY.

Zube, Ernest (1956). "Wire Mesh Reinforcing in Bituminous Resurfacing", **HRB Bulletin 131**, Highway Research Board, Washington, D.C.